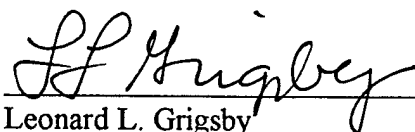


REPORT DOCUMENTATION PAGE			Form Approved OMB No. 0704-0188	
Public reporting burden for this collection of information is estimated to average 1 hour per response, including the time for reviewing instructions, searching existing data sources, gathering and maintaining the data needed, and completing and reviewing the collection of information. Send comments regarding this burden estimate or any other aspect of this collection of information, including suggestions for reducing this burden, to Washington Headquarters Services, Directorate for Information Operations and Reports, 1215 Jefferson Davis Highway, Suite 1204, Arlington, VA 22202-4302, and to the Office of Management and Budget, Paperwork Reduction Project (0704-0188), Washington, DC 20503.				
1. AGENCY USE ONLY (Leave blank)		2. REPORT DATE 4 August 1998	3. REPORT TYPE AND DATES COVERED	
4. TITLE AND SUBTITLE NONLINEAR MODELING, ANALYSIS, AND CONTROL OF INSTRUMENTS USING ROTATING UNBALANCED MASS ACTUATORS			5. FUNDING NUMBERS	
6. AUTHOR(S) Carlee A. Bishop				
7. PERFORMING ORGANIZATION NAME(S) AND ADDRESS(ES) Auburn University			8. PERFORMING ORGANIZATION REPORT NUMBER  98-017D	
9. SPONSORING/MONITORING AGENCY NAME(S) AND ADDRESS(ES) THE DEPARTMENT OF THE AIR FORCE AFIT/CIA, BLDG 125 2950 P STREET WPAFB OH 45433			10. SPONSORING/MONITORING AGENCY REPORT NUMBER	
11. SUPPLEMENTARY NOTES				
12a. DISTRIBUTION AVAILABILITY STATEMENT Unlimited distribution In Accordance With AFI 35-205/AFIT Sup 1			12b. DISTRIBUTION CODE	
13. ABSTRACT (Maximum 200 words)				
14. SUBJECT TERMS			15. NUMBER OF PAGES 145	
			16. PRICE CODE	
17. SECURITY CLASSIFICATION OF REPORT	18. SECURITY CLASSIFICATION OF THIS PAGE	19. SECURITY CLASSIFICATION OF ABSTRACT	20. LIMITATION OF ABSTRACT	

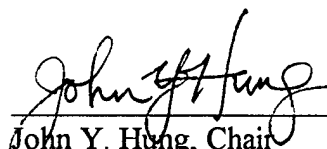
NONLINEAR MODELING, ANALYSIS, AND CONTROL OF INSTRUMENTS  
USING ROTATING UNBALANCED MASS ACTUATORS

Carlee A. Bishop

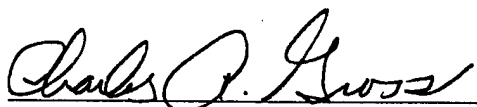
Certificate of Approval:



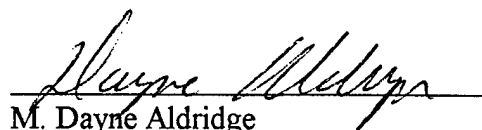
Leonard L. Grigsby  
Alabama Power Distinguished Professor  
Electrical Engineering



John Y. Hung, Chair  
Associate Professor  
Electrical Engineering



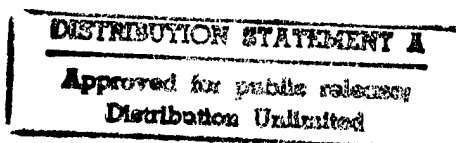
Charles A. Gross  
Square D Professor  
Electrical Engineering



M. Dayne Aldridge  
Director  
Thomas Walter Center for  
Technology Management

John F. Pritchett  
Dean  
Graduate School

DTIC QUALITY INSPECTED 1



19980811 035

NONLINEAR MODELING, ANALYSIS, AND CONTROL OF INSTRUMENTS  
USING ROTATING UNBALANCED MASS ACTUATORS

Carlee Ann Bishop

A Dissertation

Submitted to

the Graduate Faculty of

Auburn University

in Partial Fulfillment of the

Requirements for the

Degree of

Doctor of Philosophy

Auburn, Alabama

June 12, 1998

## VITA

Carlee Ann (Murphy) Bishop, daughter of William Murphy and Janice (Reich) Murphy, was born on January 21, 1958, in Russell, Kansas. She graduated from Lakeview High School, Lakeview, Oregon in 1976 and joined the United States Air Force working as a radar technician. In 1977, she was accepted to the United States Air Force Academy Preparatory School and in 1978 she entered the United States Air Force Academy with the class of 1982. She graduated on June 2, 1982 with a Bachelor of Science in Electrical Engineering and a commission in the United States Air Force. She married Sean Patrick Bishop on June 12, 1982. She went on to Undergraduate Pilot Training (UPT) and flew C-141B aircraft until 1991. During her flying career, she flew as an aerial refueling pilot, instructor pilot, and flight examiner pilot on world wide missions including the Persian Gulf during Operation Dessert Storm. In March 1991, she entered the Georgia Institute of Technology in Atlanta, GA and graduated with a Master of Electrical Engineering degree in June 1992. From 1992 to 1995 she was a flight instructor and Assistant Professor in the Astronautical Engineering Department at the United States Air Force Academy. In the Summer of 1995, she joined the doctoral program in Electrical Engineering at Auburn University, Auburn, Alabama. She is blessed with two wonderful daughters, Murphy Ann Bishop and Kelsey Michael Bishop.

DISSERTATION ABSTRACT  
NONLINEAR MODELING, ANALYSIS, AND CONTROL OF INSTRUMENTS  
USING ROTATING UNBALANCED MASS ACTUATORS

Carlee Ann Bishop

Doctor of Philosophy, June 12, 1998  
(MSEE, Georgia Institute of Technology, 1992)  
(BSEE, United States Air Force Academy, 1982)

158 Typed Pages

Directed by John Y. Hung

The Rotating Unbalanced Mass (RUM) device was originally developed at NASA's Marshall Space Flight Center by Dr. Michael Polites to provide an efficient, accurate means of scanning space/balloon-borne gamma ray and x-ray telescopes. The special optics in a gamma ray or x-ray telescope only allow for physical scanning of the telescope to image the radiation source. Physical scanning requires that the entire telescope be moved in a manner to generate the particular patterns required to image the radiation source. Employing the RUM device on a space or balloon-borne system reduces the complexity and power requirements compared to standard scanning actuators such as control moment gyros (CMG), reaction wheels, or torque

motors. To further enhance the benefits of utilizing the RUM device, pointing actuation is currently being researched.

This dissertation focuses on the development of a complete model of the RUM actuated system and on the feasibility study of RUM actuated pointing. This research effort involves extensive modeling using a robotics approach known as the Lagrange Formulation. Applying well-developed robotic kinematic and kinetic concepts to this problem provides a systematic approach to system modeling and identifies how individual components of the system interact. The RUM actuated system, however, is unique in a robotics sense because of its configuration and actuation. Therefore, the Lagrange Formulation must be modified when applying it to the RUM system. This detailed modeling approach reveals previously unmodeled inertia, centripetal, and coriolis terms in the equations of motion for the RUM actuated system. Obtaining this complete model facilitates detailed control analysis, which helps determine the feasibility of pointing actuation using the RUM device. This analysis draws from non-linear reachability conditions and the dynamic coupling index. These discoveries give considerable insight into control schemes and computer simulations confirm that pointing actuation may be possible using the RUM device. An additional control scheme, which cancels undesirable dynamic components including certain inertia, centripetal and coriolis terms, is necessary along with possible configuration changes.

## ACKNOWLEDGMENTS

The author would like to express her deepest gratitude to her advisor Dr. John Y. Hung, Associate Professor, Department of Electrical Engineering for his invaluable guidance, support and encouragement towards the completion of this dissertation. Additionally, the author would like to thank the other members of the advisory committee, including Dr. L. L. Grigsby, Dr. M. D. Aldridge and Dr. C. A. Gross. The author would also like to thank NASA Marshall Space Flight Center and the United States Air Force for supporting this work. Finally, the author wishes to express her gratitude to her husband and family for their faith and encouragement and to the many people at Auburn University that have made the past three years fulfilling and enjoyable.

Style manual of journal used IEEE Transactions on Automatic Control

---

Computer software used Microsoft Word 97, MapleV for Windows (Release 2),

Matlab for Windows 4.2c.1

---

## TABLE OF CONTENTS

LIST OF TABLES .....	xi
LIST OF FIGURES .....	xii
CHAPTER 1 INTRODUCTION .....	1
1.1 Problem Statement .....	3
1.2 Problem Approach .....	3
1.3 Dissertation Overview .....	4
CHAPTER 2 BACKGROUND INFORMATION .....	6
2.1 Optical Requirements for Gamma Ray and X-ray .....	6
2.1.1 Space and Balloon-Borne Systems .....	6
2.1.2 Special Optics .....	8
2.1.3 Scanning .....	9
2.1.4 Traditional Scanning Methods .....	11
2.2 The RUM Device .....	12
2.2.1 Basic Concept .....	12
2.2.2 Equations of Motion .....	13
2.2.3 Auxiliary Control System .....	17
2.3 Prior Work on Pointing Control .....	18
2.3.1 Dynamical Analysis .....	19
2.3.2 Control Analysis .....	21
2.4 Necessary Technical Study .....	25
2.4.1 Modeling Issues .....	25
2.4.2 Control Issues .....	26
2.5 Conclusions .....	27
CHAPTER 3 SYSTEMS APPROACH TO MODELING .....	29
3.1 Lagrange Formulation - Basic Concepts .....	30
3.1.1 Potential Energy .....	32
3.1.2 Kinetic Energy .....	34
3.2 Kinematics .....	38
3.2.1 Position Kinematics .....	38
3.2.2 Denavit- Hartenberg (DH) Convention .....	42
3.2.3 Velocity Kinematics .....	45

3.2.3.1 Angular Velocity Jacobian .....	45
3.2.3.2 Linear Velocity Jacobian .....	47
3.3 Summary of Lagrange Formulation Steps .....	51
<b>CHAPTER 4 RUM-ACTUATED SYSTEM MODELING .....</b>	<b>55</b>
4.1 Kinematic Modifications .....	56
4.1.1 Modeling Assumptions and System Properties .....	56
4.1.2 Position Kinematic Modifications .....	57
4.1.2.1 Homogeneous Transformation Modifications .....	60
4.1.2.2 Potential Energy Simplification .....	61
4.1.3 Velocity Kinematic Modifications .....	62
4.2 Dynamic Modifications .....	64
4.3 Summary .....	68
<b>CHAPTER 5 MODEL VALIDATION .....</b>	<b>69</b>
5.1 Kinematic Model Validation .....	69
5.2 Dynamic Model Validation .....	70
5.2.1 Pendulum Example .....	71
5.2.2 Verifying Matrix Properties .....	73
5.2.3 Model Analysis .....	74
5.2.3.1 Model Descriptions .....	74
5.2.3.2 Model Comparisons .....	77
5.2.4 Experimental Validation .....	78
5.2.4.1 Model Form .....	79
5.2.4.2 Matlab <sup>TM</sup> Simulations .....	81
5.2.4.3 Constant RUM Speed Analysis .....	84
5.2.4.4 Start-Up Transient Behavior .....	86
5.2.4.5 Variable RUM Speed Analysis .....	88
5.3 Summary .....	91
<b>CHAPTER 6 FEASIBILITY OF RUM ACTUATED POINTING CONTROL .....</b>	<b>93</b>
6.1 Pointing Control Using RUM Rate Variations .....	95
6.2 Pointing Control using Feedback ‘Cancellation’ .....	96
6.3 Controllability Analysis Tools .....	98
6.3.1 Linear System Control Analogy .....	98
6.3.2 Nonlinear System Controllability (Reachability) .....	99
6.3.3 Coupling index .....	100
6.4 Reachability Analysis – RUM Actuated System .....	102
6.4.1 Model 1 Controllability Condition .....	104
6.4.2 Model 2 Reachability Condition .....	106
6.4.3 Model 3 Reachability Condition .....	107
6.5 Coupling index – RUM Actuated System .....	108

6.5.1 Model 1 Coupling index .....	108
6.5.2 Model 2 Coupling index .....	109
6.5.3 Model 3 Coupling index .....	111
6.5.4 Summary .....	112
6.6 Modifications to Control Input .....	112
6.7 System Configuration Changes .....	118
6.7.1 Variable Gimbal Braking .....	119
6.7.2 Pointing Control using Variable RUM Arm Length .....	120
6.8 Conclusions .....	122
CHAPTER 7 FUTURE WORK AND CONCLUSIONS .....	124
7.1 Future Research .....	125
7.2 Summary of Contributions .....	129
7.3 Closing Thoughts .....	130
BIBLIOGRAPHY .....	131
APPENDIX A KINEMATIC MODELING DETAILS .....	134
APPENDIX B VELOCITY JACOBIANS .....	136
APPENDIX C H AND C MATRIX VALUES .....	138
APPENDIX D COUPLING INDEX .....	144

## LIST OF TABLES

Table 1 - Joint Parameters .....	44
Table 2 - RUM System Joint Parameters .....	60

## LIST OF FIGURES

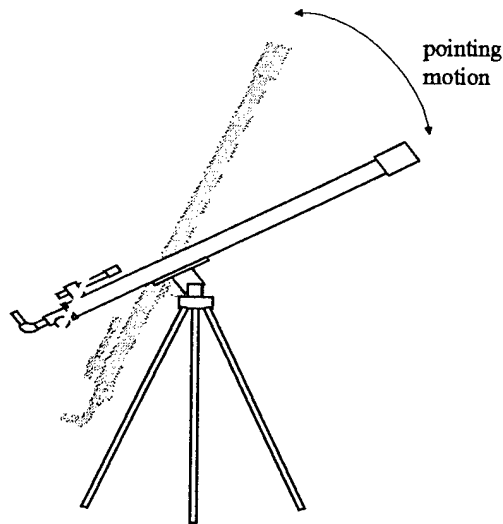
Figure 1 Telescope Pointing Motions .....	1
Figure 2 Telescope Scanning Motion .....	2
Figure 3 Atmospheric Blocking of EM Radiation .....	7
Figure 4 Spark Chamber Gamma Ray Detector .....	8
Figure 5 Grazing Incidence X-Ray Detector .....	9
Figure 6 Scanning Example .....	10
Figure 7 Typical Scanning Patterns .....	10
Figure 8 Balloon-Borne Experiment in a Circular Scan .....	14
Figure 9 Balloon-borne experiment in a linear scan .....	16
Figure 10 Test Configuration .....	18
Figure 11 Torque Profile about the Center of Mass .....	19
Figure 12 Control System Overview .....	23
Figure 13 Elevation Axis Disturbance Response .....	24
Figure 14 N Link Manipulator .....	31
Figure 15 Relative Position of Link Center of Mass .....	33
Figure 16 Manipulator Jacobian Mapping .....	35
Figure 17 Position Representation .....	39
Figure 18 Example Transformation .....	41
Figure 19 DH Convention Example .....	44
Figure 20 Angular Velocity Vectors for Revolute Joints .....	46
Figure 21 Linear Velocity Vectors for Prismatic Joints .....	48
Figure 22 Linear Velocity Vector for Revolute Joints .....	49
Figure 23 Position Vector Representation .....	50
Figure 24 RUM Actuated System Diagram .....	58
Figure 25 RUM System Coordinate Frames (DH Convention) .....	59
Figure 26 Links of the RUM Actuated System .....	63
Figure 27 Kinematic Simulations .....	70
Figure 28 Simple Pendulum .....	72
Figure 29 Flow Diagram for RUM Simulations .....	83
Figure 30 Constant RUM Velocity Simulation Results .....	86
Figure 31 Start-Up Transient Response Simulation Results .....	87
Figure 32 RUM Velocity Profile .....	89
Figure 33 Variable RUM Velocity Simulation Results .....	90
Figure 34 General Open-Loop Control Scheme .....	94
Figure 35 Variable Speed Control on Model 3 without Reaction Forces .....	97

Figure 36	Speed Profile Comparison .....	113
Figure 37	Cross-Elevation Axis Motion with New Control (30 sec simulation) .....	115
Figure 38	Elevation Axis Motion with New Control ( $\Delta$ times 10).....	116
Figure 39	Variable Gimbal Braking Pointing Actuation .....	120
Figure 40	Variable RUM Arm Length Pointing Actuation.....	121

## CHAPTER 1

### INTRODUCTION

Remote sensing of gamma ray and x-ray sources poses unique attitude control challenges for balloon or space borne telescopes. The challenges include pointing and scanning of the telescope optical systems. Pointing is two dimensional motion that turns the telescope in a given direction for target acquisition and centering a scan on the target. Figure 1 shows an example of a ground based telescope in pointing motion.



**Figure 1 Telescope Pointing Motions**

Scanning is small, localized two dimensional motion accomplished by electronically or physically changing or moving the optics of the sensor. Figure 2 shows an example of a ground based telescope in physical scanning motion.

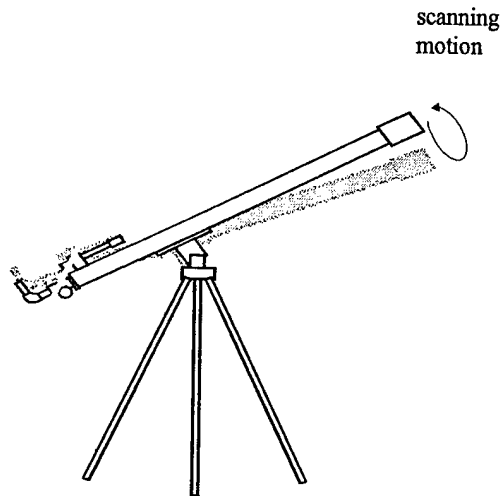


**Figure 2 Telescope Scanning Motion**

The special optics in a gamma ray or x-ray telescope only allow for physical scanning of the telescope to image the radiation source. Physical scanning requires that the entire telescope be moved in a manner to generate the particular patterns required to image the radiation source. An innovative new type of actuator called the rotating unbalanced mass (RUM) device was recently developed at NASA (National Aeronautics and Space Administration) by Dr. Michael Polites [1,2] to accomplish the scanning requirements of these optical systems. The RUM has proven to provide an efficient, accurate means of scanning space/balloon-borne gamma ray and x-ray telescopes during ground testing [3]. Employing the RUM device on a space or

balloon-borne system reduces the complexity and power requirements compared to standard scanning actuators such as control moment gyros (CMG), reaction wheels, or torque motors. The next challenge is to use the device to accomplish the pointing necessary for target acquisition and proper imaging. If the RUM device proves to be as effective at pointing actuation as it has been at scanning actuation, considerable actuator hardware reductions are possible.

### **1.1 Problem Statement**

Attitude control for balloon and space-borne gamma ray and x-ray telescopes is divided into two areas: scanning and pointing. Currently, the telescope is pointed using an auxiliary control system (ACS) consisting of the standard CMG's, reaction wheels or torque motors and scanning is accomplished using the RUM actuator. The research conducted for this dissertation is motivated by the prospect of simplifying or eliminating the ACS by using a pointing control scheme incorporating RUM devices for pointing actuation.

### **1.2 Problem Approach**

Since linearized scanning models of the RUM actuated systems appear to be inaccurate for pointing control, a systems approach to modeling and control is incorporated that draws from dynamic modeling of robots using the Lagrange Formulation. Applying well-developed robotic kinematic and kinetic concepts to this problem provides a systematic approach to system modeling and identifies how

individual components of the system interact. The RUM actuated system, however, is unique in a robotics sense because of its configuration and actuation. Therefore, the Lagrange Formulation must be modified when applying it to the RUM system. This unique approach provides equations of motion that give the designer physical insight into the behavior of the overall system and is critical in the development of pointing control schemes.

### **1.3 Dissertation Overview**

This dissertation describes the approach used to analyze pointing control using the RUM device. This research focuses on the development of a complete model of the RUM actuated system and on the feasibility study of RUM actuated pointing. The dissertation is divided into the following chapters: Chapter 2 presents background information on the special scanning requirements of gamma ray and x-ray optics and how this scanning is accomplished using the RUM device. This chapter also presents previous work on pointing control using the RUM device. Chapter 3 introduces robotic modeling concepts that are used in Chapter 4 for the development of the RUM equations of motion; e.g. Denavit-Hartenberg (DH) convention and Lagrange Formulation. Chapter 4 covers RUM system kinematic modeling based on the DH convention and RUM system dynamic modeling based on the Lagrange Formulation. It covers, in detail, the modifications necessary when applying these robotic modeling techniques to the RUM actuated system. Since this modeling approach is unique in a robotics sense, the dynamic model is validated in Chapter 5. Chapter 6 examines the

feasibility of RUM actuated pointing control by investigating several control approaches that might achieve pointing control. This chapter addresses the nonlinear control aspects of the system and points out control considerations for RUM actuated systems. Chapter 7, the concluding chapter, presents a summary of research discoveries and suggestions for future work in numerous areas related to the RUM analysis.

## **CHAPTER 2**

### **BACKGROUND INFORMATION**

The RUM device was originally developed to provide an efficient means of scanning space and balloon borne telescopes. This chapter provides background information on the unique requirements of gamma ray and x-ray detectors and how they influenced the development of the RUM device. Next, it presents an overview of RUM actuator concepts when used for scanning purposes. Finally, prior work accomplished toward pointing control is discussed along with the necessary technical study involving modeling and control issues.

#### **2.1 Optical Requirements for Gamma Ray and X-ray**

This section presents the needs of the user based on optical requirements of this special remote sensing equipment.

##### **2.1.1 Space and Balloon-Borne Systems**

Gamma ray and X-ray detectors require a balloon-borne or space borne platform for several reasons [4]:

1. Atmospheric absorption prevents much of the radiation from ever reaching ground based telescopes. Figure 3 depicts the electromagnetic (EM) frequencies reaching

the surface of the Earth and those absorbed or blocked by the atmosphere. X-ray and gamma ray radiation is blocked at rather high altitudes (approximately 25 to 30 thousand feet) making it very difficult if not impossible to detect these radiation sources from ground based sensors. In order to detect gamma ray or X-ray sources accurately, the imaging system must be above the level of the atmosphere that is distorting and blocking the radiation.

2. Images of astronomical objects are blurred when light travels through the turbulent and clumpy air around the Earth.
3. Ground based telescopes receive stray light interference from cities and from atmospheric auroras.
4. Angular resolution is dramatically increased when using space based optical telescopes. Space telescopes can generally distinguish details separated in angle ten times better than ground based systems.

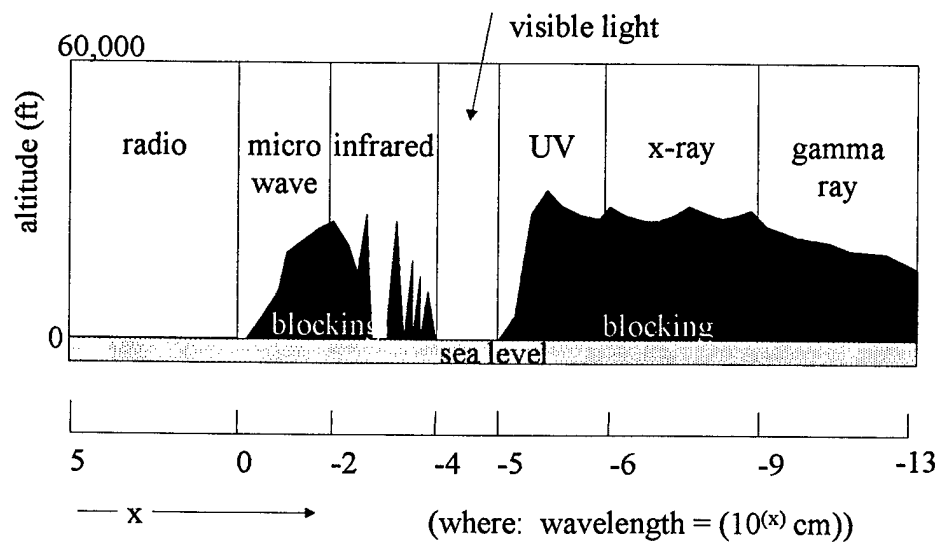


**Figure 3 Atmospheric Blocking of EM Radiation [ 4]**

### 2.1.2 Special Optics

Gamma rays and X-rays penetrate the normal 'mirror' optics of standard telescopes without being detected. Gamma ray detectors require unique hardware such as used in the spark detector shown in Figure 4. Gamma ray detectors track the gamma-ray photon as it passes close to the nucleus of an atom in the target. The photon disappears and a pair of electrons take its place. The electrons absorb the photon's energy and retain much of its trajectory leaving trails of ions in the detector.

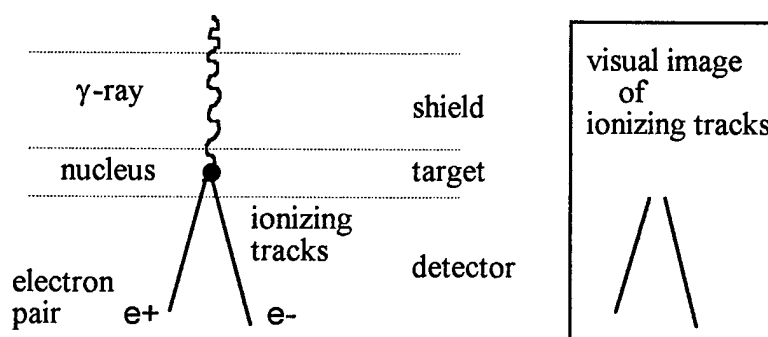


**Figure 4 Spark Chamber Gamma Ray Detector [ 4]**

Similarly, the X-ray detector requires special optics such as the grazing incidence telescope shown in Figure 5. It uses highly polished glass tubes to direct the X-ray radiation by placing them at high incidence angles to the source. Applying Snell's Law to gamma-ray and X-ray radiation provides the incidence angles needed for proper focusing of the image.

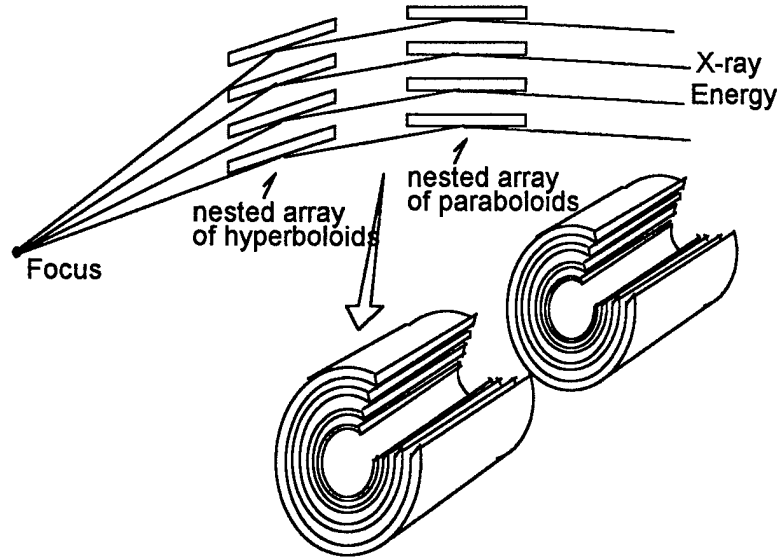


**Figure 5 Grazing Incidence X-Ray Detector [ 4]**

### 2.1.3 Scanning

The special optics and the sources to be detected present some unique control requirements for the imaging process. First, the limited field of view (FOV) requires that the imaging device be scanned to give proper dimension to the image [5]. Referring to Figure 6, a simple example of electro-optical scanning would include a one dimensional scan of an object orthogonal to the flight path of an aircraft. The motion of the aircraft generates the second dimension of the image and is an example of physical scanning.

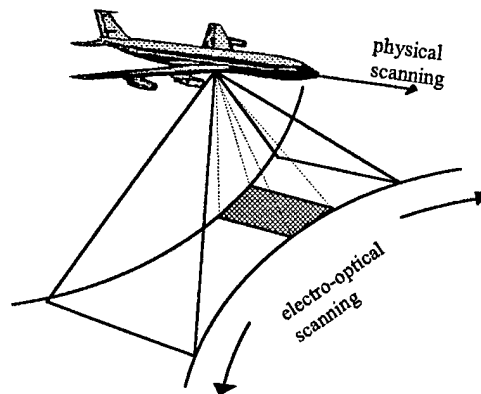


**Figure 6 Scanning Example**

Second, since gamma ray and X-ray radiation is always present as background radiation, it is necessary to distinguish between background radiation and source radiation when imaging a gamma ray or X-ray source. Scanning “on target” and “off target” identifies the flux coming from the background so it can be compared to that coming from the source [6]. Typical scanning patterns include linear, circular, and raster scanning as depicted in Figure 7 [5,6,1]. Gamma ray and X-ray detectors generally require adjustable scan periods and radii to meet user needs.

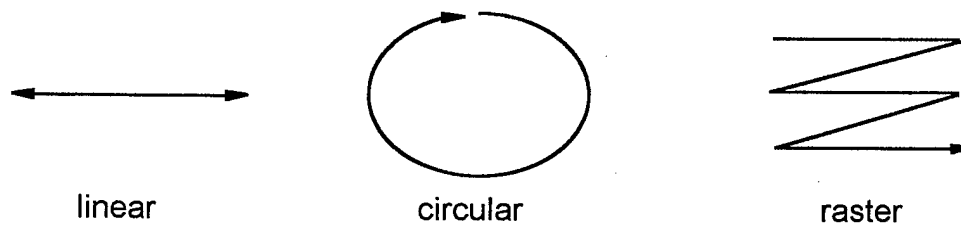


**Figure 7 Typical Scanning Patterns**

#### 2.1.4 Traditional Scanning Methods

The special make-up of gamma ray and X-ray detectors prevent them from being electro-optically scanned. Physical scanning is the only option for these detectors. Prior scanning techniques incorporated torque motors, reaction wheels, control moment gyros or reaction control devices to generate the desired scan patterns. A detailed description of these components is covered in Reference [7]. Basic operation and advantages/disadvantages of each are described as follows:

1. Momentum control devices actively vary the angular momentum of small masses within the spacecraft to change attitude. Reaction wheels and control moment gyros are momentum control devices. Reaction wheels vary spin speed to effect a change in the angular momentum. They provide highly accurate, fast response attitude control. They are complex and expensive, however, and have a large power consumption in the scanning mode of operation. Control moment gyros (CMG) vary spin direction to effect a change in angular momentum. The advantages and disadvantages are similar to reaction wheels.
2. Reaction control devices are basically jet thrusters. The thrusters apply a force at a distance from the center of mass (CM) to effect a torque about the CM. They can produce fast responses but have limited use since they require propellant, which is exhaustible. Because of their nonlinear 'on-off' behavior, they are difficult to control and very inefficient for scanning use since excessive propellant is required.

3. Torque motors provide the simplest means of attitude control. Electronic motors apply torque to a gimbaled system by ‘pushing’ against the gimbal platform. The ‘pushing’, however, can cause instability for balloon-borne gondola systems [8]. Torque motors require excessive power during scanning operation and they cannot be used for free flying spacecraft because there is no platform to ‘push’ against [1].

## **2.2 The RUM Device**

All of the traditional methods of scanning have serious drawbacks including excessive weight, cost, and limited lifetime. The primary motivation for developing the RUM device was reducing payload mission requirements. Major factors influencing space and balloon-borne payloads are efficiency, low cost, and reliability; the RUM device was developed to meet all these requirements. Simulation and prototype test results have shown that the RUM device has a great advantage over reaction wheels and torque motors in the areas of weight and power consumption [1,3]. This section presents a brief overview of the RUM concepts. References [1] and [3] provide excellent explanations of the RUM device.

### **2.2.1 Basic Concept**

The concept of scanning using rotating unbalanced masses is a geometry and physics problem involving the mechanical properties of the system. The RUM device consists of a mass on a lever arm rotating at a constant angular velocity. The mass rotation generates a centripetal force that has constant magnitude but changing

direction. This force applied through a distance from the center of mass generates a torque about the center of mass that also has time varying direction. The time varying torque produces the necessary scan motion, which can be circular, linear, or raster depending on the configuration of the RUM devices [1]. In developing this concept, several assumptions were made:

1. The center of mass is along the line of sight.
2. The line of sight is the axis of minimum principal moment of inertia ( $I_{\min}$ ).
3. The other two principal moments of inertia are equal ( $I_{\max}$ ).
4. Localized RUM motion (i.e. small angle of movement of the experiment).
5. Constant RUM velocity (constant  $\omega_R$ ).
6. The RUM device is treated as a simple actuator decoupled from the experiment dynamics except as an input to the system.

Note: Assumptions 7 and 8 specifically apply to only balloon-borne systems.

7. The Experiment is attached to the gondola by a 2 axis gimbal system.
8. Balloon rotations are isolated from the experiment by a separate azimuth control system.

Based on these assumptions, a linearized equation of motion for the balloon-borne gondola system is developed in the next section.

### **2.2.2 Equations of Motion**

For the balloon-borne gondola system configured with a RUM device as depicted in Figure 8, torque about the center of mass (CM) of the experiment is given

by Equation (1) [1]. The masses are 180° spatially displaced from each other and rotate in the same direction.

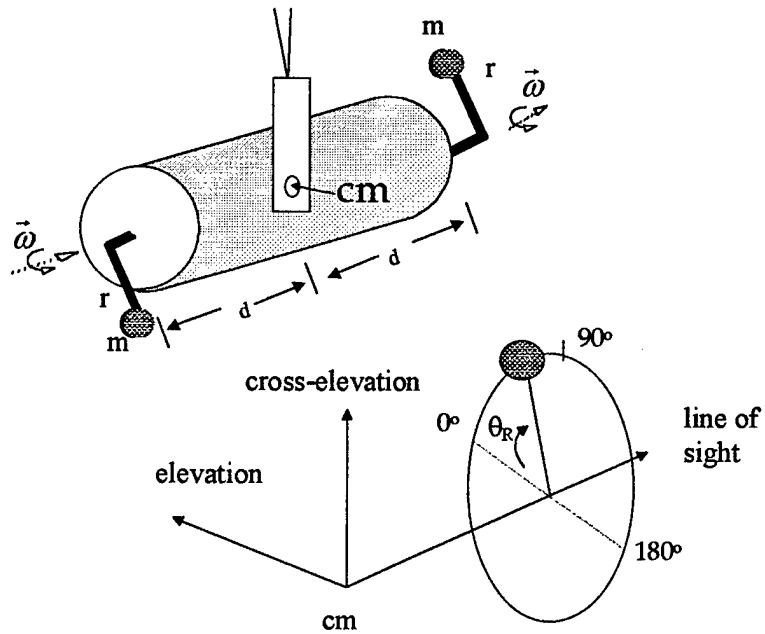


**Figure 8 Balloon-Borne Experiment in a Circular Scan**

$$\begin{bmatrix} T_{LOS} \\ T_E \\ T_X \end{bmatrix} = 2m\omega_R^2 r d \begin{bmatrix} 0 \\ -\sin(\theta_R) \\ +\cos(\theta_R) \end{bmatrix} \quad (1)$$

where:

$T_{(LOS,E,X)}$  = torque about the line of sight (LOS), elevation (E), or cross-elevation (X) axis respectively (ft-lbs),

$m$  = mass on end of lever arm of RUM (slugs),

$r$  = length of lever arm (feet),

$d$  = distance from CM to attachment point of RUM (feet),

$\omega_R$  = angular velocity of rotating mass (radians/sec),

$\theta_R = \omega_R \cdot t$  = angular position of rotating mass (radians).

Using these torques in the linearized equation of motion given by Equation (2) and integrating twice gives the steady state scan motion given by Equation (3).

$$\begin{bmatrix} \ddot{\theta}_{LOS} \\ \ddot{\theta}_E \\ \ddot{\theta}_X \end{bmatrix} = \begin{bmatrix} I_{\max}^{-1} & 0 & 0 \\ 0 & I_{\max}^{-1} & 0 \\ 0 & 0 & I_{\min}^{-1} \end{bmatrix} \begin{bmatrix} T_{LOS} \\ T_E \\ T_X \end{bmatrix} \quad (2)$$

where:  $\ddot{\theta}_{( )}$  = angular acceleration about the respective axis (rad/sec<sup>2</sup>) and  $I$  = the payload moment of inertia (slug-ft<sup>2</sup>).

$$\begin{bmatrix} \theta_E \\ \theta_X \end{bmatrix} = \frac{2mrd}{I_{\max}} \begin{bmatrix} +\sin(\theta_R) \\ -\cos(\theta_R) \end{bmatrix} \quad (3)$$

where:  $\theta_{(E,X)}$  = angular rotation about the elevation and cross-elevation axis (rad). This results in the circular scanning motion depicted in Figure 7. The radius of the scan is given by Equation (4) and the period of the scan is given by Equation (5). Note that the radius and period of the scan are independent of each other. This is a valuable design benefit, making it possible to adjust the period of the scan without changing the radius of the scan and change the radius without changing the period.

$$\rho = \frac{2mrd}{I_{\max}} \quad (4)$$

$$T_{period} = \frac{2\pi}{\omega_R} \quad (5)$$

For the balloon-borne experiment configured as depicted in Figure 9, torque about the center of mass of the experiment is given by Equation (6) and results in the steady state scan motion given by Equation (7) resulting in the linear scan motion depicted in Figure 7.

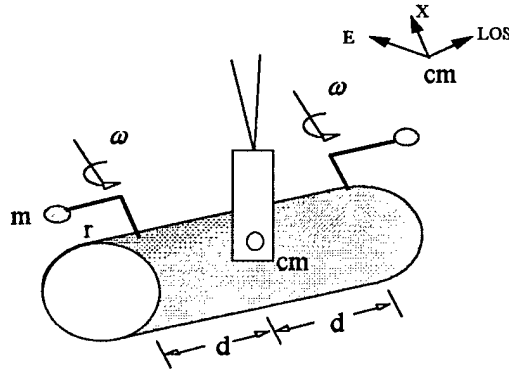


**Figure 9 Balloon-borne experiment in a linear scan**

$$\begin{bmatrix} T_{LOS} \\ T_E \\ T_X \end{bmatrix} = 2m\omega_R^2 r d \begin{bmatrix} 0 \\ 0 \\ \cos(\theta_R) \end{bmatrix} \quad (6)$$

$$\theta_X = -\frac{2mrd}{I_{max}} \cos(\theta_R) \quad (7)$$

The raster scan is generated by using the linear scan configuration and superimposing complementary motion from an auxiliary control system (ACS) that will be described

in the next section. The development is similar for the free flying spacecraft and the gimbaled space platform experiment. See Reference [1] or [3] for details.

### **2.2.3 Auxiliary Control System**

An auxiliary control system is needed to supplement the RUM devices and is usually made of traditional control devices such as reaction wheels, torque motors, etc. The auxiliary control system is used for the following pointing and scanning purposes:

1. Target acquisition.
2. Keeping the center-of-scan on target.
3. Producing the complementary motion for raster scanning.

Figure 10 shows the test configuration of the gimbaled system using torque motors for the ACS. The elevation and cross-elevation axis are controlled independently with low frequency/low amplitude torques where as the RUM devices are controlled by high frequency/high amplitude torques [1]. Low pass filtering keeps the ACS from fighting the motion generated by the RUM devices.

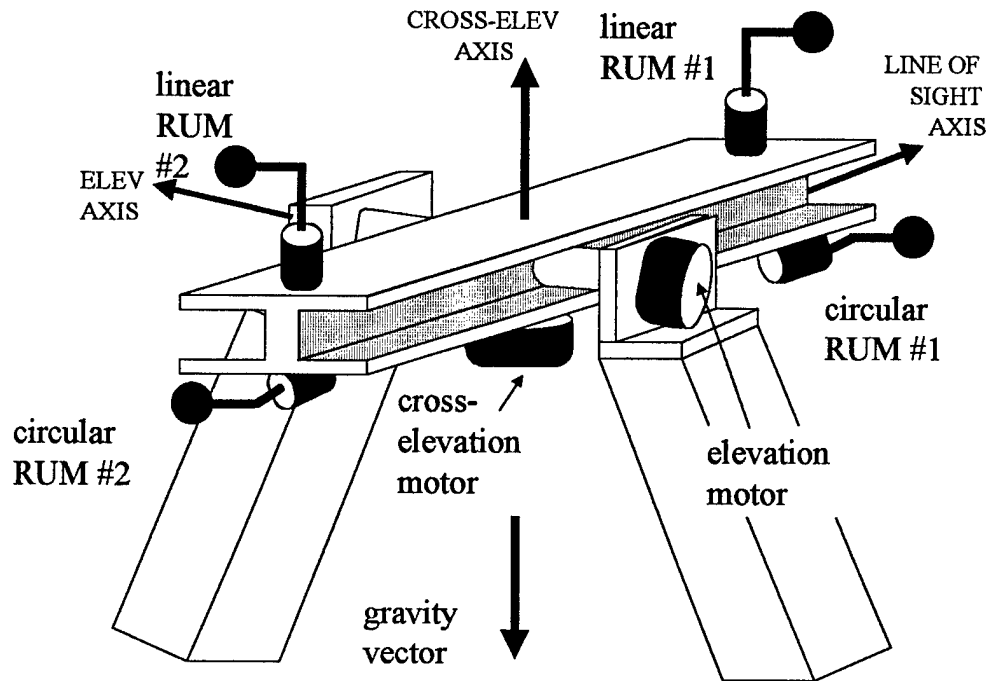


**Figure 10 Test Configuration**

### 2.3 Prior Work on Pointing Control

It has been suggested by Dr. Polites that the RUM device can be used for not only scanning motion but also to control pointing motion. The research work conducted through the NASA/ASEE Summer Faculty Fellowship Program during the summer of 1996 produced promising results in the area of RUM actuated pointing control [9]. The goals of the research program included further dynamical analysis of the experimental system and development of microcontroller code to achieve pointing control. The following two sections cover dynamical analysis and control analysis of the RUM actuated pointing system.

### 2.3.1 Dynamical Analysis

The dynamical analysis centers around the basic concept that a time varying RUM velocity ( $\omega_R$ ) will produce a centripetal force having both time varying magnitude and direction [2,9]. This force can generate a torque about the center of mass that also has time varying magnitude and direction. Figure 11 shows a comparison between a constant  $\omega_R$  torque profile and a time varying  $\omega_R$  torque profile. Note that a net torque can be generated, depending on how the RUM velocity is varied, which in turn can generate the necessary pointing motion.

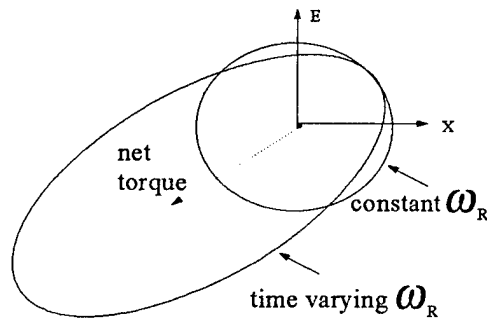


**Figure 11 Torque Profile about the Center of Mass**

The gimbal mounted experiment is configured in the circular scan mode to ensure both the elevation axis and cross-elevation axis have ‘steering’ opportunities. In other words, for the circular scan configuration, RUM rotation generates torques about both the elevation and cross elevation axis as compared to the linear scan configuration where torque is generated about only one axis. Dynamical analysis starts with

Equation (8) which represents the equations of motion for constant RUM angular velocity resulting from combining Equations (1) and (2). Assuming reaction forces from the acceleration of the RUM masses are small, pointing control will be achieved by varying RUM angular velocity, ( $\omega_R$ ), in Equation (8).

$$\begin{aligned}\ddot{\theta}_E &= -\frac{2dmr}{I_E} \sin(\theta_R) \omega_R^2 \\ \ddot{\theta}_X &= \frac{2dmr}{I_X} \cos(\theta_R) \omega_R^2\end{aligned}\quad (8)$$

Equation (8) yields some interesting observations [9]:

1. The elevation and cross-elevation angle dynamics are functions of RUM position ( $\theta_R$ ) and velocity ( $\omega_R$ ).
2. The control input,  $\omega_R$ , varies based on the position of the RUM (i.e. is weighted by  $\sin(\theta_R)$  and  $\cos(\theta_R)$  for elevation and cross-elevation respectively).
3. The control input,  $\omega_R$ , enters the equation of motion as a squared term. Negative  $\omega_R$  has the same effect as positive  $\omega_R$  and must rely on the sign changes of cosine and sine factors to effect positive and negative accelerations.

These observations are used in the next section to develop the control input necessary for pointing motion.

### 2.3.2 Control Analysis

Dr. Polites originally proposed to use a control signal that introduces periodic variations in the RUM rate  $\omega_R$ . The basic approach for determining the control input is to start with a nominal RUM velocity and vary it slightly about each axis. The nominal velocity will provide the scanning motion necessary while the rate variation will provide the change in the net torque necessary for pointing motion. The control input is defined in Equation (9) as:

$$\omega_R = \omega_{r_0} + \Delta\omega_X \cos(\theta_R) - \Delta\omega_E \sin(\theta_R) \quad (9)$$

where:

$\omega_{r_0}$  = a constant (nominal RUM rate of rotation),

$\Delta\omega_X$  = a rate variation to compensate for cross-elevation gimbal error ,

$\Delta\omega_E$  = a rate variation to compensate for elevation gimbal error .

Since the control input is based on the position of the RUM, the rate variations must be 'timed' properly to effect the desired input. The sine and cosine terms in Equation (9) weight the rate variations to give them the proper 'timing'. Substituting the control input into the dynamical model of Equation (8) and eliminating small higher order terms results in the elevation and cross-elevation axis acceleration approximations in Equation (10).

$$\begin{aligned}
\ddot{\theta}_E &\approx -\frac{2dmr}{I_E} \left( \omega_{ro}^2 \sin(\theta_R) - \frac{\omega_{ro}}{2} \Delta\omega_E \right) \\
\ddot{\theta}_X &\approx \frac{2dmr}{I_X} \left( \omega_{ro}^2 \cos(\theta_R) + \frac{\omega_{ro}}{2} \Delta\omega_X \right)
\end{aligned} \tag{10}$$

$\uparrow \qquad \qquad \uparrow$   
scanning      pointing

There are several interesting observations made from this analysis:

1. The first sinusoidal terms cause the periodic ‘scanning’ motion of the main body.
2. The second terms affect the ‘pointing’ motion.

Therefore, pointing control can be accomplished by introducing periodic RUM rate variations  $\Delta\omega_X$  and  $\Delta\omega_E$  for cross-elevation and elevation axis errors, respectively, without interfering with the scanning motion controlled by  $\omega_{ro}$ . The control developed around this model required a pointing controller and a RUM speed controller as shown in Figure 12. Note that this is the control system for a single RUM device. Control for the second RUM device is identical with the exception that the second RUM is  $180^\circ$  spatially displaced from the first RUM.

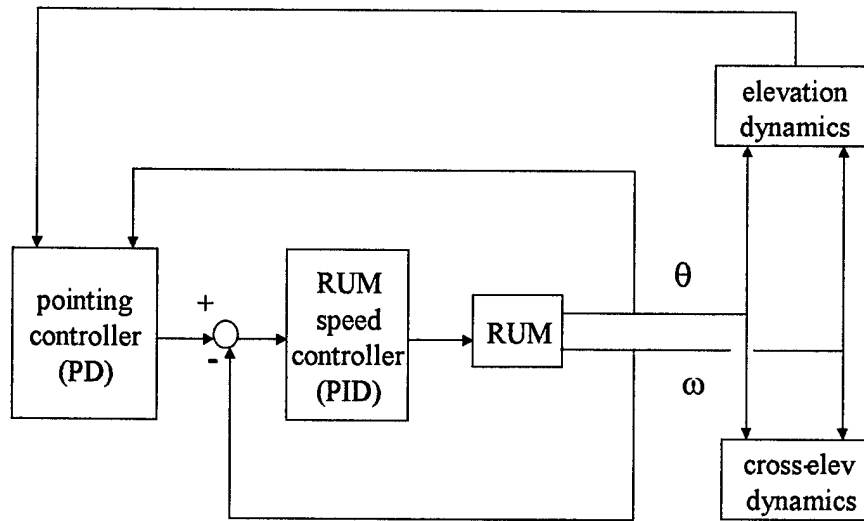


**Figure 12 Control System Overview**

The pointing controller uses a proportional derivative control design (PD) to provide gimbal control via coupling to the RUM speed controller which uses proportional - integral - derivative (PID) control. The elevation and cross elevation torque motors are disabled leaving the RUM devices for actuation of pointing and scanning motion. The test results are shown in Figure 13 for a small impulse disturbance input in the elevation axis.

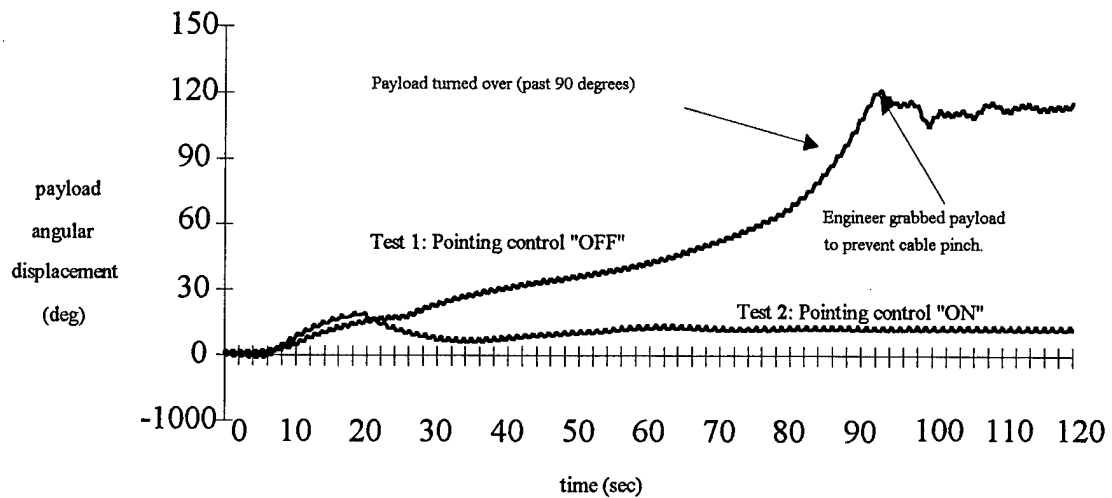


**Figure 13 Elevation Axis Disturbance Response**

Pointing control test result observations:

1. Scanning motion is shown as high frequency oscillation on the plots.
2. Without pointing control, the system has no disturbance rejection.
3. With pointing control off, the system demonstrates a non-linear behavior even before it turns over  $90^\circ$ . A linear system would have displayed a ramp-type response to an impulse input instead of the exponential type response shown. This seems to indicate there is some coupling between the RUM dynamics and the motion of the experiment beyond simple scanning or pointing movement.
4. There is a large steady state error (approximately  $10^\circ$ ) with pointing control on.
5. Test 2, in Figure 13, shows the best result obtained from the pointing control test and was difficult to duplicate.
6. Further testing indicated there was a small stability margin.

## 2.4 Necessary Technical Study

Work accomplished in the summer of 1996 indicates that pointing control may be possible using the RUM device as an actuator. There are several open issues that arise, however, when incorporating the RUM device and a RUM control algorithm to accomplish the pointing control. The issues are divided into two primary areas: Modeling issues and control issues. These issues are briefly introduced in the next two sections with detailed treatment presented in subsequent chapters.

### 2.4.1 Modeling Issues

The modeling approach taken thus far has been to use the RUM device as an actuator basically independent of plant dynamics. The dynamic model developed previously used the RUM device as strictly a torque input. This was a valid approach when the small angle and constant  $\omega$  assumptions were valid. A different modeling approach may be necessary if these assumptions are not valid. Time varying  $\omega_R$  generates additional reaction force terms in the modeling of the RUM device that are neglected in the original dynamical analysis. A more accurate model should include these terms as shown in Equation (11).

$$\begin{bmatrix} \ddot{\theta}_{LOS} \\ \ddot{\theta}_E \\ \ddot{\theta}_X \end{bmatrix} = \frac{2mrd}{I_{max}} \begin{bmatrix} 0 \\ -\omega^2 \sin(\theta_R) + \frac{u}{J} \cos(\theta_R) \\ +\omega^2 \cos(\theta_R) + \frac{u}{J} \sin(\theta_R) \end{bmatrix} \quad (11)$$

$\uparrow$   
centripetal components

$\uparrow$   
reaction component

where:

$u$  = torque applied to the RUM (control input)

$J$  = moment of inertia of the RUM

$$\frac{u}{J} = \dot{\omega}_R$$

Even this model, however, may not be completely accurate. Coupling between the system dynamics and the RUM dynamics would invalidate previous systems models. A systems approach to modeling should be used in order to account for the possible coupling of the RUM device to the experiment dynamics. Robotics provides a large body of knowledge that may be applicable to the proposed model. The physical makeup of the plant and RUM devices as seen in Figure 10 resembles the make-up of robotic mechanisms. Using a robotics approach will allow for the mechanics of the problem by addressing how individual components of the system interact. Applying well-developed robotic kinematics and kinetics concepts to this problem provides a systematic approach to system modeling. The Lagrange Formulation [10] is an important modeling technique that appears to be applicable. The RUM actuated system is unique in a robotic sense, however, requiring modifications to the Lagrange Formulation.

#### **2.4.2 Control Issues**

The technical study must address several control issues that result from the development of equations of motion for a time varying RUM velocity. Even though

Equation (11) may not be completely accurate, it brings up the following control issues:

1. RUM control actuation is unique in a robotics sense. Robots generally use torques at the base and subsequent joints to generate motion at the end effector. In the RUM actuated system, the actuator is at an end effector equivalent and is used to generate motion about the base (or center of mass). Also, the RUM actuator is relying on centripetal force to generate torques that cause movement at the center of mass of the experiment instead of using directly applied torques.
2. A nonlinear system model and large angular motion require a different control method. Well-developed robotic control methods involving feedback linearization, adaptive control, or nonlinear trajectory control appear to be more appropriate than linear control methods [10,11,12,13].
3. The system displays “periodic controllability” [14]. Periodic controllability is a term used to indicate the periodic nature of the control signal. The RUM device generates the sine and cosine terms in the centripetal and reaction components of Equation (11). These terms have a periodic effect on the “steering” opportunities for each axis.

## 2.5 Conclusions

This chapter presents a brief summary of the RUM development and preliminary research in the area of RUM actuated pointing control. The basic concept employed uses a time varying RUM velocity that produces torques about the center of

mass of the experiment having time varying magnitude and direction. These torques, in turn, effect pointing motion. Experimental testing indicates that pointing control may be possible but considerable research is necessary. The technical study must address several issues to improve pointing performance of the RUM actuated system. Modeling and control issues indicate a systems approach is necessary to account for “periodic controllability” and possible coupling of the RUM device to experiment dynamics. Chapters 3, 4 and 5 treat the modeling issues in detail and Chapter 6 treats the control issues.

## CHAPTER 3

### SYSTEMS APPROACH TO MODELING

The modeling approach presented in References [1] and described in Chapter 2 treats the RUM device as an actuator that operates independent of plant dynamics. The dynamic model developed in Chapter 2 treats the RUM device as strictly a torque producing device. This is a valid approach when the small angle and constant  $\omega$  assumptions are satisfied. A different modeling approach is necessary if these assumptions are not valid, as in a pointing control application. Equations (1) through (7) are developed under the small angle and constant  $\omega$  assumption. Equation (11), developed for time varying  $\omega$ , does not consider large angle motion seen in the experiment or coupling dynamics linking the RUM to the payload (or telescope). A systems-level modeling approach must be used to accurately account for the coupling of the RUM device to the telescope dynamics.

Robotics provides a large body of knowledge that is applicable to the model. The physical makeup of the plant and RUM devices, as seen in Figure 8, resembles the make-up of robotic mechanisms. The robotics approach addresses individual component interaction thus identifying detailed dynamics not found in simpler modeling techniques. Well-developed robotic kinematics and kinetics concepts

provide a systematic approach to system modeling of this problem. This chapter presents an overview of the general modeling approach applying the Lagrange Formulation. It is organized in a 'top-down' manner starting with basic concepts of the Lagrange Formulation including expressions for the kinetic and potential energy. Since these expressions require kinematic calculations, kinematics is presented next. Finally, an outline of the Lagrange Formulation steps is given to summarize the entire process. The formulation results in a dynamical model of the entire manipulator in terms of all joint variables. The equations of motion give the designer physical insight needed to understand the behavior of the overall system. Chapter 4 describes the Lagrange Formulation specifically applied to the RUM actuated system.

### 3.1 Lagrange Formulation - Basic Concepts

The Lagrange formulation [10] is derived from Hamilton's principle, one of the most basic principles of mechanics [15]. The development presented here is based on a robotics application. Figure 14 shows a general system of  $N$  components or links. The variable  $q_i$  at each joint defines the link's motion within its own frame of reference, thus making the  $q_i$ 's independent from each other. The  $q_i$  can be a rotational variable for a **revolute joint** (Joints 1 and 2 of Figure 14) or a translational variable for a **prismatic joint** (as in Joint  $N$  of Figure 14). The motion of link  $i$  affects the motion of links  $i+1$  to  $N$  for an  $N$  link system.

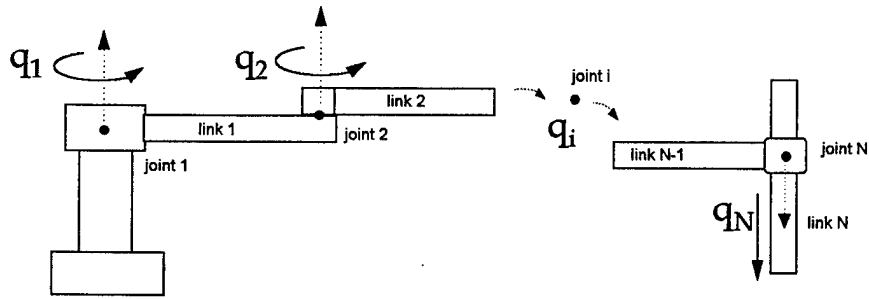


**Figure 14 -  $N$  Link Manipulator**

The Lagrange Formulation provides a systematic approach to dynamic modeling that accounts for the effects of the joint motions on system dynamics. The objective of the Lagrange Formulation is to relate the joint position variable,  $q_i$ , and the joint velocity variable,  $\dot{q}_i$ , to the potential and kinetic energies of the system. The kinetic and potential energies are then used to develop the Lagrange Energy Function which in turn is used to calculate the equations of motion for the entire system. The Lagrange energy function for a system is defined in Equation (12). The variable  $\vec{q}$  is a vector of  $N$  independent variables as previously defined,  $\vec{q}(t) = [q_1(t) \ \cdots \ q_N(t)]^T$ , describing the motion of a manipulator with  $N$  joints.  $K(\bullet)$  and  $P(\bullet)$  are the kinetic energy and potential energy expressions for the manipulator respectively.

$$L(\vec{q}, \dot{\vec{q}}, t) = K(\vec{q}, \dot{\vec{q}}, t) - P(\vec{q}, t) \quad (12)$$

Once the energy function is specified, the equations of motion for the manipulator are obtained through the Euler-Lagrange equation defined in Equation (13).

$$\frac{d}{dt} \left[ \frac{\partial L(\bar{q}, \dot{\bar{q}}, t)}{\partial \dot{q}_i} \right] - \frac{\partial L(\bar{q}, \dot{\bar{q}}, t)}{\partial q_i} = F_i \quad (13)$$

Where:  $i = 1, \dots, N$  and  $F_i$  is the generalized, non-conservative force acting in the direction of the  $q_i$  coordinate (i.e. external forces, frictions, etc.). The general model resulting from the Lagrange Formulation is of the form defined in Equation (14). The first term on the left side of the equation is associated with the manipulator inertia. The second term represents the coriolis and centripetal forces and is associated with the manipulator kinetic energy. The third term signifies the gravity effects and is associated with the potential energy. The term on the right side of Equation (14) specifies the generalized forces acting on each joint. In robotics, this term represents the control input(s) to the system.

$$H(\bar{q})\ddot{\bar{q}} + C(\bar{q}, \dot{\bar{q}})\dot{\bar{q}} + G(\bar{q}) = F \quad (14)$$

Expressions for the kinetic and potential energies as functions of the joint variables,  $\bar{q}$  and  $\dot{\bar{q}}$ , must be developed for each link of the system to use the formulation in Equations (14). The kinetic and potential energy expressions are developed in the next few sections.

### 3.1.1 Potential Energy

Potential energy is a function of the position of the manipulator components therefore it is configuration dependent. The configuration can be described as a function of the joint variables,  $\bar{q}$ , thus making potential energy a function of  $\bar{q}$  as well

[16]. Equation (15) represents the general form of potential energy for the  $i$ th link of the system connected to the  $i-1$  coordinate frame as shown in Figure 15.

$$P_i = m_i g^T \vec{r}_{i-1,ci} \quad (15)$$

where:  $m_i$  = mass of  $i$ th link,  $g$  = gravity vector, and  $\vec{r}_{i-1,ci}$  = position vector for  $i$ th link center of mass in reference to the  $i-1$  coordinate frame.

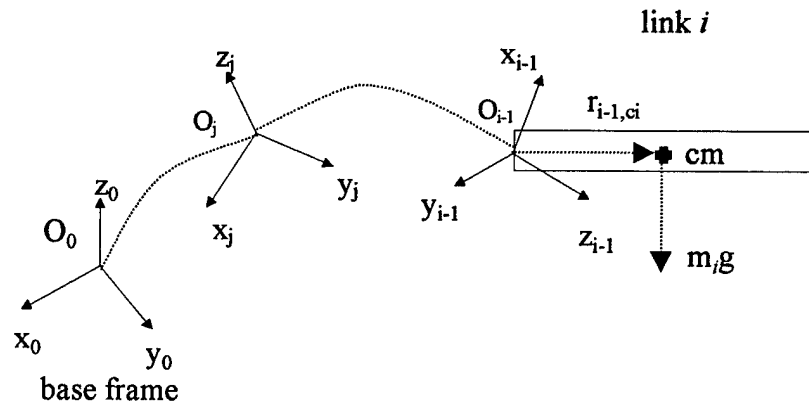


**Figure 15 - Relative Position of Link Center of Mass**

The total potential energy of the system is the sum of the potential energy of each link, since potential energy is a scalar quantity. To accomplish this summation, each term in the summation must be represented in a common reference frame. In robotics, the base coordinate frame is generally used as the common reference and the gravity vector is expressed in that frame. Therefore the position vector,  $\vec{r}_{i-1,ci}$ , must be represented in the base coordinate frame. This involves a homogeneous

transformation which accounts for translation and rotation between coordinate frames based on  $q_i$ , the joint variable. Let  $A_0^{i-1}$  be the homogeneous transformation between frames  $i-1$  and 0, the base frame. Then the total potential energy,  $P$ , can be expressed as in Equation (16).

$$P = \sum_{i=1}^N m_i g^T A_0^{i-1} \vec{r}_{i-1,ci} \quad (16)$$

This concept will be discussed further in the development of kinematic equations in Section 3.2 to follow. In summary, the potential energy is a function of  $\vec{q}$  because the position vector represented in the base frame involves homogeneous transformations that are a function of  $\vec{q}$ .

### 3.1.2 Kinetic Energy

The kinetic energy of each link is developed in a manner similar to that for potential energy. However, the calculations are complicated by the fact that the total kinetic energy is composed of translational and rotational components. Equation (17) represents the kinetic energy for the  $i$ th link of the system. The first term is the translational kinetic energy based on linear velocity vector,  $\vec{v}_{ci}$ , of the center of mass of the link. The second term is the rotational kinetic energy based on the angular velocity vector of the link and the moment of inertia of the link,  $\vec{\omega}_i$  and  $I_i$  respectively.

$$K_i = \frac{1}{2} m_i \vec{v}_{ci}^T \vec{v}_{ci} + \frac{1}{2} \vec{\omega}_i^T I_i \vec{\omega}_i \quad (17)$$

Since kinetic energy is a scalar function, the total kinetic energy of the system is the sum of the kinetic energy of each link provided there is a common frame of reference for the calculations. This requires a mapping function called the manipulator Jacobian that relates the joint velocities,  $\dot{q}_i$ , to linear and angular velocity in base frame coordinates (Figure 16).

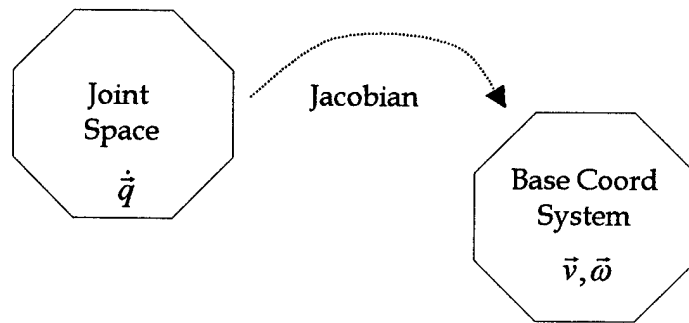


**Figure 16 - Manipulator Jacobian Mapping**

The relationship between the linear velocity,  $\vec{v}_{ci}$ , and joint velocities is described in Equation (18) [16].

$$\vec{v}_{ci} = J_L^i \dot{\vec{q}} \quad (18)$$

where:  $J_L^i$  = the  $3 \times N$  linear velocity Jacobian for the  $i$ th link,

$\dot{\vec{q}}$  = the vector of  $N$  joint velocities for an  $N$  link system.

Similarly, the relationship between the angular velocity,  $\vec{\omega}_i$ , and joint velocities is described by Equation (19).

$$\vec{\omega}_i = J_A^i \dot{\vec{q}} \quad (19)$$

where:  $J_A$  = the  $3 \times N$  angular velocity Jacobian for the  $i$ th link. Since these Jacobians are configuration dependent, they are functions of  $\vec{q}$ . Thus, kinetic energy is generally a function of  $\vec{q}$  and  $\dot{\vec{q}}$ . The calculations for the Jacobians are addressed in Section 3.2.3 to follow. The manipulator Jacobian accounts for the mapping of  $\dot{\vec{q}}$  to  $\vec{v}$  and  $\vec{\omega}$  in the base coordinate frame but does not take into account how these terms are multiplied in Equation (17). The linear terms can be multiplied without reference to any particular frame since the product  $\vec{v}_{ci}^T \vec{v}_{ci}$  is simply the square length of the vector  $\vec{v}_{ci}$ . Transforming  $\vec{v}_{ci}$  into a different reference frame does not change its length, but only rotates it [17]. Therefore, the translational kinetic energy for link  $i$  can be expressed as in Equation (20).

$$\frac{1}{2} m_i \vec{v}_{ci}^T \vec{v}_{ci} = \frac{1}{2} m_i \dot{\vec{q}}^T J_L^{iT} J_L^i \dot{\vec{q}} \quad (20)$$

Similarly, the triple product of  $\vec{\omega}_i^T I_i \vec{\omega}_i$  in the rotational kinetic energy term does not need to be referenced to any particular coordinate frame thus making the summation of the translational kinetic energy and the rotational kinetic energy in Equation (17) possible without regard to any particular reference frame. There is a requirement,

however, that  $\vec{\omega}_i$  and  $I$  be in the same frame in order to calculate the triple product.

In the calculation of  $\vec{\omega}_i$  in Equation (19), multiplying  $\dot{\vec{q}}$  by  $J_A^i$  puts  $\vec{\omega}_i$  into the base coordinate frame. Therefore,  $I_i$  must be expressed in the base frame or  $\vec{\omega}_i$  must be transformed into the same frame in which  $I_i$  is expressed. It is generally simpler to express  $I_i$  in the link coordinate frame. Therefore,  $\vec{\omega}_i$  will be expressed in the link frame as shown in Equation (21).

$$\vec{\omega}_i = (R_0^{i-1})^T J_A^i \dot{\vec{q}} \quad (21)$$

where:  $R_0^{i-1}$  is the rotational transformation from the base frame to the  $i$ th link frame.

Note that  $R_0^{i-1}$  is an orthogonal submatrix of the homogeneous transformation  $A_0^{i-1}$ .

Therefore,  $(R_0^{i-1})^T$  is the inverse of  $R_0^{i-1}$ . Thus, the rotational kinetic energy can be expressed as in Equation (22).

$$\frac{1}{2} \vec{\omega}_i^T I_i \vec{\omega}_i = \frac{1}{2} \dot{\vec{q}}^T J_A^{iT} R_0^{i-1} I_i (R_0^{i-1})^T J_A^i \dot{\vec{q}} \quad (22)$$

It follows from Equations (21) and (22), the total kinetic energy of an  $N$  link system can be expressed as in Equation (23).

$$K = \frac{1}{2} \dot{\vec{q}}^T \left[ \sum_{i=1}^N m_i J_L^{iT} J_L^i + J_A^{iT} R_0^{i-1} I_i (R_0^{i-1})^T J_A^i \right] \dot{\vec{q}} \quad (23)$$

In summary, the kinetic energy requires a mapping between joint space velocity variables,  $\dot{\vec{q}}$ , and the base coordinate frame velocity variables,  $\vec{v}$  and  $\vec{\omega}$  thus

making kinetic energy a function of  $\vec{q}$  and  $\dot{\vec{q}}$  since the Jacobian (mapping function) is a function of  $\vec{q}$ . The next several sections discuss the calculations of the kinematics of a mechanical system. These kinematics are required in order to accomplish the mapping necessary for the potential and kinetic energy calculations.

## 3.2 Kinematics

Kinematics is the branch of mechanics that deals with the motion of rigid bodies without reference to their masses or forces producing the motion [10]. Basically, kinematics defines the geometry of the system, and the coordinate systems chosen determine the mathematical relations developed. The objective of kinematic modeling is to determine the cumulative effects of the entire set of joint variables. Kinematic modeling can be divided into two areas: Position kinematics and velocity kinematics. In each area the goal is to relate knowledge of the manipulator joint variables,  $\vec{q}$  and  $\dot{\vec{q}}$ , to the movement of the entire system. The next several sections describe this relationship.

### 3.2.1 Position Kinematics

Position kinematics involves the representation of points in one reference frame to that of another frame. Figure 17 shows the position vector of point P in reference to different frames. If knowledge about point P is obtained in one frame, position kinematics enables that knowledge to be represented in another frame.

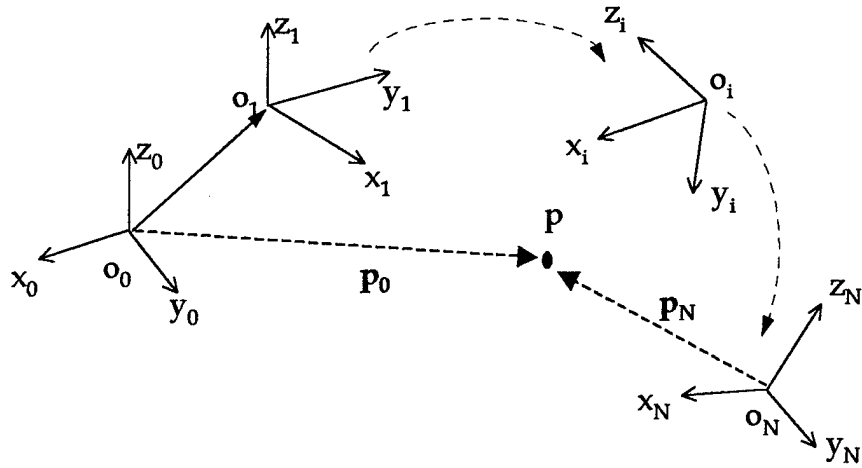


**Figure 17 - Position Representation**

The tool for accomplishing these different representations is called the homogeneous transformation [16]. In general, this transformation accounts for rotations and translations in three dimensional space by using a matrix of the form shown in Equation (24).

$$A_{i-1}^i = \begin{bmatrix} R_{3 \times 3} & d_{3 \times 1} \\ f_{1 \times 3} & s_{1 \times 1} \end{bmatrix} = \begin{bmatrix} \text{rotation submatrix} & \text{translation vector} \\ \text{perspective vector} & \text{scaling vector} \end{bmatrix} \quad (24)$$

This matrix converts the coordinates of a point expressed in the  $i$ th  $(x_i, y_i, z_i)$  coordinate frame to the coordinates of the same point described in the  $i-1$   $(x_{i-1}, y_{i-1}, z_{i-1})$  coordinate system. The translation vector describes the translation between the origins of the  $i-1$  and  $i$ th coordinate systems. The rotation matrix is a  $3 \times 3$  submatrix specifying the rotation of the  $i$ th coordinate system relative to the  $i-1$  coordinate system. The scaling factor can be used to adjust the desired scale for the components of the translation

vector but is generally specified as 1 for robotics applications. The perspective vector may be applied to determine the position (size) of an object image using the focal length of a camera for optical sensing but will be zero in this robotics application. The components in this matrix are functions of the joint variable  $\vec{q}$  and the manipulator configuration. Therefore, in order to represent point P (in Figure 17) in terms of reference frame 0 given its position vector in reference frame  $N$ , the following transformations must be used.

$$\begin{aligned} \begin{bmatrix} P_0 \\ 1 \end{bmatrix} &= A_0^1 A_1^2 \dots A_{N-1}^N \begin{bmatrix} P_N \\ 1 \end{bmatrix} \\ &= A_0^N \begin{bmatrix} P_N \\ 1 \end{bmatrix} \end{aligned} \quad (25)$$

Note that the position vectors must be augmented by 1 to account for the translational part of the transformation. If the transformation is purely rotational, then  $A_{i-1}^i$  simplifies to Equation (26). A short hand notation given for Equation (26) is  $Rot_{axis,angle}$  which specifies the axis and angle of rotation.

$$A_{i-1}^i = \begin{bmatrix} R_{3 \times 3} & 0 \\ 0 & 1 \end{bmatrix} \quad (26)$$

If the transformation is purely translational, then  $A_{i-1}^i$  simplifies to Equation (27). A short hand notation given for Equation (27) is  $Trans_{axis,distance}$  which specifies the axis and distance of translation.

$$A_{i-1}^i = \begin{bmatrix} I_{3 \times 3} & d_{3 \times 1} \\ 0 & 0 \end{bmatrix} \quad (27)$$

Different combinations of these two simple forms can result in the representation of transformations between any two reference frames. For example, point P in Figure 18 can be represented in two reference frames. The frames are separated by a distance -a along the  $x_0$  axis and the rotation  $\theta$  about the  $z_0$  axis.  $\theta$  is measured from the  $x_0$  axis to the projection of the  $x_1$  axis into the  $0^{th}$  frame.

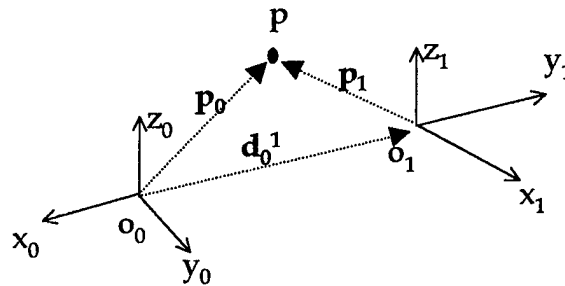


**Figure 18 - Example Transformation**

Letting  $R_0^1$  be the rotation submatrix of  $A_0^1$ , the problem can be broken down into a simple rotation and a simple translation as shown in Equation (28).

$$\begin{aligned}
 P_0 &= R_0^1 P_1 + d_0^1 & (28) \\
 \begin{bmatrix} P_0 \\ 1 \end{bmatrix} &= Rot_{z,\theta} Trans_{x,a} \begin{bmatrix} P_1 \\ 1 \end{bmatrix} = \begin{bmatrix} \cos\theta & -\sin\theta & 0 & -a \\ \sin\theta & \cos\theta & 0 & 0 \\ 0 & 0 & 1 & 0 \\ 0 & 0 & 0 & 1 \end{bmatrix} \begin{bmatrix} P_1 \\ 1 \end{bmatrix} \\
 &= A_0^1 \begin{bmatrix} P_1 \\ 1 \end{bmatrix}
 \end{aligned}$$

Multiplying the rotation and translation matrices results in the homogeneous transformation,  $A_0^1$ , between frames 0 and 1. This approach allows for a large amount of flexibility in determining transformations between reference frames. A more systematic approach is the Denavit-Hartenberg (DH) convention addressed in the next section.

### 3.2.2 Denavit- Hartenberg (DH) Convention

The DH convention is a systematic approach that uses the minimum number of parameters to describe kinematic relationships by restricting the types of rotations and translations allowed [10]. Rotations and translations are only allowed about or along the x and/or z axis. The joint variable,  $q_i$ , is also restricted to a single variable per joint always about or along the z axis defined for that reference frame. The joint variable is further restricted to be either a single translational variable or a single rotational variable but not both. Applying the DH convention to the homogeneous transformation results in an  $A_{i-1}^i$  matrix defined in Equation (29).

$$A_{i-1}^i = Rot_{z,\theta_i} Trans_{z,d_i} Trans_{x,a_i} Rot_{x,\alpha_i} \quad (29)$$

where[10]:

$\theta_i$  = angle of rotation about the positive  $z_{i-1}$  axis measured from the positive  $x_{i-1}$  axis to the positive  $x_i$  axis (or its parallel projection) where the positive direction is counterclockwise (joint variable for a revolute joint),

$d_i$  = offset distance measured along the  $z_{i-1}$  axis from the origin of the  $i-1$  frame to the intersection of the  $z_{i-1}$  axis and the  $x_i$  axis (joint variable for a prismatic joint),

$a_i$  = link length measured along the  $x_i$  axis from the origin of the  $i^{th}$  frame to the to the intersection of the  $z_{i-1}$  axis and the  $x_i$  axis (constant),

$\alpha_i$  = twist angle between two joint axes measured about the positive  $x_i$  axis from the positive  $z_{i-1}$  axis (or its parallel projection) to the positive  $z_i$  axis where the positive direction is counterclockwise (constant).

Figure 19 shows an example of applying the DH convention to a simple manipulator. Table 1 lists the parameters for each joint of the system. Note that the ( )<sup>\*</sup> signifies the joint variable,  $q_i$ , and that the joints are numbered starting with 1 at reference frame 0.

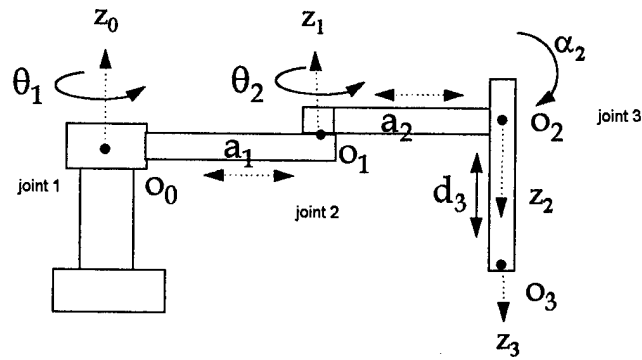


Figure 19 - DH Convention Example

Joint	$a_i$	$\alpha_i$	$d_i$	$\theta_i$
1	$a_1$	0	0	$\theta_1^*$
2	$a_2$	$180^\circ$	0	$\theta_2^*$
3	0	0	$d_3^*$	0

Table 1 - Joint Parameters

The general form of the homogeneous transformation incorporating the DH convention is shown in Equation (30).

$$A_{i-1}^i = \begin{bmatrix} \cos \theta_i & -\sin \theta_i \cos \alpha_i & \sin \theta_i \sin \alpha_i & a_i \cos \theta_i \\ \sin \theta_i & \cos \theta_i \cos \alpha_i & -\cos \theta_i \sin \alpha_i & a_i \sin \theta_i \\ 0 & \sin \alpha_i & \cos \alpha_i & d_i \\ 0 & 0 & 0 & 1 \end{bmatrix} \quad (30)$$

There are several advantages to using the DH convention in the development of kinematic relationships. It provides a systematic approach to defining these relationships with only 4 parameters. It also makes the manipulator Jacobian calculations simpler since the joint variable,  $q_i$ , is always defined with reference to the z axis in the local frame. There are some disadvantages, however, to using the DH convention. The main drawback is that a “dummy link” or “dummy joint” may have to be incorporated to abide by the restrictions placed on the homogeneous transformation. In the RUM actuated system development presented in the next chapter, a “dummy link” and 2 “dummy joints” are required in order to apply the DH convention to this system.

### 3.2.3 Velocity Kinematics

Velocity kinematics involves the development of the manipulator Jacobian discussed in Section Kinetic Energy which relates the joint velocities,  $\dot{\vec{q}}$ , to linear and angular velocities in the base coordinate frame. The following development assumes the DH convention is used to set up the kinematic relationships.

#### 3.2.3.1 Angular Velocity Jacobian

The angular velocity of link  $j$  attached to the **revolute joint**  $j$  is the vector  $\vec{\omega}_j = \vec{z}_{j-1}\dot{q}_j$  as shown in Figure 20. If the angular velocity of link  $j$  is written in the base coordinate frame, it can simply be added to angular velocities from other revolute joints when they are also written in the base frame.

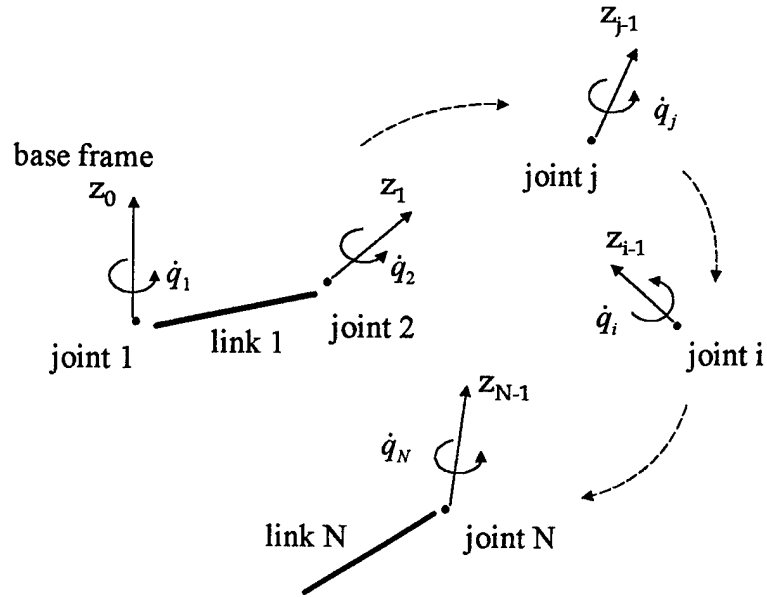


**Figure 20 Angular Velocity Vectors for Revolute Joints**

A **prismatic joint** adds no angular velocity to the system. Therefore, the total angular velocity of the  $i$ th link, in reference to the base frame, is the sum of all the angular velocities contributed by the 1 to  $i$  revolute joints. Joints  $i+1$  to  $N$  do not contribute to the angular velocity of the  $i$ th link. Equation (31) demonstrates this vector addition.

$$\begin{aligned}
 \vec{\omega}_i^{tot} &= \vec{\omega}_1 + \vec{\omega}_2 + \cdots + \vec{\omega}_j + \cdots + \vec{\omega}_i \\
 &= \vec{b}_0 \dot{q}_1 + \vec{b}_1 \dot{q}_2 + \cdots + \vec{b}_{j-1} \dot{q}_j + \cdots + \vec{b}_{i-1} \dot{q}_i \\
 &= J_{A1}^i \dot{q}_1 + J_{A2}^i \dot{q}_2 + \cdots + J_{Aj}^i \dot{q}_j + \cdots + J_{Ai}^i \dot{q}_i \\
 &= J_A^i \vec{\dot{q}}
 \end{aligned} \tag{31}$$

where:  $\vec{b}_{j-1} = R_0^{j-1} \vec{z}_{j-1}$ , the representation of  $\vec{z}_{j-1}$  in the base frame

$J_A^i$  = the angular velocity Jacobian for the  $i^{\text{th}}$  link.

Therefore, the  $j$ th component of the angular velocity Jacobian for the  $j$ th joint is simply  $\vec{b}_{j-1}$  for a revolute joint and zero for a prismatic joint. Equation (32) summarizes the construction of the angular velocity Jacobian,  $J_A^i$ , for the  $i$ th link.

$$J_A^i = [J_{A1}^i \quad \cdots \quad J_{Aj}^i \quad \cdots \quad J_{Ai}^i \quad 0 \quad \cdots \quad 0] \quad (32)$$

$$\text{where: } J_{Aj}^i = \begin{cases} \vec{b}_{j-1} & \text{for a revolute joint} \\ 0 & \text{for a prismatic joint} \end{cases}$$

### 3.2.3.2 Linear Velocity Jacobian

Similarly, the linear velocity of the center of mass of link  $j$  attached to the **prismatic joint**  $j$  is the vector  $\vec{v}_{cj} = \vec{z}_{j-1}\dot{q}_j$  as shown in Figure 21. If the linear velocity of link  $j$  is written in the base coordinate frame, it can simply be added to linear velocities from other prismatic joints when they are also written in the base frame. Therefore, the  $j$ th component of the linear velocity Jacobian for the  $j$ th prismatic joint is  $\vec{b}_{j-1}$ , the representation of  $\vec{z}_{j-1}$  in the base frame.

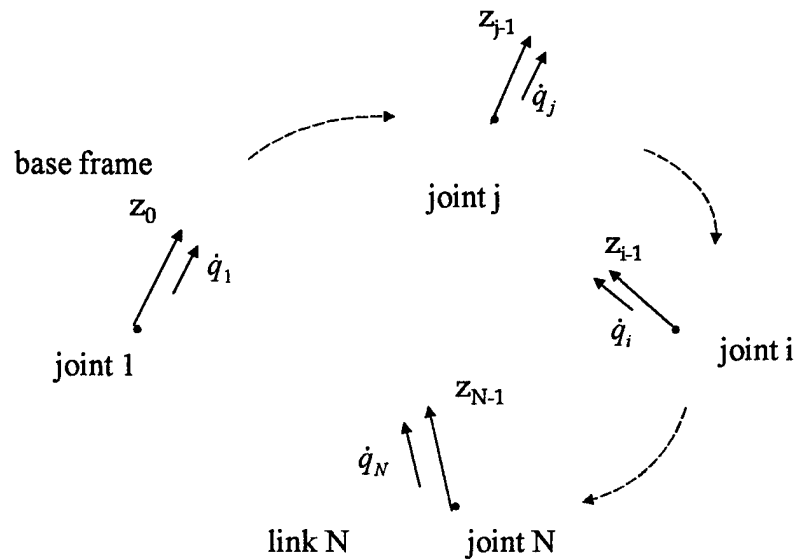


**Figure 21 - Linear Velocity Vectors for Prismatic Joints**

The development of the linear velocity Jacobian for a **revolute joint** is more complicated, however, since a revolute joint contributes a linear velocity term that is tangential to the motion of the link. Figure 22 shows the linear velocity contribution of revolute joint  $j$  to the center of mass of link  $i$ .

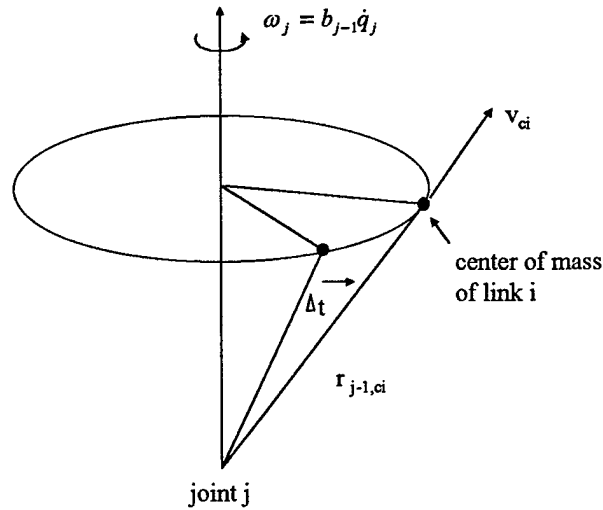


**Figure 22 - Linear Velocity Vector for Revolute Joints**

The velocity vector of the center of mass of link  $i$  can be written as in Equation (33).

$$\vec{v}_{ci} = \vec{\omega}_j \times \vec{r}_{j-1,ci} \quad (33)$$

Where:  $\vec{r}_{j-1,ci}$  is the position vector from the  $j$ th joint to the center of mass of the  $i$ th link. Once this velocity vector is written in terms of the joint variable and the base coordinate frame, it can also be added to other linear velocity terms. This requires that  $\vec{\omega}_j$  and  $\vec{r}_{j-1,ci}$  be written in terms of the base frame. The angular velocity vector is equal to  $\vec{\omega}_j = \vec{b}_{j-1} \dot{q}_j$  as presented previously. To represent the position vector,  $\vec{r}_{j-1,ci}$ , in the base coordinate frame requires vector addition as shown in Figure 23.

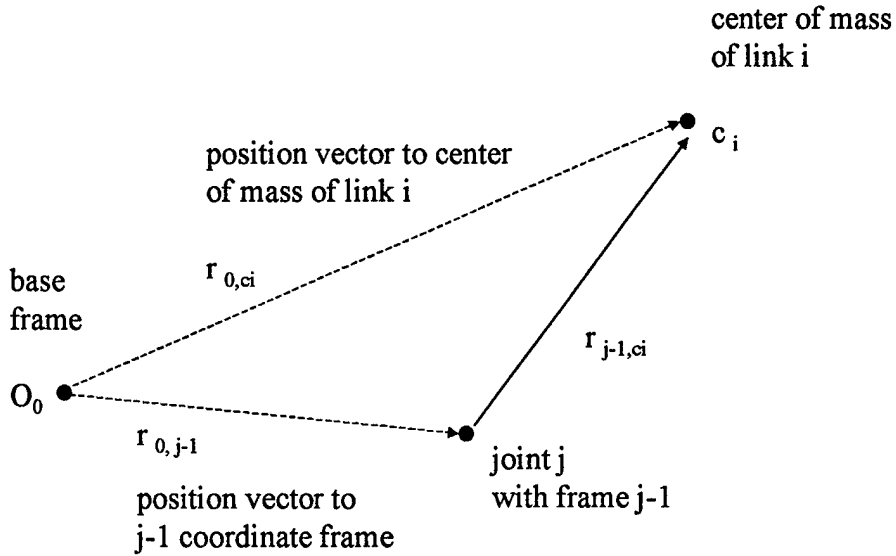


**Figure 23 - Position Vector Representation**

Since  $\vec{r}_{o,ci}$  and  $\vec{r}_{o,j-1}$  can be represented in the base frame by using the homogeneous transformations developed for the system,  $\vec{r}_{j-1,ci}$  is represented in the base frame by their vector subtraction as seen in Equation (34).

$$\vec{r}_{o,ci} - \vec{r}_{o,j-1} = \vec{r}_{j-1,ci} \quad (34)$$

Where  $\vec{r}_{o,ci}$  and  $\vec{r}_{o,j-1}$  are represented in the base coordinate frame. Therefore, the  $i$ th link's linear velocity contribution from the  $j$ th revolute joint is represented in Equation (35).

$$\begin{aligned} \vec{v}_{ci} &= \vec{\omega}_j \times \vec{r}_{j-1,ci} \\ &= (\vec{b}_{j-1} \dot{q}_j) \times (\vec{r}_{o,ci} - \vec{r}_{o,j-1}) \\ &= (\vec{b}_{j-1} \times (\vec{r}_{o,ci} - \vec{r}_{o,j-1})) \dot{q}_j \end{aligned} \quad (35)$$

The total linear velocity of the  $i$ th link, in reference to the base frame, is the sum of all the linear velocities contributed by the 1 to  $i$  prismatic and revolute joints. Joints  $i+1$  to  $N$  do not contribute to the linear velocity of the  $i$ th link. Equation (36) demonstrates this vector addition.

$$\begin{aligned}
 \vec{v}_{ci}^{tot} &= \vec{v}_{c1} + \vec{v}_{c2} + \cdots + \vec{v}_{cj} + \cdots + \vec{v}_{ci} \\
 &= J_{L1}^i \dot{q}_1 + J_{L2}^i \dot{q}_2 + \cdots + J_{Lj}^i \dot{q}_j + \cdots + J_{Li}^i \dot{q}_i \\
 &= J_L^i \dot{\vec{q}}
 \end{aligned} \tag{36}$$

Where  $J_L^i$  is the linear velocity Jacobian for the  $i$ th link. Equation (37) summarizes the construction of the linear velocity Jacobian for the  $i$ th link.

$$J_L^i = [J_{L1}^i \quad \cdots \quad J_{Lj}^i \quad \cdots \quad J_{Li}^i \quad 0 \quad \cdots \quad 0] \tag{37}$$

$$\text{Where : } J_{Lj}^i = \begin{cases} \vec{b}_{j-1} \times (\vec{r}_{0,ci} - \vec{r}_{o,j-1}) & \text{for a revolute joint} \\ \vec{b}_{j-1} & \text{for a prismatic joint} \end{cases}$$

### 3.3 Summary of Lagrange Formulation Steps

In summary, the Lagrange Formulation results in the dynamic equations of motion for mechanical systems. The process involves several steps in determining the relationships between joint variables and kinetic and potential energy. This

information is then used to calculate the Euler-Lagrange equations of motion. This section provides a brief outline of the steps to the Lagrange formulation using the DH convention.

Step 1. Assign a coordinate frame to each joint of the manipulator.

- Use the DH convention when it is appropriate.

Step 2. Define coordinate frame parameters for each joint:  $a_i$ ,  $\alpha_i$ ,  $d_i$ ,  $\theta_i$ .

Step 3. Determine the homogeneous transformations between each coordinate frame using Equation (3.19) repeated here.

$$A_{i-1}^i = \begin{bmatrix} \cos \theta_i & -\sin \theta_i \cos \alpha_i & \sin \theta_i \sin \alpha_i & a_i \cos \theta_i \\ \sin \theta_i & \cos \theta_i \cos \alpha_i & -\cos \theta_i \sin \alpha_i & a_i \sin \theta_i \\ 0 & \sin \alpha_i & \cos \alpha_i & d_i \\ 0 & 0 & 0 & 1 \end{bmatrix}$$

Step 4. Determine the position kinematic equations relating each link of the manipulator to the base coordinate frame.

Step 5. Determine the velocity kinematics.

- Requires calculation of the Manipulator Jacobian for each link using Equations (32) and (37) repeated here.

$$J_A^i = [J_{A1}^i \quad \cdots \quad J_{Aj}^i \quad \cdots \quad J_{Ai}^i \quad 0 \quad \cdots \quad 0]$$

$$J_{Aj}^i = \begin{cases} \vec{b}_{j-1} & \text{for a revolute joint} \\ 0 & \text{for a prismatic joint} \end{cases}$$

$$J_L^i = [J_{L1}^i \quad \cdots \quad J_{Lj}^i \quad \cdots \quad J_{Li}^i \quad 0 \quad \cdots \quad 0]$$

$$J_{Lj}^i = \begin{cases} \vec{b}_{j-1} \times (\vec{r}_{0,ci} - \vec{r}_{o,j-1}) & \text{for a revolute joint} \\ \vec{b}_{j-1} & \text{for a prismatic joint} \end{cases}$$

- Use Manipulator Jacobian to calculate linear and angular velocities from joint velocities using Equations (31) and (35) repeated here.

$$\vec{\omega}_i = J_A^i \dot{\vec{q}}$$

$$\vec{v}_{ci} = J_L^i \dot{\vec{q}}$$

- Step 6. Calculate the potential energy for each link with reference to the base coordinate frame using Equation (16) repeated here.

$$P = \sum_{i=1}^N m_i g^T A_0^{i-1} \vec{r}_{i-1,ci}$$

Note that  $r_i$  will have to be augmented by 1 when multiplying by  $A_0^i$  to account for the translational part of the homogeneous transformation.

- Requires calculation of the position vector of the center of mass of each link relative to the base coordinate frame using the kinematic equations from step 4.

- Step 7. Calculate the kinetic energy for each link with reference to the base coordinate frame using Equation (23) repeated here.

$$K = \frac{1}{2} \dot{\vec{q}}^T \left[ \sum_{i=1}^N m_i J_L^{iT} J_L^i + J_A^T R_0^{i-1} I_i (R_0^{i-1})^T J_A^i \right] \dot{\vec{q}}$$

- Step 8. Calculate the Lagrangian energy function,  $L(\vec{q}, \dot{\vec{q}}, t)$ , by subtracting potential energy from kinetic energy.
- Step 9. Calculate the equations of motion for the manipulator through the Euler-Lagrange equation defined in Equation (13) repeated here.

$$\frac{d}{dt} \left[ \frac{\partial L(\vec{q}, \dot{\vec{q}}, t)}{\partial \dot{q}_i} \right] - \frac{\partial L(\vec{q}, \dot{\vec{q}}, t)}{\partial q_i} = F_i$$

## CHAPTER 4

### RUM-ACTUATED SYSTEM MODELING

There are several benefits to applying Chapter 3 concepts to modeling the RUM actuated system. It is a systematic approach to modeling complex systems and it produces a complete dynamic model. Applying the Denavit-Hartenburg coordinate convention and the Lagrange Formulation to standard robotic manipulators is generally straightforward since robots are designed specifically and efficiently to perform certain tasks. There are certain drawbacks, however, to directly applying this formulation to the RUM actuated system. The RUM system is unique in a robotics sense since it is not an efficient use of joints or links and is under-actuated, having only the RUM torque motors for actuation. It would take six links and joints (some dummy) to represent this system that only has three degrees of freedom. Certain physical properties of the RUM system can be used to reduce the system order and complexity if taken into account during the modeling process. Therefore, in order to benefit from the systematic, detailed aspects of the Lagrange Formulation without unduly complicating the model, special insight and some modifications are required. All RUM actuated systems will require similar modifications and considerations when applying the Lagrange Formulation. The modifications are divided up into two

groups: Kinematic modifications and dynamic modifications. The development of the RUM actuated system equations of motion using these modifications is presented in this chapter.

## **4.1 Kinematic Modifications**

Recall that the objective of kinematic modeling is to determine the cumulative effects of the entire set of joint variables. The next several sections will discuss physical properties of the RUM system along with modeling assumptions, position kinematic modifications and velocity kinematic modifications used to reduce model order and complexity.

### **4.1.1 Modeling Assumptions and System Properties**

Three modeling assumptions are made during the development of the equations of motion. The first assumption is that no rotational motion about the line of sight axis is possible. This is a valid assumption for the test configuration described in Chapter 2 since the gimbal mount only allows cross-elevation and elevation axes motion. The second assumption is that the RUM mass arms are controlled to maintain the  $180^\circ$  spatial displacement. Note that the masses are not physically held in these positions by hardware but must be controlled to maintain this displacement. This property allows a model reduction since the RUMs can be treated as a single actuator. The last assumption, that the mass of the RUM link may be treated as a 'point mass' located at the center of mass of that link, is a valid assumption since the mass of the

RUM is much larger than the mass of the rod attaching the RUM to the telescope and the center of mass of the RUM link is located near the end of the link arm. This assumption also allows for a simplified model as discussed in Section 4.1.3 to follow.

#### **4.1.2 Position Kinematic Modifications**

Position kinematics must be used to properly model the RUM positions, regardless of the modeling approach used. Certain considerations in position kinematics, however, will simplify the velocity kinematics and system dynamics developed in Sections 4.1.3 and 4.2 respectively. Figure 24 shows the RUM actuated system diagram. Since the circular scan RUMs are the only actuators used in this model development, the elevation and cross-elevation torque motors have been removed, as well as the linear scan RUMs. The joint variables are identified with  $\theta_i$  as indicated.

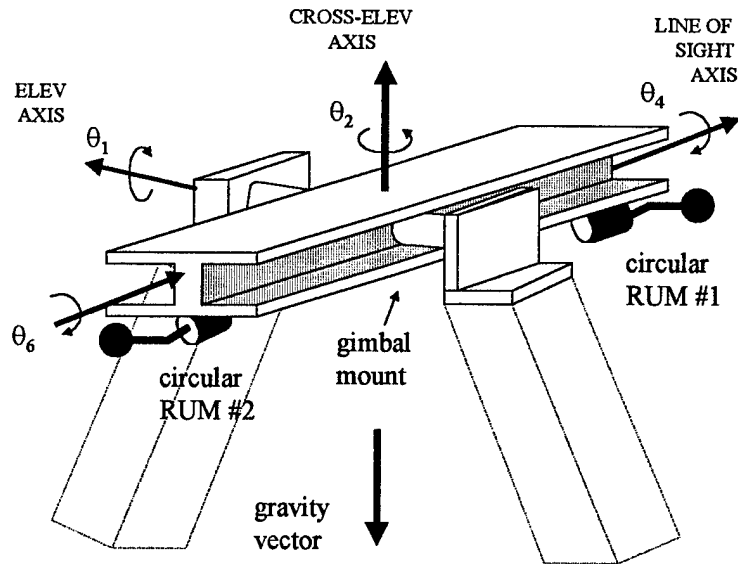


**Figure 24 - RUM Actuated System Diagram**

There is a 2-degree-of-freedom gimbal joint at the center mount of the beam (or telescope). Since the DH convention is used, this joint will be modeled with two distinct coordinate frames with origins separated by a distance of zero. The telescope body can be modeled in several ways. Each method results in the same equations of motion but requires different calculations for the velocity kinematics. The telescope is treated as a single link to simplify the velocity kinematics in Section 4.1.3. However, several dummy frames and joints must be included in the model to ensure the proper configuration of the RUM system and to account for the geometry of the system. Figure 25 shows the coordinate frames used to model the RUM system. Reference frame 0 signifies the elevation axis motion while reference frame 1 signifies the cross-elevation axis motion. The DH convention also requires that a “dummy” link and

joint be used between reference frames 1 and 2. Reference frames 3 and 5 signify the attachment points of the RUM actuator. Reference frames 4 and 6 are attached to the end of the RUM mass and are required to determine the relative displacement of the RUM mass from the other reference frames.

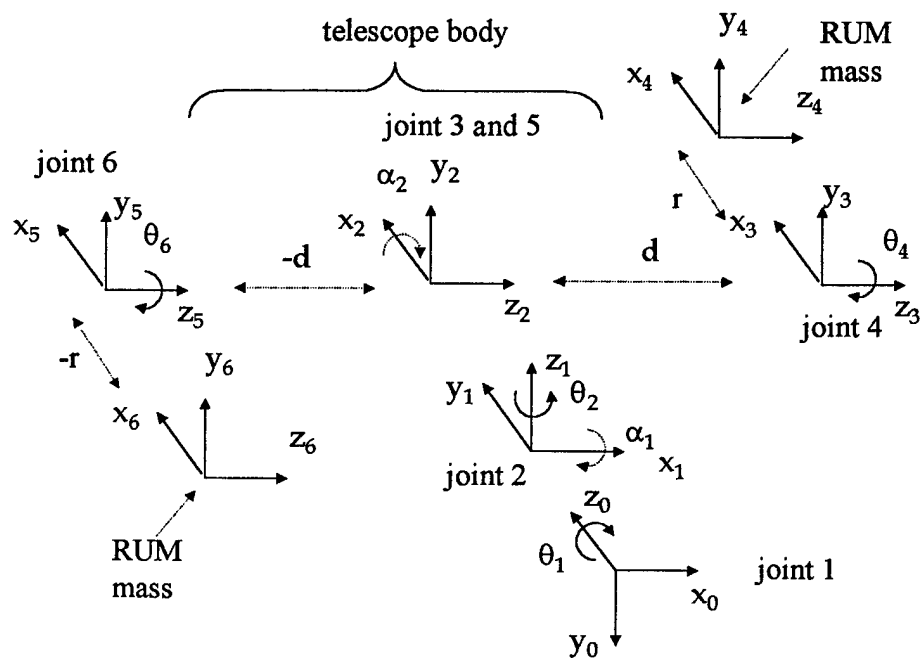


**Figure 25 - RUM System Coordinate Frames (DH Convention)**

Table 2 defines the joint parameters for the RUM actuated system. In order to maintain the correct telescope orientation,  $90^\circ$  must be added to the  $\theta_2$  variable. The parameters defined by  $( )^*$  are the joint variables,  $q_i$ . To ensure that the RUMs are kept at the  $180^\circ$  spatial displacement,  $'-r'$  is used in the  $6^{th}$  joint parameter and the

RUM rotation variables,  $\theta_6$  and  $\theta_4$ , will be set equal to each other in the dynamic modifications in Section 4.2. This modification simplifies the calculations and enables a reduction of the system order later in the development. Note that joints 3 and 5 have all constant parameters. These are required for kinematic ‘bookkeeping’ to ensure compliance with the DH convention and the proper orientation of the telescope and RUMs. Although the position kinematics are complicated because of two ‘dummy’ joints, the velocity kinematics can be simplified since the constant parameters do not add dynamics to the system model.

Joint	$a_i$	$\alpha_i$	$d_i$	$\theta_i$
1	0	$+90^\circ$	0	$\theta_1^*$
2	0	$+90^\circ$	0	$\theta_2^* + 90^\circ$
3	0	0	d	0
4	r	0	0	$\theta_4^*$
5	0	0	-d	0
6	-r	0	0	$\theta_6^*$

**Table 2 - RUM System Joint Parameters**

#### 4.1.2.1 Homogeneous Transformation Modifications

The RUM system is unique in terms of robotic homogeneous transformations. Normally, a kinematic chain of equations relates the  $N^{\text{th}}$  link to the base coordinate

frame by passing through all the other links. However, a RUM link (or arm) is attached to each end of the telescope requiring distinctly different kinematic chains. Therefore, the homogeneous transformations and the kinematic equations go from the base frame 0 out to frame 4 for the first RUM. For the second RUM, the transformations and equations go from the base frame 0 through frames 1 and 2 again, and then to frames 5 and 6. MapleV<sup>tm</sup>, a symbolic computation program, was used to facilitate these calculations. Appendix A provides detailed results of the homogeneous transformations. The kinematic equations for the first and second RUMs are shown in Equations (38) and (39) respectively.

$$A_0^4 = A_0^1 A_1^2 A_2^3 A_3^4 \quad (38)$$

$$A_0^6 = A_0^1 A_1^2 A_2^5 A_5^6 \quad (39)$$

#### 4.1.2.2 Potential Energy Simplification

Since the system is gimbaled at the center of mass of the telescope, the potential energy of one half of the telescope is equal and opposite to the other half of the telescope when calculated in terms of the base coordinate frame. Therefore, the potential energy of the entire telescope is equal to zero since the two halves cancel each other when added. If the 180° spatial displacement is maintained between the masses of the RUM arms, their potential energy will be equal and opposite as well thus resulting in a zero potential energy. Therefore, assuming a 180° RUM spatial displacement, the total potential energy of the entire system is zero.

### 4.1.3 Velocity Kinematic Modifications

The physical properties analyzed in the previous sections facilitate the development of velocity kinematics. The different links of the RUM actuated system contribute different components to the kinetic energy. Each link can contribute a linear velocity term, an angular velocity term or both as shown in Equation (40) repeated here from Chapter 3.

$$K = \frac{1}{2} \dot{\mathbf{q}}^T \left[ \sum_{i=1}^N m_i J_L^{iT} J_L^i + J_A^{iT} R_i I_i R_i^T J_A^i \right] \dot{\mathbf{q}} \quad (40)$$

$\uparrow$   
 linear velocity  
 terms

$\uparrow$   
 angular velocity  
 terms

These terms are based on the mass of each link, the inertia about the center of mass of each link, and the velocity of the center of mass of each link. Figure 26 shows the five links of the RUM actuated system and RUM and telescope centers of mass necessary for analysis.

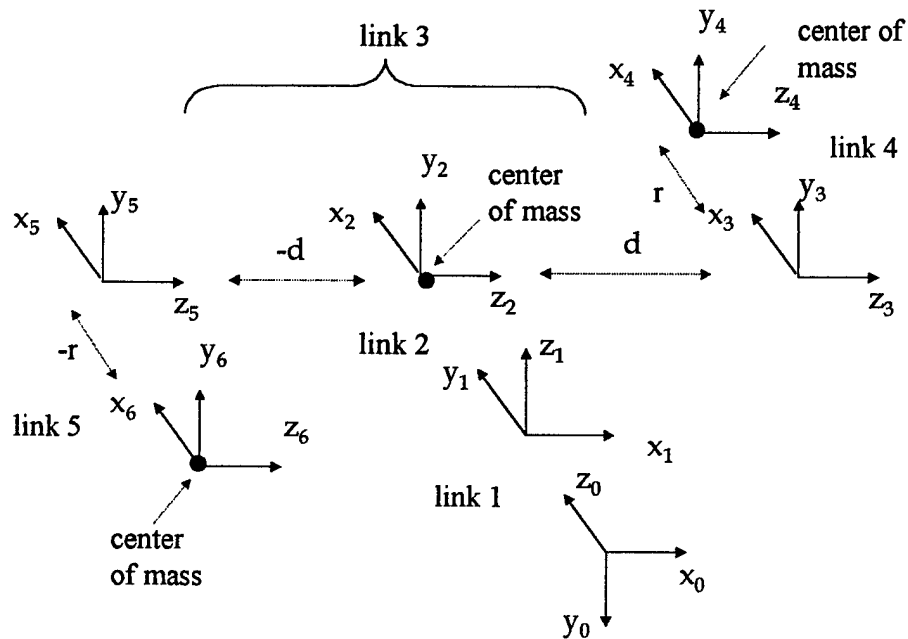


**Figure 26 - Links of the RUM Actuated System**

Links 1 and 2 have zero kinetic energy since there is no mass or inertia in either link. The mass and inertia of the telescope is contained entirely in link 3. Modeling the telescope as a single link simplifies the kinetic energy calculation for link 3 since it rotates about its center of mass. This motion produces only rotational kinetic energy since the link rotates about its center of mass and the center of mass does not translate. Modeling links 4 and 5, the RUM arms, as point masses further reduces the complexity of the velocity kinematics. Even though the RUM arms are rotating, they contribute only a linear velocity term to the kinetic energy. This is due to the fact that for a point mass model, there is no inertia about the center of mass and the rotation

occurs about a point other than the center of mass. These modifications result in a total kinetic energy consisting of only three terms as described in Equation (41).

$$\mathbf{K}_{\text{Total}} = \mathbf{K}_{3,\text{Rotational}} + \mathbf{K}_{4,\text{Translational}} + \mathbf{K}_{5,\text{Translational}} \quad (41)$$

There is one drawback, however, to these modifications. The notation used in Chapter 3 is no longer valid and considerable care must be taken when calculating the manipulator Jacobians. A systematic approach must still be used since there are intricate kinematics involved primarily because of the complexity of the RUM motion in reference to the base frame. Appendix B shows detailed calculations for the RUM system Jacobians.

## 4.2 Dynamic Modifications

The kinematic modifications made in the previous sections reduce the complexity of calculating the system's kinetic energy and allow further reductions of the dynamic model presented in this section. Although the specific notation used in Chapter 3 is no longer useful because of the modifications necessary for modeling the RUM system, the basic concepts are still valid. The Lagrange energy function,  $L(\vec{q}, \dot{\vec{q}}, t)$ , requires the calculation of only three kinetic energy terms since potential energy is zero. Applying the Euler-Lagrange equation discussed in Chapter 3, (repeated here in Equation (42) below), will result in the desired equations of motion but in a very unstructured form.

$$\frac{d}{dt} \left[ \frac{\partial L(\bar{q}, \dot{\bar{q}}, t)}{\partial \dot{q}_i} \right] - \frac{\partial L(\bar{q}, \dot{\bar{q}}, t)}{\partial q_i} = F_i \quad (42)$$

The results of Equation (42), require significant manipulation to separate the sixteen inertia terms and sixteen coriolis/centripetal terms into a form similar to Equation (43) (repeated from Chapter 3). Note there are no gravitational terms in the RUM system, since potential energies cancel.

$$\begin{array}{ccc} H(\bar{q})\ddot{\bar{q}} & + C(\bar{q}, \dot{\bar{q}})\dot{\bar{q}} & + G(\bar{q}) = F \\ \uparrow & \uparrow & \uparrow \\ \text{inertia} & \text{coriolis/} & \text{gravity} \\ \text{term} & \text{centripetal} & \text{term} \\ & \text{term} & \end{array} \quad (43)$$

The form presented in Equation (43) is desirable since it provides considerable insight into model validation and controllability (discussed in Chapters 5 and 6). A more systematic and algorithmic approach, presented by Spong and Asada [17,16], takes advantage of the relationship between the kinetic energy coefficients, the inertia terms, and the coriolis / centripetal terms. Recalling that the Jacobians,  $J$ , and the rotation matrices,  $R$ , are functions of the joint variables,  $q_i$ , Equation (44) shows the relationship between the kinetic energy coefficients and the inertia matrix,  $H(\bar{q})$ .

$$\begin{aligned}
K &= \frac{1}{2} \dot{\vec{q}}^T \left[ \overbrace{\sum_{i=1}^N m_i J_L^{iT} J_L^i + J_A^{iT} R_i I_i R_i^T J_A^i}^{\text{coefficient matrix}} \right] \dot{\vec{q}} \\
&= \frac{1}{2} \dot{\vec{q}}^T H(\vec{q}) \dot{\vec{q}} \\
&= \frac{1}{2} \sum_{i=1}^N \sum_{j=1}^N h_{i,j}(\vec{q}) \dot{q}_i \dot{q}_j
\end{aligned} \tag{44}$$

where:  $h_{i,j}(\vec{q})$  is the (i,j) component of  $H(\vec{q})$ . There are four independent joint variables,  $q_1$  through  $q_4$ , corresponding to  $\theta_1$ ,  $\theta_2$ ,  $\theta_4$ , and  $\theta_6$  for the RUM system. Therefore, the Jacobians,  $J_L^i$  and  $J_A^i$ , are  $3 \times 4$  matrices, resulting in a  $4 \times 4$  coefficient matrix for the kinetic energy equal to the  $H(\vec{q})$  matrix. Equation (45) shows a further relationship between the inertia matrix,  $H(\vec{q})$ , and the coriolis / centripetal matrix,  $C(\vec{q}, \dot{\vec{q}})$ . [17]

$$c_{k,j} = \sum_{i=1}^N \frac{1}{2} \left\{ \frac{\partial h_{k,j}}{\partial q_i} + \frac{\partial h_{k,i}}{\partial q_j} - \frac{\partial h_{i,j}}{\partial q_k} \right\} \dot{q}_i \tag{45}$$

where:  $c_{k,j}$  is the (k,j) component of the  $C(\vec{q}, \dot{\vec{q}})$  matrix, which is also a  $4 \times 4$  matrix for the RUM system. These calculations result in the system of equations in the form of Equation (46) below. Detailed values are given in Appendix C.

$$\begin{bmatrix} h_{11} & h_{12} & h_{13} & h_{14} \\ h_{21} & h_{22} & h_{23} & h_{24} \\ h_{31} & h_{32} & h_{33} & 0 \\ h_{41} & h_{42} & 0 & h_{44} \end{bmatrix} \begin{bmatrix} \ddot{q}_1 \\ \ddot{q}_2 \\ \ddot{q}_3 \\ \ddot{q}_4 \end{bmatrix} + \begin{bmatrix} c_{11} & c_{12} & c_{13} & c_{14} \\ c_{21} & c_{22} & c_{23} & c_{24} \\ c_{31} & c_{32} & 0 & 0 \\ c_{41} & c_{42} & 0 & 0 \end{bmatrix} \begin{bmatrix} \dot{q}_1 \\ \dot{q}_2 \\ \dot{q}_3 \\ \dot{q}_4 \end{bmatrix} = \begin{bmatrix} \tau_1 \\ \tau_2 \\ \tau_3 \\ \tau_4 \end{bmatrix} \quad (46)$$

where:  $h_{ij}$  is a function of  $\bar{q}$  and  $c_{kj}$  is a function of  $\bar{q}$  and  $\dot{\bar{q}}$ . Analysis of the components of the  $H(\bar{q})$  and  $C(\bar{q}, \dot{\bar{q}})$  matrices reveal certain relationships allowing further simplifications. The  $H(\bar{q})$  matrix is symmetric and, due to system configuration,  $h_{13}=h_{14}$  and  $h_{23}=h_{24}$ . Therefore,  $h_{31}=h_{41}$  and  $h_{32}=h_{42}$ . System configuration also helps simplify the  $C(\bar{q}, \dot{\bar{q}})$  matrix with the following relationships:  $c_{13}=c_{14}$ ,  $c_{23}=c_{24}$ ,  $c_{31}=c_{41}$ , and  $c_{32}=c_{42}$ . Assuming that  $\theta_6 = \theta_4$ ,  $\dot{\theta}_6 = \dot{\theta}_4$ ,  $\ddot{\theta}_6 = \ddot{\theta}_4$  (i.e. position references, velocities and accelerations are the same for both RUM devices) and noting that torque is applied only at the RUM torque motor, Equation (46) reduces to Equation (47).

$$\begin{bmatrix} h_{11} & h_{12} & 2h_{13} \\ h_{21} & h_{22} & 2h_{23} \\ h_{13} & h_{23} & h_{33} \end{bmatrix} \begin{bmatrix} \ddot{q}_1 \\ \ddot{q}_2 \\ \ddot{q}_3 \end{bmatrix} + \begin{bmatrix} c_{11} & c_{12} & 2c_{13} \\ c_{21} & c_{22} & 2c_{23} \\ c_{31} & c_{32} & 0 \end{bmatrix} \begin{bmatrix} \dot{q}_1 \\ \dot{q}_2 \\ \dot{q}_3 \end{bmatrix} = \begin{bmatrix} 0 \\ 0 \\ \tau_3 \end{bmatrix} \quad (47)$$

### 4.3 Summary

Efficient modeling of the RUM actuated system requires numerous modifications to the standard Lagrange Formulation presented in Chapter 3. The modifications void the standard notation used in Chapter 3 but result in a simplified model. Directly applying the Lagrange Formulation to the RUM system would result in six equations of motion with only three degrees of freedom present. The modifications presented in this chapter enable a reduction of system order, without loss of system details, resulting in three equations of motion for the system model. The approach taken in this chapter, however, is unconventional in robotic applications. Therefore, it is critical to validate the model to ensure that the modifications were accomplished correctly. Chapter 5 discusses this validation using several different methods.

## CHAPTER 5

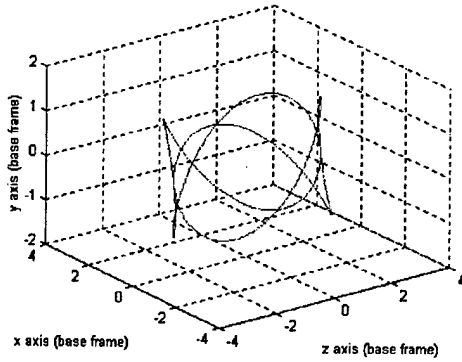
### MODEL VALIDATION

The modeling approach described in Chapter 4 borrows from robotic modeling methods, but is unconventional in a robotic modeling sense. Therefore, it is necessary to validate the model. Analytic analysis, simulation tools (including Maple<sup>TM</sup> and Matlab<sup>TM</sup>), and experiments provide model validation. This chapter discusses kinematic model validation and dynamic model validation.

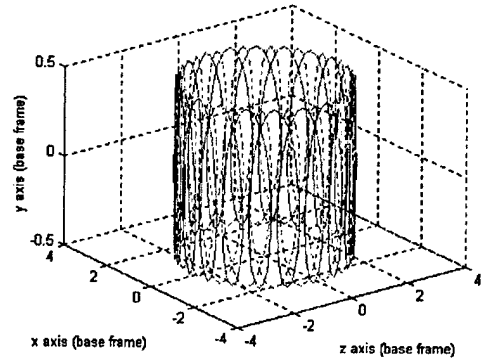
#### 5.1 Kinematic Model Validation

Validation of the kinematic model is critical to subsequent development of the dynamic equations of motions. Kinematics errors will result in errors in the model dynamics due to misrepresentation of the system configuration. Matlab<sup>TM</sup> simulation results, shown in Figure 27a. – 1d, validate the kinematic equations for the following parameters: RUM radius ( $r$ ) = 0.5 feet, distances between telescope gimbal and RUMs ( $d$ ) = 2.5 feet. A different joint variable is put into motion for each simulation. The patterns traced indicate the end position of the mass of each RUM. Comparison of these simulations to analytical solutions confirms that the kinematic model is correct. This validation helped identify and correct a configuration error in the orientation of

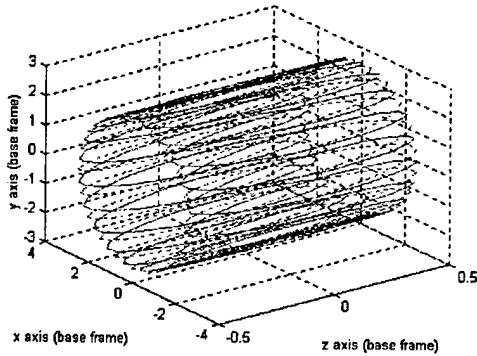
the telescope resulting in the  $\theta_2 + 90^\circ$  term for the joint 2 parameters seen in Table 2 of Chapter 4.



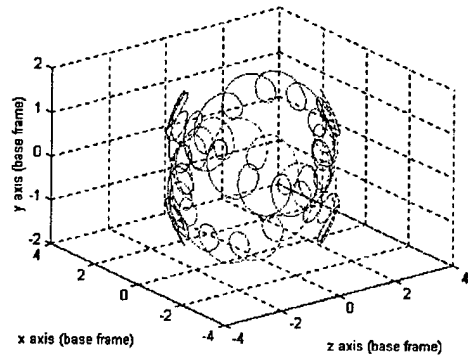
a. Elev and X-Elev axis motion w/out RUM motion



b. X-Elev axis motion w/ RUM motion



c. Elev axis motion w/ RUM motion



d. Elev and X-Elev axis motion w/RUM motion

**Figure 27 Kinematic Simulations**

## 5.2 Dynamic Model Validation

The dynamic model is validated in several steps detailed in the following subsections. An analytic validation is accomplished by first applying the Lagrange

Formulation to a simple, known, mechanical system to ensure the approach is valid for a known system and to gain insight into application to the RUM actuated system. Then, the RUM system inertia and the coriolis/centripetal matrices are investigated to ensure they have the proper form. Next, the RUM model developed in Chapter 4 is compared to other models presented in Chapter 2. Finally, an experimental validation is accomplished by comparing the experimental results with the Matlab™ simulations of the system in the different modes of operation (i.e. scanning and pointing).

### **5.2.1 Pendulum Example**

The first validation uses a robotics approach to apply the Lagrange Formulation to a simple, known, mechanical system to confirm the validity of its use and provides some understanding into how to apply it to more complex systems. The kinetic energy calculations of a pendulum system can help identify errors in the RUM model. A simple pendulum system, shown in Figure 28, is used to validate the approach.

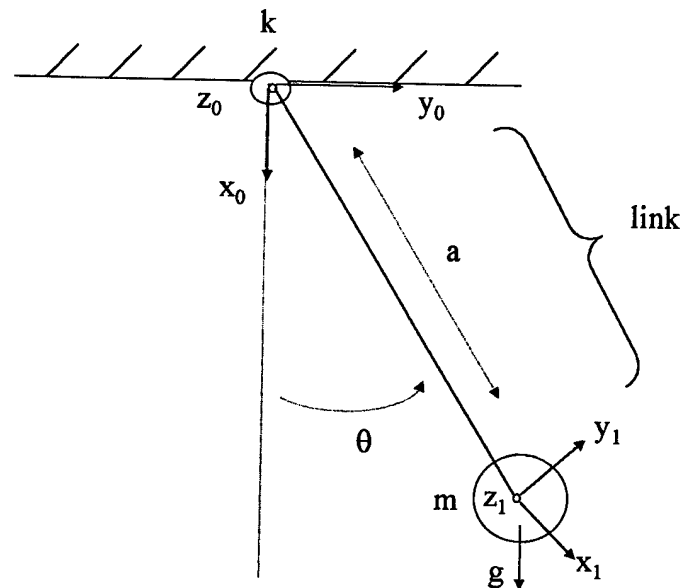


Figure 28 Simple Pendulum

The pendulum has a known equation of motion [18] given by Equation (48).

$$ma^2\ddot{\theta} + mga \sin \theta = -k\dot{\theta} \quad (48)$$

or

$$ma^2\ddot{\theta} + k\dot{\theta} + mga \sin \theta = 0$$

where:  $k\dot{\theta}$  is the generalized friction torque at the joint.

Applying the Lagrange Formulation to the pendulum system results in the same equation of motion. The process of modeling the pendulum gives considerable insight into application of the Lagrange Formulation to the RUM actuated system. The "link" of the pendulum system is similar to the link of the telescope system containing the RUM mass. Each is modeled as a point mass with center of mass at the end of the

link arm. Since the links are modeled as point masses, the inertia about the center of mass of each link is zero. Therefore, the kinetic energy will only have a translational component and not a rotational component. This is an important discovery that can help identify inertia errors in the RUM model.

### 5.2.2 Verifying Matrix Properties

Certain properties of the inertia and coriolis/centripetal matrices can also be used as analytical tools to validate the model. The inertia matrix,  $H$ , will be symmetric if the modeling process is performed properly [17]. Results from Chapter 4 indicate that the 4x4  $H$  matrix (before the model reduction) is symmetric for the RUM system. In fact, this symmetry is one of several properties used to reduce the order of the model. Further investigation of the  $H$  matrix and the coriolis/centripetal matrix,  $C$ , is performed by investigating the properties of  $N(\vec{q}, \dot{\vec{q}})$  defined in Equation (49).

$$N(\vec{q}, \dot{\vec{q}}) = \dot{H}(\vec{q}) - 2C(\vec{q}, \dot{\vec{q}}) \quad (49)$$

If the calculations for  $C$  and  $H$  are correct,  $N(\vec{q}, \dot{\vec{q}})$  will be skew symmetric. That is,  $n_{jk}$  of  $N$  satisfies  $n_{jk} = -n_{kj}$ . The proof of this property is given in [17]. Calculating  $N(\vec{q}, \dot{\vec{q}})$  for the RUM actuated system results in a skew symmetric matrix.

### 5.2.3 Model Analysis

Two models are available for comparison with the model developed in Chapter 4. These models have certain limitations and assumptions associated with their development. The purpose of this section is to determine if the model developed in Chapter 4 yields the simple models under the same assumptions. The next subsections briefly describe the different models, including their attributes and limitations, followed by an analytical comparison of each model.

#### 5.2.3.1 Model Descriptions

The models described in this section are the equations of motion developed using the different modeling techniques employed in Chapter 2 and Chapter 4. **Model 1**, repeated here in Equation (50), was developed in Chapter 2 assuming a constant speed RUM and treats the RUM as an actuator independent of telescope dynamics.

$$\begin{bmatrix} \ddot{\theta}_{LOS} \\ \ddot{\theta}_E \\ \ddot{\theta}_X \end{bmatrix} = 2mrd \begin{bmatrix} 0 \\ -I_E^{-1} \dot{\theta}_R^2 \sin(\theta_R) \\ I_X^{-1} \dot{\theta}_R^2 \cos(\theta_R) \end{bmatrix} \quad (50)$$

The attributes of Model 1 include:

1. Simplicity permits a closed form solution.
2. Elevation and cross-elevation axes are not coupled.
3. RUM arm is coupled to the telescope only through the centripetal terms.

4. Constant RUM speed is assumed.
5. Small angular displacement in the elevation and cross-elevation axes is assumed.

Since Model 1 does not account for variations in the RUM speed, **Model 2** was developed in Chapter 2 assuming a variable speed RUM and is repeated here in Equation (51).

$$\begin{bmatrix} \ddot{\theta}_{LOS} \\ \ddot{\theta}_E \\ \ddot{\theta}_X \end{bmatrix} = 2mrd \begin{bmatrix} 0 \\ I_E^{-1}[-\dot{\theta}_R^2 \sin(\theta_R) + \ddot{\theta}_R \cos(\theta_R)] \\ I_X^{-1}[\dot{\theta}_R^2 \cos(\theta_R) + \ddot{\theta}_R \sin(\theta_R)] \end{bmatrix} \quad (51)$$

$\uparrow$   
centripetal  
components

$\uparrow$   
reaction  
components

The attributes of Model 2 include:

1. Model 2 is slightly more complex than Model 1 but still fairly simple.
2. Elevation and cross-elevation axes are not coupled.
3. RUM arm is coupled to the telescope only through the centripetal terms and reaction terms.
4. Variable RUM speed is assumed.
5. Small angular displacement in the elevation and cross-elevation axes is assumed.

**Model 3** is the reduced order, detailed model developed in Chapter 4. It has equations of motion shown in Equation (52) where  $h_{ij}$  and  $c_{ij}$  are as previously defined in Chapter 4 and Appendix C.

$$\begin{bmatrix} h_{11} & h_{12} & 2h_{13} \\ h_{21} & h_{22} & 2h_{23} \\ h_{13} & h_{23} & h_{33} \end{bmatrix} \begin{bmatrix} \ddot{q}_1 \\ \ddot{q}_2 \\ \ddot{q}_3 \end{bmatrix} + \begin{bmatrix} c_{11} & c_{12} & 2c_{13} \\ c_{21} & c_{22} & 2c_{23} \\ c_{31} & c_{32} & 0 \end{bmatrix} \begin{bmatrix} \dot{q}_1 \\ \dot{q}_2 \\ \dot{q}_3 \end{bmatrix} = \begin{bmatrix} 0 \\ 0 \\ \tau_3 \end{bmatrix} \quad (52)$$

Equation (52) must be put into a form similar to Equations (50) and (51) using the equations of motion for the line of sight, elevation and cross-elevation axes to allow for comparison of the models. From the model developed in Chapter 4,  $q_1$  represents  $\theta_X$ ,  $q_2$  represents  $\theta_E$ , and  $q_3$  represents  $\theta_R$ . The line-of-sight angular motion is physically constrained to zero by the gimbal mount, allowing the equations of motion for the line of sight, elevation and cross-elevation axes for Model 3 to be written as shown in Equation (53).

$$\begin{bmatrix} \ddot{\theta}_{LOS} \\ \ddot{\theta}_E \\ \ddot{\theta}_X \end{bmatrix} = \begin{bmatrix} 0 \\ h_{22}^{-1}(-h_{21}\ddot{\theta}_X - 2h_{23}\ddot{\theta}_R - c_{21}\dot{\theta}_X - c_{22}\dot{\theta}_E - 2c_{23}\dot{\theta}_R) \\ h_{11}^{-1}(-h_{12}\ddot{\theta}_E - 2h_{13}\ddot{\theta}_R - c_{11}\dot{\theta}_X - c_{12}\dot{\theta}_E - 2c_{13}\dot{\theta}_R) \end{bmatrix} \quad (53)$$

The Model 3 attributes include:

1. Model 3 is a detailed model involving complicated, nonlinear terms.
2. Shows coupling between the elevation and cross-elevation axes.
3. Shows coupling of the telescope with the RUM arm through inertia terms and coriolis/centripetal terms.
4. No assumptions made about RUM speed; valid for all operating conditions.
5. Also provides an equation of motion for the RUM link (i.e.  $\ddot{\theta}_R$ ) when in the form of Equation (52).

### 5.2.3.2 Model Comparisons

The models developed in Chapter 2 and described in the previous section contain only the equations of motion (*eom*) for the line of sight, elevation, and cross-elevation axes of the RUM actuated telescope. Model analysis is accomplished by comparing the line of sight axis *eom*, elevation axis *eom*, and the cross-elevation axis *eom* between models. An analytic comparison of the models reveals that under certain assumptions, the model developed in Chapter 4 (Model 3) reduces to Model 1 and Model 2. Reducing Model 3 to Model 2 requires the following assumptions:

1. No cross-coupling in the inertias of the elevation and cross-elevation telescope axes. The RUM is coupled to the telescope inertias only through the  $h_{13}$  and  $h_{23}$  terms.

Result: Inertia matrix has constant diagonal elements and two, time varying, off diagonal elements.

2. Zero telescope centripetal and coriolis effects. Also, zero coriolis effects between telescope and RUM axes. The only effects retained in the model are the RUM centripetal terms.

Result: All C-matrix elements are zero, except for  $c_{13}$  and  $c_{23}$  in Equation (53).

3. Let  $\theta_E$  be small, so  $\cos(\theta_E) = 1$  and  $\sin(\theta_E) = 0$ .

Result: Equation (54), which is the Model 2 with a few minor differences.

$$\begin{bmatrix} \ddot{\theta}_{LOS} \\ \ddot{\theta}_E \\ \ddot{\theta}_X \end{bmatrix} = 2mrd \begin{bmatrix} 0 \\ I_E^{-1}[\dot{\theta}_R^2 \sin(\theta_R) - \ddot{\theta}_R \cos(\theta_R)] \\ + I_X^{-1}[-\dot{\theta}_R^2 \cos(\theta_R) - \ddot{\theta}_R \sin(\theta_R)] \end{bmatrix} \quad (54)$$

Note that the terms in Equation (54) are shifted 180 degrees from the terms in Model 2 shown in Equation (51). Since the choice of reference frame changes all the relationships by 180 degrees, the *com*'s are not altered by the difference in frame selection. Therefore, the results show that Model 3 contains the reaction force model.

Reducing Model 3 to Model 1 requires the same three assumptions listed previously plus an additional assumption:

4. Constant RUM speed. The  $\ddot{\theta}_R$  (RUM acceleration) is zero and  $\dot{\theta}_R$  (RUM velocity) is constant.

Result: Equation (55), which is Model 1 with terms shifted 180 degrees similar to Model 2.

$$\begin{bmatrix} \ddot{\theta}_{LOS} \\ \ddot{\theta}_E \\ \ddot{\theta}_X \end{bmatrix} = 2mrd \begin{bmatrix} 0 \\ I_E^{-1}\dot{\theta}_R^2 \sin(\theta_R) \\ -I_X^{-1}\dot{\theta}_R^2 \cos(\theta_R) \end{bmatrix} \quad (55)$$

Therefore, the results show that Model 3 contains Model 1 as well.

#### 5.2.4 Experimental Validation

Experimental validation is performed by comparing Matlab™ simulation results with the actual NASA test system experimental results. Numerous tests were

conducted on the NASA experiment and documented in [19]. There is an important distinction between these tests and those reported earlier by Polites [3,20]. Earlier tests confirmed accurate scanning and pointing performance when auxiliary gimbal control actuators and closed-loop gimbal control are employed. The tests described here are conducted without gimbal control thus evaluating the open-loop response of the system. Since the goal of the present testing is to validate a new model of the open-loop system dynamics, these test results cannot be compared to the findings reported earlier. This section describes how the simulations were accomplished by introducing different representations for Models 1 and 2. This section also compares simulation results with experimental results under different modes of operation including a constant RUM speed mode of operation, start-up transient response, and a variable RUM speed mode of operation.

#### 5.2.4.1 Model Form

Putting Model 3 into a robotics framework helps identify the input to the RUM torque motors necessary for different operating modes. The models are put into the same format, namely  $H(\vec{q})\ddot{\vec{q}} + C(\vec{q}, \dot{\vec{q}})\dot{\vec{q}} = \tau$ , to facilitate simulation. The control input is through the  $\tau$  term, which is the input torque vector to the different joints. This is significantly different than Polites' original model in which he used a torque input about the elevation and cross-elevation axes generated by the centripetal force of the RUM. In the above form, however, the torque input to the RUM actuated system

is  $\tau = [0 \ 0 \ \tau_3]^T$  showing that the cross-elevation and elevation joints are unactuated (i.e.  $\tau_1$  and  $\tau_2$  are zero).  $\tau_3$  controls the speed of the RUM arms through input torque to the RUM torque motors. Equation (52) shows Model 3 already in this form. Since Model 1 and Model 2 are contained in Model 3, they can easily be put into this same form as shown below in Equation (56) and (57). Note that these equations are shifted by 180 degrees to permit comparison with Model 3.

$$\begin{bmatrix} I_X & 0 & 0 \\ 0 & I_E & 0 \\ 0 & 0 & I_{RUM} \end{bmatrix} \begin{bmatrix} \ddot{q}_1 \\ \ddot{q}_2 \\ \ddot{q}_3 \end{bmatrix} + \begin{bmatrix} 0 & 0 & 2(mrd\dot{q}_3 \sin(q_3)) \\ 0 & 0 & 2(mrd\dot{q}_3 \cos(q_3)) \\ 0 & 0 & 0 \end{bmatrix} \begin{bmatrix} \dot{q}_1 \\ \dot{q}_2 \\ \dot{q}_3 \end{bmatrix} = \begin{bmatrix} 0 \\ 0 \\ \tau_3 \end{bmatrix} \quad (56)$$

$$\begin{bmatrix} I_X & 0 & -2mrd \cos(q_3) \\ 0 & I_E & 2mrd \sin(q_3) \\ 0 & 0 & I_{RUM} \end{bmatrix} \begin{bmatrix} \ddot{q}_1 \\ \ddot{q}_2 \\ \ddot{q}_3 \end{bmatrix} + \begin{bmatrix} 0 & 0 & 2(mrd\dot{q}_3 \sin(q_3)) \\ 0 & 0 & 2(mrd\dot{q}_3 \cos(q_3)) \\ 0 & 0 & 0 \end{bmatrix} \begin{bmatrix} \dot{q}_1 \\ \dot{q}_2 \\ \dot{q}_3 \end{bmatrix} = \begin{bmatrix} 0 \\ 0 \\ \tau_3 \end{bmatrix} \quad (57)$$

In this form, both models contain an equation of motion for the RUM arm. This gives the designer considerable insight into how to apply the desired torque to the RUM arm. This form also gives model flexibility by allowing friction or disturbances at the different joints through the torque inputs ( $\tau_1, \tau_2, \tau_3$ ).

### 5.2.4.2 Matlab™ Simulations

In the Matlab™ simulations, the equations of motion are numerically integrated to solve for  $\vec{q}$  and  $\dot{\vec{q}}$ . A numerical integration is required for the detailed model because of the complexity of  $C$ ,  $H$  and  $H^{-1}$  and the lack of a closed form solution for  $\ddot{\vec{q}}$ . Model 1 and Model 2 are simulated using the same techniques to ensure that differences in numerical techniques do not contribute to differences in the simulations. Matlab™ contains numerous numerical integration procedures called ordinary differential equations (ODE) solvers. They are intended to solve a general system of differential equations of the form  $\dot{y} = f(t, y)$ , where  $t$  is the scalar independent variable and  $y = y(t)$  is the vector of dependent variables. This ODE solver is based on the classic Runge - Kutta method [21]. This method treats  $f(t, y)$  as a function of two independent variables, samples the function for several different values of these variables, combines the samples to approximate the Taylor series, and integrates the resulting approximation over one time step. ODE 45 is used in the RUM system simulations. The digits 4 and 5 refer to the order of the underlying method. ODE 45 employs two approximations, one of order 4 and one of order 5, and uses their difference to estimate the error in each step. The order is roughly the number of terms in the Taylor series approximation.

To put the RUM actuated system into ‘first order’ form consistent with  $\dot{y} = f(t, y)$ , the six state variables are defined as:

$$\begin{array}{ll}
 x_1 = q_1 & \text{(elev postion)} \\
 x_2 = q_2 & \text{(x-elev position)} \\
 x_3 = q_3 & \text{(RUM position)} \\
 x_4 = \dot{q}_1 & \text{(elev velocity)} \\
 x_5 = \dot{q}_2 & \text{(x-elev velocity)} \\
 x_6 = \dot{q}_3 & \text{(RUM velocity)}
 \end{array}$$

The resulting 'first order' differential equation is shown in Equation (58):

$$\dot{\vec{x}} = \begin{bmatrix} 0_{3 \times 3} & I_{3 \times 3} \\ 0_{3 \times 3} & -H^{-1}C \end{bmatrix} \vec{x} + \begin{bmatrix} 0_{3 \times 3} \\ H^{-1} \end{bmatrix} \tau \quad (58)$$

where: H and C were previously defined in the Chapter 4 calculations. The control input,  $\tau$ , is the single torque input to the RUM torque motors. The Matlab<sup>TM</sup> simulations use several M-files containing RUM system parameters. Figure 29 shows the flow diagram for the simulations.

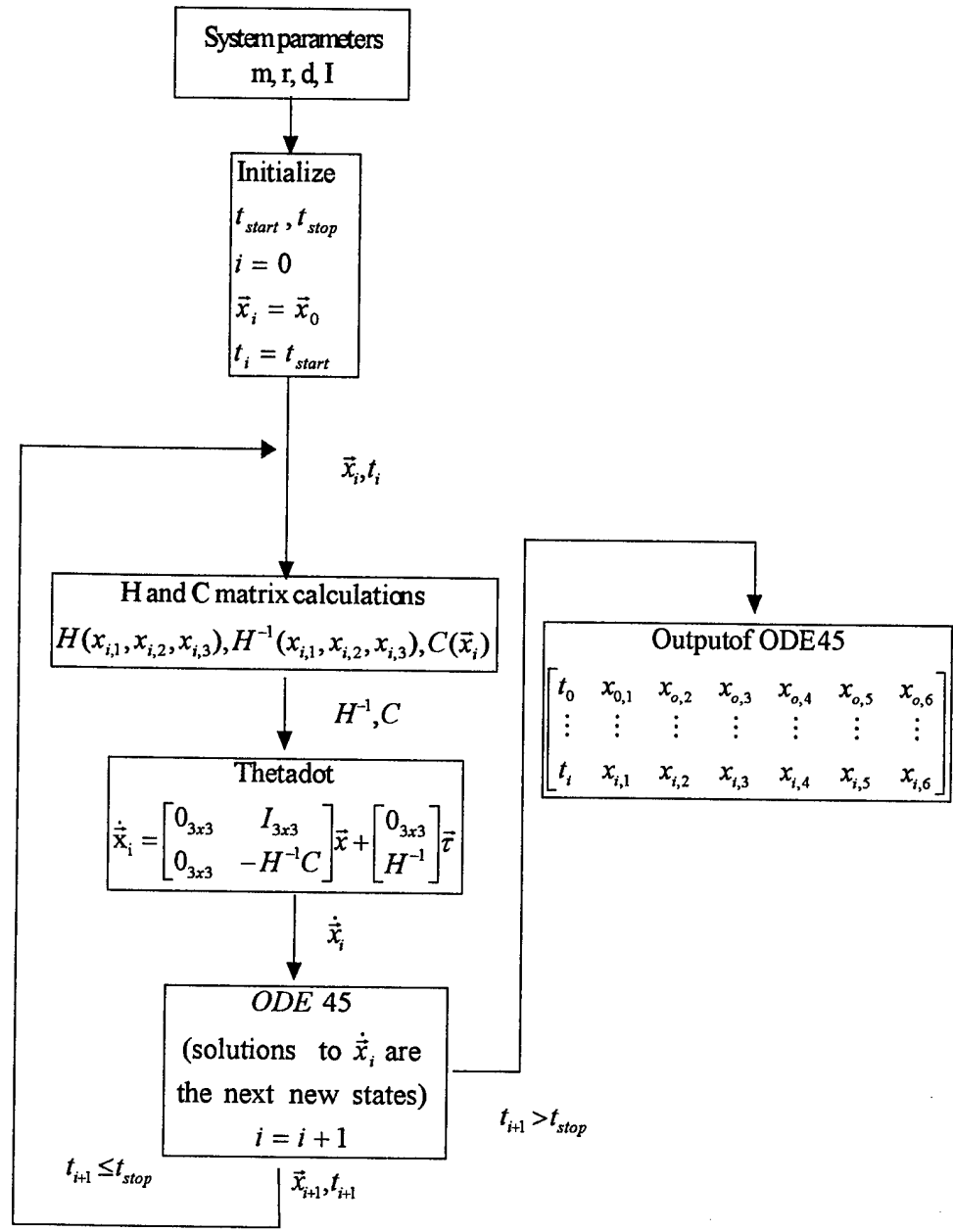


Figure 29 Flow Diagram for RUM Simulations

The system parameters used for the RUM actuated system simulation are specified below and are consistent with the test configuration shown in Chapter 2.

$$m = .155 \text{ slugs}$$

$$d = 2.5 \text{ feet}$$

$$r = 0.5 \text{ feet}$$

$$I_{(\text{telescope along x axis})} = I_{(\text{telescope along y axis})} = 26 \text{ slug} \cdot \text{ft}^2 \text{ (specified in reference frame 2)}$$

Note that this numerical integration technique was successfully tested on the simple pendulum system to validate its use for the RUM system.

#### 5.2.4.3 Constant RUM Speed Analysis

Polites' analysis in Chapter 2 and [3,20] indicates that a constant RUM speed should generate a circular scanning motion. Constant RUM speed is implemented using a RUM torque command based on velocity feedback. Proportional control is used to generate the commanded torque given in Equation (59).

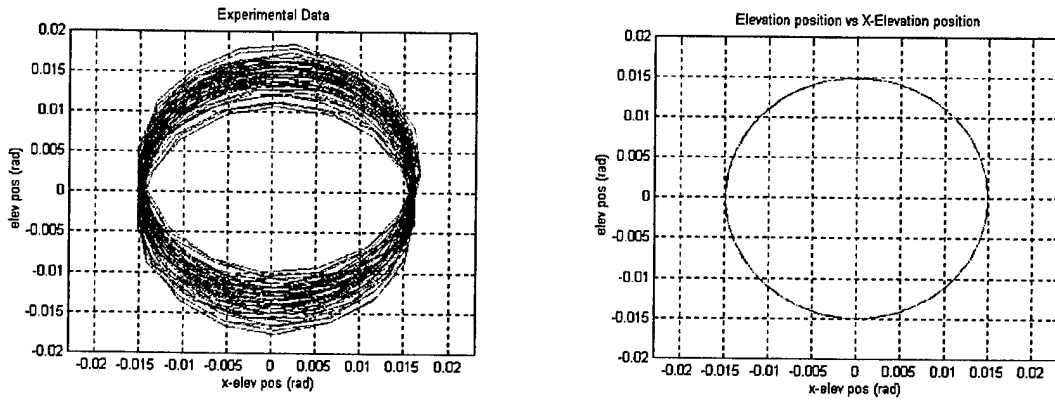
$$\begin{aligned} \tau_3 &= \text{proportional gain}(\text{Velocity}_{RUM,reference} - \text{Velocity}_{RUM,actual}) \\ &= k_p(\text{constant} - \dot{q}_3) \end{aligned} \quad (59)$$

This torque is generated in the Matlab<sup>TM</sup> thetadot.m program. The initial conditions are based on the assumption that the system is in the steady state scanning mode already. That is, the RUM is rotating at a constant speed and the telescope is

scanning. For a RUM reference speed of  $\pi$  rad/sec and RUM position ( $q_3$ ) of 0 radians, the initial conditions are:

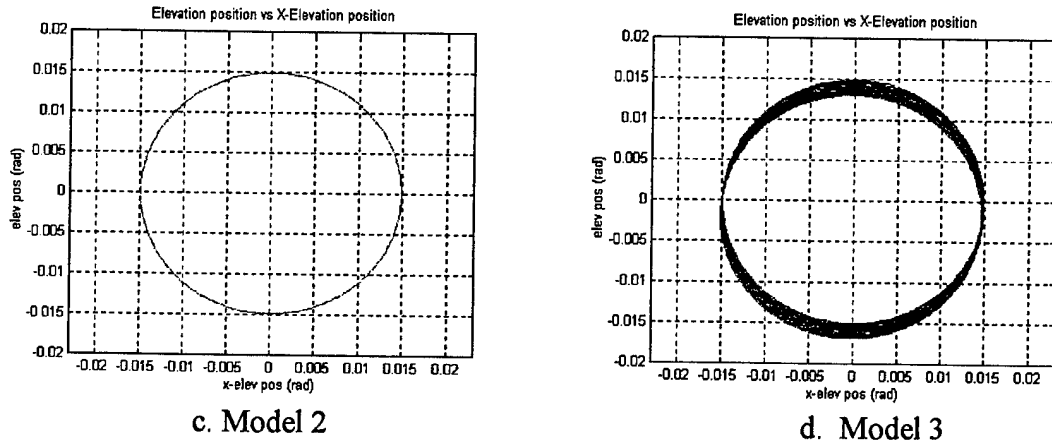
$$\begin{aligned} x_0 &= [x_{0,1} \quad x_{0,2} \quad x_{0,3} \quad x_{0,4} \quad x_{0,5} \quad x_{0,6}]^T \\ &= \left[ 0 \quad \frac{2mrd}{I_y} \quad 0 \quad \frac{2mrd}{I_x} \pi \quad 0 \quad \pi \right]^T \end{aligned} \quad (60)$$

Figure 30 shows a comparison between the experiment and simulation results for each of the models. Note that the initial offset bias is removed from the experimental data.



a. Actual Experiment

b. Model 1



**Figure 30 Constant RUM Velocity Simulation Results**

Observations:

1. Scanning is a “steady state” mode.
2. The experiment radius of the scan is .015 radians with a period of 2 sec.
3. There are some unmodeled disturbances in the experiment observed by the fluctuations in the scan pattern. There are a number of possible sources for the disturbances including imbalances in the system, control cable interference, friction, etc.
4. All 3 models closely approximate the experiment in the scanning mode with a radius of approximately 0.015 radians and a 2 second scan period.

#### **5.2.4.4 Start-Up Transient Behavior.**

The start-up transient response simulation is conducted with all initial conditions set to zero (i.e. the system is at rest). Torque is then applied to the RUM

actuator to accelerate to and maintain a constant speed of  $\pi$  rad/sec. The simulation results are compared to the experimental results in Figure 31.

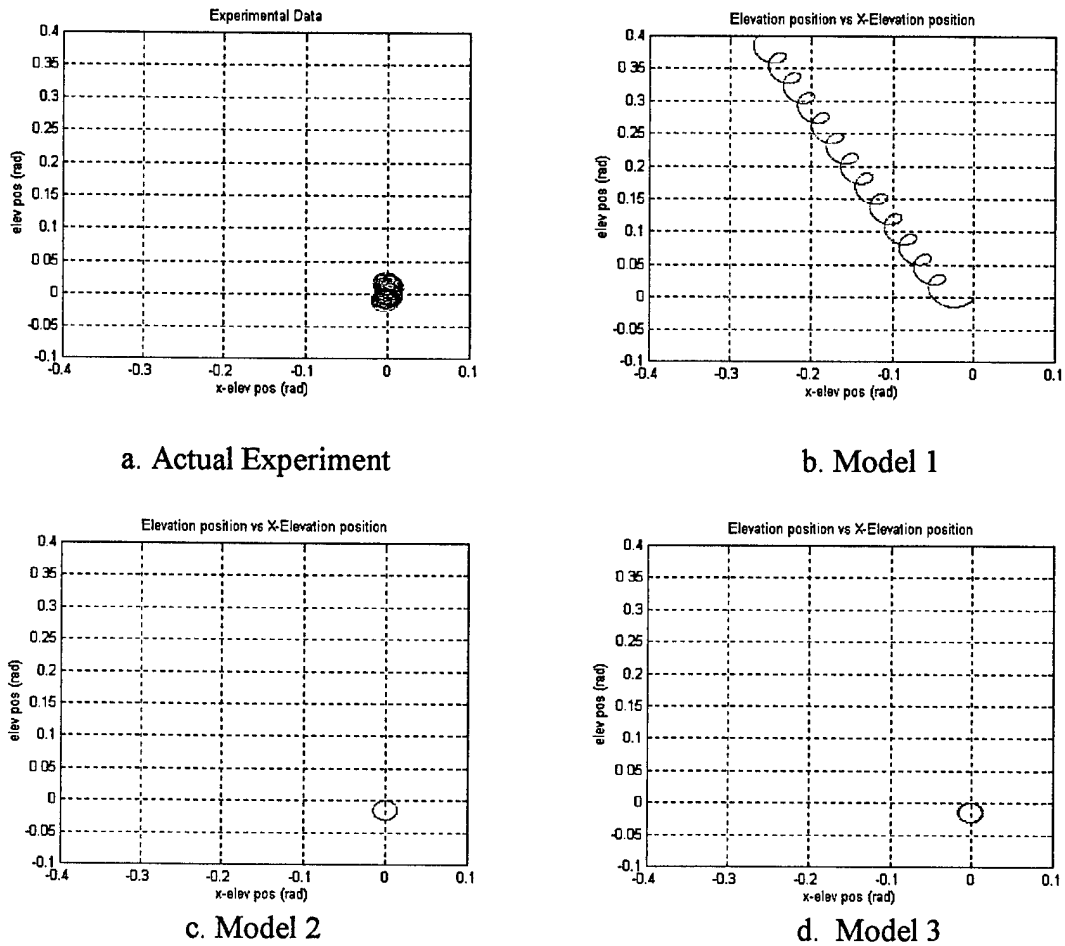


**Figure 31 Start-Up Transient Response Simulation Results**

Observations:

1. The experiment shows small fluctuations in the transient response presumably caused by the synchronization of the RUM arms to the  $180^\circ$  spatial displacement

position. After the fluctuations settle out, a fairly constant steady state scan is observed with no significant offset.

2. Model 1 shows significant errors in the transient behavior of the model compared to the experimental results. It shows a large offset in both the elevation and cross-elevation axis.
3. Models 2 and 3 show similar results observed on the experiment.

#### 5.2.4.5 Variable RUM Speed Analysis.

This section investigates the behavior of the experiment and all three models when a variable RUM speed is introduced to the system. A variable RUM speed can be generated by adjusting the RUM joint torque input ( $\tau_3$ ). Equation (61) shows one such possibility for varying the RUM speed.

$$\begin{aligned}\dot{q}_{3(ref)} &= \text{nominal speed} + \frac{\Delta}{2} \cos(q_3 + \phi) \\ \tau_3 &= k_p (\dot{q}_{3(ref)} - \dot{q}_3)\end{aligned}\tag{61}$$

Where  $\Delta$  is the change in maximum to minimum RUM speed and  $\phi$  is a phase shift term used to adjust the location of RUM acceleration and deceleration in each revolution. Applying the torque in this manner generates a RUM velocity profile shown in Figure 32. Note that the nominal speed is  $\pi$  rad/sec and  $\phi = \pi/4$ .

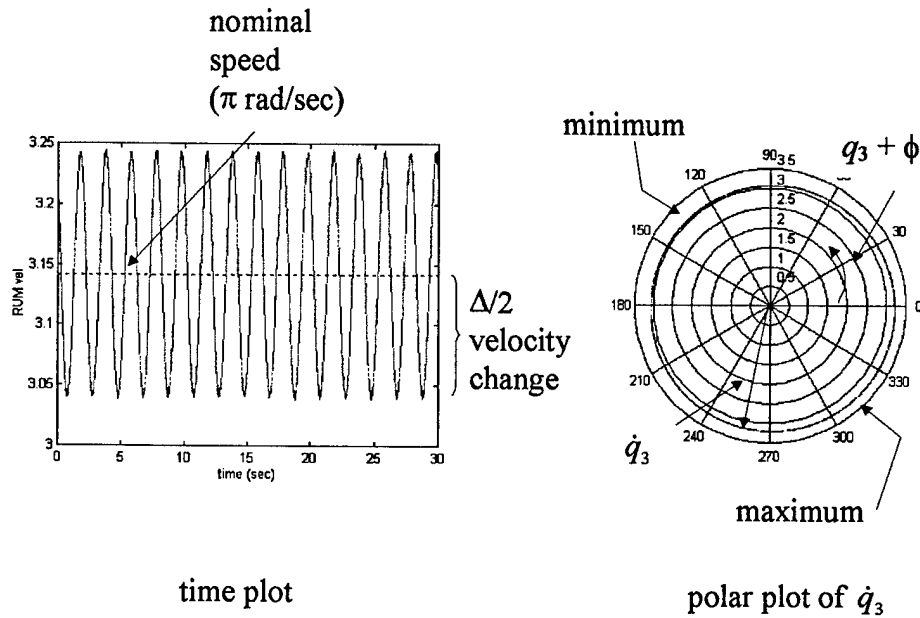
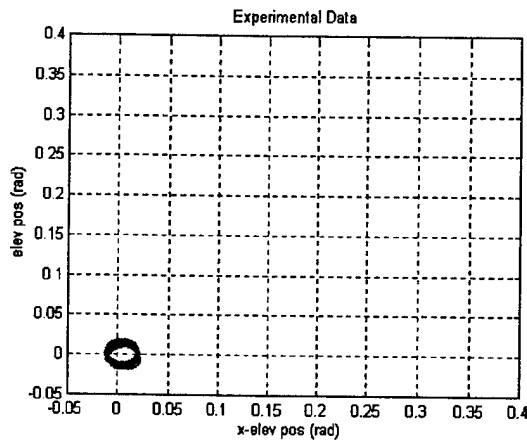
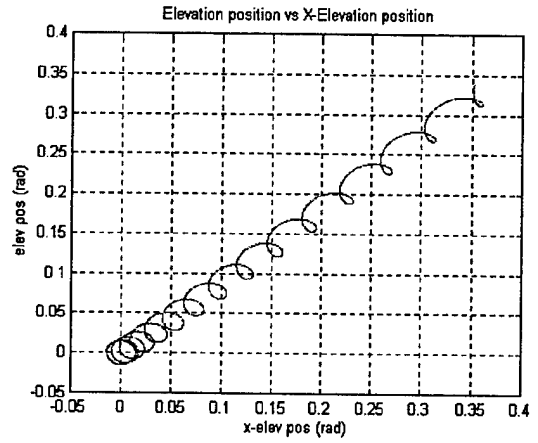


**Figure 32 RUM Velocity Profile**

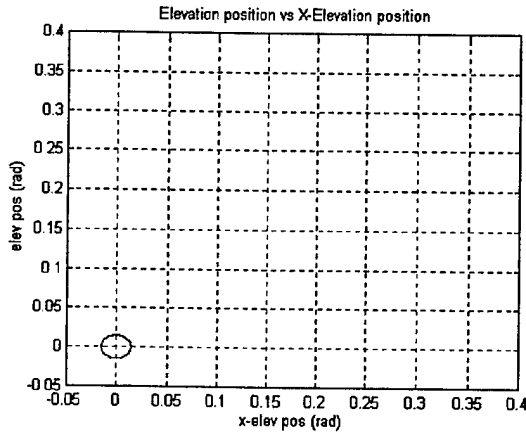
Viewing the velocity profile on a polar plot in Figure 32 reveals where the RUM is accelerating and decelerating in each revolution. Note that since there is no feedback from the elevation and cross-elevation axes present in  $\tau_3$ , these simulations address the open loop behavior of the system. The results of applying this torque to the experiment and models are shown in Figure 33. Note that  $\Delta = 0.1$  for the Model 1 simulation and  $\Delta = 1.0$  for the other simulations. The larger  $\Delta$  is used to determine if a larger velocity change may increase the offset in the elevation and/or cross-elevation axes.



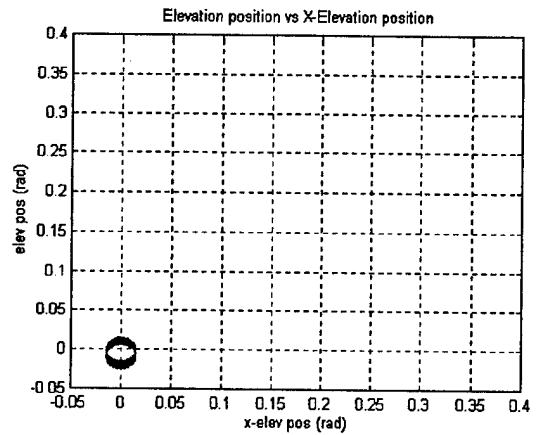
a. Actual Experiment



b. Model 1



c. Model 2



d. Model 3

**Figure 33 Variable RUM Velocity Simulation Results**

Observations:

1. The control input from Equation (61) alone has little noticeable effect on the experimental systems pointing motion. That is, significant changes in the average

cross-elevation and elevation angles are not possible using the control input (61) alone.

2. Model 1 predicts significant effects on the instrument pointing motion by using the control input (61) alone. It shows a large offset in both the elevation and cross-elevation axis.
3. The reaction force model predicts no noticeable effect on the instrument pointing by using control input (61) alone. Even the larger  $\Delta$  has no noticeable effect.
4. The detailed model predicts a very small, long term effect on the pointing angles. The detailed model is in agreement with the behavior observed in the experimental system. The predicted effect is small, however, and may be easily washed out by imperfections in the actual experiment (e.g. nonlinear friction at the gimbals, gravity, cable tensions, etc.). Again, the larger  $\Delta$  has no significant effect.
5. Even though Model 1 does not agree with either the experiment or the other two models, it does give insight to how instrument pointing can be achieved by a modified control. In other words, the control input (61) may not be suitable alone, but may be effective if augmented by other control effort. This is explained further in Chapter 6.

### 5.3 Summary

Validation of the RUM actuated system model involves several techniques. Since all of the dynamics depend on the position and velocity of each component, the kinematics of the system must be validated to ensure proper system configuration.

The data presented in this chapter has validated the dynamic model analytically and experimentally. Further, the dynamic model is shown to contain the simple models and does not contradict the experimental results.

## CHAPTER 6

### FEASIBILITY OF RUM ACTUATED POINTING CONTROL

A detailed model is very important when considering the control of the RUM-actuated system. The difference between the models is significant. Model 1 and Model 2 have limited use in pointing control design since they do not consider large angular motion in the elevation and cross-elevation axes which is the goal for the pointing control schemes. They also neglect coupling between the elevation axis and the cross-elevation axis and some coupling between the RUM arm and these axes. Knowledge of this coupling may be essential when considering a control scheme because of the limited number of actuators in the system. Therefore, the model developed in Chapter 4 and validated in Chapter 5 is necessary when investigating pointing control schemes. Models 1 and 2, however, can lend insight into the controllability of the RUM actuated system. In this chapter, the feasibility of RUM actuated pointing is examined by analyzing the open loop response of the system to different control inputs. Open loop response here means no cross-elevation or elevation motion information is used for the feedback control. Figure 34 shows the general control scheme used in this chapter. Note that the RUM motion is used for feedback control of the RUM velocity only.

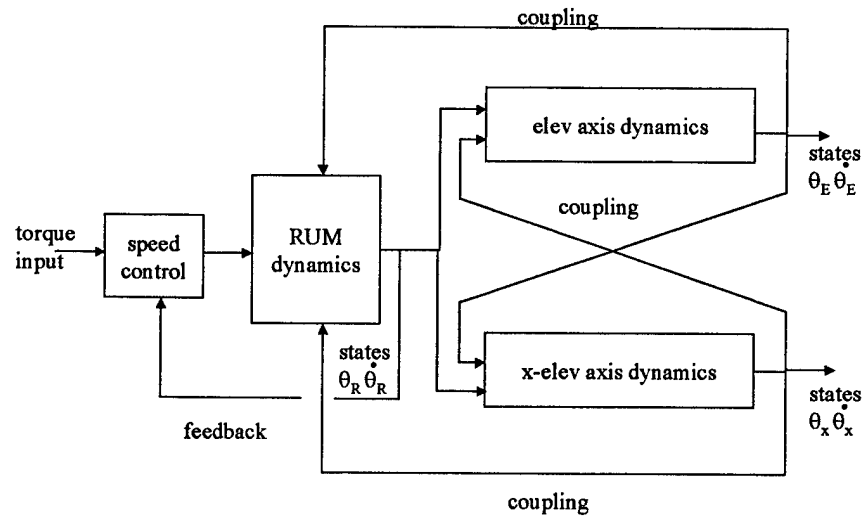


**Figure 34 General Open-Loop Control Scheme**

Several different control schemes are investigated for pointing actuation using the RUM devices. Pointing control using simple RUM rate variations is examined first, followed by feedback ‘cancellation’ analysis. Next, since these two control schemes raise issues regarding the controllability of the system, system controllability (or reachability) and a coupling index are discussed. Finally, variable gimbal braking and variable RUM arm length are considered as possible additions to the pointing control configurations and schemes.

## 6.1 Pointing Control Using RUM Rate Variations

In this section, Polites' control scheme presented in Chapter 2 is investigated. Polites proposed to use a control signal that introduces periodic variations in the RUM rate,  $\omega_R$ . The suggested control input is repeated here in Equation (62).

$$\omega_R = \omega_{R_0} + \Delta\omega_X \cos(\theta_R) - \Delta\omega_E \sin(\theta_R) \quad (62)$$

where:

$\omega_{R_0}$  : a constant (nominal RUM rate of rotation)

$\Delta\omega_X$  : a rate variation to compensate for cross-elevation gimbal error

$\Delta\omega_E$  : a rate variation to compensate for elevation gimbal error

Recall that the sine and cosine terms in Equation (62) weight the rate variations to give them the proper 'timing'. In Chapter 2, this control scheme was implemented in a disturbance rejection test. Here, the control scheme is applied to Model 3 (full model) and is used to determine the feasibility of pointing control. The variable RUM speed analysis conducted in the Chapter 5 investigates this type of control input for constant rate variations ( $\Delta\omega_X$  and  $\Delta\omega_E$ ). Note that since there is no feedback from the elevation and cross-elevation axes, these studies address the open loop behavior of the system.

The following conclusions can be drawn:

1. The control input from Equation (62) alone has little noticeable effect on the experimental systems pointing motion. That is, significant changes in the average

cross-elevation and elevation angles are not possible using the control input (62) alone.

2. Model 1 predicts significant effects on the instrument pointing motion by using the control input (62) alone.
3. Model 2 predicts no noticeable effect on the instrument pointing by using control input (62) alone.
4. Model 3 predicts a very small, long term effect on the pointing angles. Model 3 is in agreement with the behavior observed in the experimental system. The predicted effect is small, however, and may be easily washed out by imperfections in the actual experiment (e.g. nonlinear friction at the gimbals, gravity, cable tensions, etc.).
5. Even though Model 1 does not agree with either the experiment or the other two models, it does give insight to how instrument pointing can be achieved by a modified control. In other words, the control (62) may not be suitable alone, but may be effective if augmented by other control effort. This is explained further in the next section.

## **6.2 Pointing Control using Feedback ‘Cancellation’**

Analysis of the Model 1 suggests that pointing control of the system should be possible if the undesirable dynamic effects of the RUM acceleration and deceleration can be cancelled. The more detailed models 2 and 3 indicate that cross-coupling and other nonlinear dynamics are significant and cannot be ignored. From the controller

design viewpoint, it is suggested that these nonlinear effects be cancelled by feedback control [19]. The idea is very similar to feedback linearizing control, which has been proven in robotics control (but called “computed torque control”) to give linear closed-loop dynamics to systems that are inherently nonlinear [17]. In the RUM application, however, closed-loop dynamics consistent with that predicted by the nonlinear Model 1 is the goal, rather than linear closed-loop dynamics. From the previous variable RUM speed analysis, reaction forces can be identified that prevent pointing from happening. When the reaction terms are taken out, pointing is possible as shown in Figure 35.

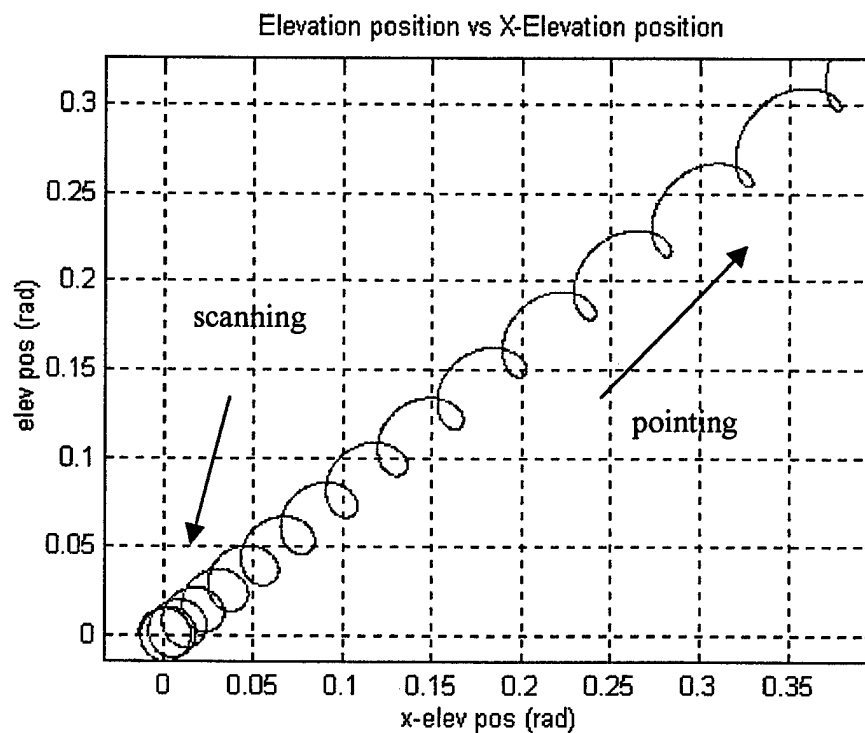


**Figure 35 Variable Speed Control on Model 3 without Reaction Forces**

In order to accomplish this feedback cancellation a significant amount of cross-coupling must be present since the system is under-actuated. That is, the system has more joints (and degrees of freedom) than actuators. The RUM actuated system has three degrees of freedom and a single actuator since the RUMs are held at  $180^\circ$  spatial displacement. The restriction on the RUM phasing ties their motion together and causes them to become a single actuator. Dynamic coupling between the RUM arm and the telescope is necessary for the single actuator to affect motion about the elevation and cross-elevation axes. This requires the determination of system controllability, discussed in the next several sections.

### 6.3 Controllability Analysis Tools.

A system is said to be controllable at time  $t_0$  if it is possible to transfer the system, with some control ' $\vec{u}$ ', from any initial state  $\vec{x}(t_0)$  to any other state  $\vec{x}(t_1)$  in a finite interval of time [22]. This section provides several valuable tools used in the determination of system controllability. To lay the foundation for controllability of the non-linear RUM system, a linear system analogy is described first. Then, non-linear system controllability is discussed, followed by the development of a coupling index used for under-actuated system analysis.

#### 6.3.1 Linear System Control Analogy

Consider the linear system model given by Equation (63).

$$\dot{\vec{x}} = A\vec{x} + B\vec{u} \quad (63)$$

where:  $\vec{x} = n \times 1$  state vector

$\vec{u} = m \times 1$  control vector

$A = n \times n$  system matrix

$B = n \times m$  input matrix

The system is said to be completely state controllable if every state is controllable.

The states of the RUM actuated system are the position and velocity of each joint variable as discussed in Section 0 to follow. Every state is controllable if and only if the  $n \times n$  controllability matrix given by Equation (64) has rank  $n$  [22, 24].

$$\begin{bmatrix} B & AB & \dots & A^{n-1}B \end{bmatrix} \quad (64)$$

### 6.3.2 Nonlinear System Controllability (Reachability)

Consider the non-linear system model given by Equation (65).

$$\dot{\vec{x}} = f(\vec{x}) + g(\vec{x})\vec{u} \quad (65)$$

where:  $\vec{x} = n \times 1$  state vector

$\vec{u} = m \times 1$  control vector

$f(\vec{x})$  and  $g(\vec{x}) =$  vector functions of the states

The 'controllability condition' of Equation (65) is given by the linear independence of the vectors in Equation (66) similar to the linear systems described previously [13].

$$\begin{bmatrix} g, & ad_f g, & \dots, & ad_f^{n-1} g \end{bmatrix} \quad (66)$$

where:

$$\begin{aligned} ad_f g &= [f, g] = \nabla g \cdot f - \nabla f \cdot g \\ ad_f^i g &= [f, ad_f^{i-1} g] \\ \nabla f &= \partial f / \partial x \quad (n \times n \text{ matrix}) \\ \nabla g &= \partial g / \partial x \quad (n \times n \text{ matrix}) \end{aligned}$$

$[f, g]$  is known as the Lie Bracket of  $f$  and  $g$ . Note that for linear systems, Equation (66) becomes the controllability matrix  $\begin{bmatrix} B & AB & \dots & A^{n-1}B \end{bmatrix}$ .

### 6.3.3 Coupling index

Using the Lagrange Formulation (i.e.  $H(\bar{q})\ddot{\bar{q}} + C(\bar{q}, \dot{\bar{q}})\dot{\bar{q}} + G(\bar{q}) = \tau$ ) for the RUM actuated system facilitates the use of numerous robotic analysis techniques. One technique that is particularly useful for control analysis is the coupling index developed by Bergerman, Lee, and Xu [23]. The coupling index is a measure of dynamic coupling present in under-actuated systems. Under-actuated refers to systems that have more joints than control actuators. Some examples of under-actuated systems are robots with failed actuators, legged robots with passive joints and hyper-redundant (snake like) robots with passive joints. This tool will provide insight into the coupling available for control and help determine system controllability. This section briefly explains the indexing process and its use for determining controllability of a nonlinear system.

To use the coupling index technique, the system equations of motion must be put into a form that reveals the relationship between active and passive joints.

Equation (67) provides this relationship for a system with:

$n$  = total number of joints,

$r$  = number of active joints (joints with actuation),

$p$  = number of passive joints.

$$\begin{bmatrix} H_{aa} & H_{ap} \\ H_{pa} & H_{pp} \end{bmatrix} \begin{bmatrix} \ddot{\vec{q}}_a \\ \dot{\vec{q}}_p \end{bmatrix} + \begin{bmatrix} \vec{b}_a \\ \vec{b}_p \end{bmatrix} = \begin{bmatrix} \vec{\tau}_a \\ 0 \end{bmatrix} \quad (67)$$

Where:  $q_a$  = active joint angles

$q_p$  = passive joint angles

$b$  = coriolis, centripetal, and gravitational terms

Note that this H matrix may not always equal the conventional inertia matrix but the properties are preserved such as symmetry and positive-definiteness [23]. From Equation (67), the relationship between the acceleration of the active joints and the passive joints is represented by Equation (68).

$$\begin{aligned} H_{pa} \ddot{\vec{q}}_a + H_{pp} \ddot{\vec{q}}_p + \vec{b}_p &= 0 \\ \text{or} & \\ \ddot{\vec{q}}_p &= -H_{pp}^{-1} H_{pa} \ddot{\vec{q}}_a - H_{pp}^{-1} \vec{b}_p \\ &= M_c \ddot{\vec{q}}_a - H_{pp}^{-1} \vec{b}_p \end{aligned} \quad (68)$$

This can be rewritten as:

$$\ddot{\vec{q}}_p + H_{pp}^{-1}\vec{b}_p = M_c \ddot{\vec{q}}_a \quad (69)$$

The term on the left side of Equation (69) is viewed as the virtual acceleration of the passive joints. Therefore, analysis of how active joint acceleration ( $\ddot{\vec{q}}_a$ ) effects passive joint acceleration ( $\ddot{\vec{q}}_p$ ) involves careful study of the  $M_c$  matrix. The following results apply to the  $M_c$  matrix [23]:

1. If row  $i$ ,  $1 \leq i \leq p$ , in matrix  $M_c$  contains only zeros, the  $i$ th passive joint cannot be controlled via dynamic coupling with the active joints.
2. If  $r < p$ , then  $r$  passive joints can be controlled at every instant, while  $p - r$  passive joints cannot. The  $p - r$  passive joints will depend linearly on the acceleration of the other  $r$  joints.
3. In order to independently control all  $p$  passive joints, at least  $p$  actuators are necessary.

This analysis tool is used in Section 6.5 to help determine the dynamic coupling and controllability of the RUM actuated system.

#### 6.4 Reachability Analysis – RUM Actuated System

This section uses the controllability condition tool to make comparisons between the three models representing the RUM actuated system. Model 1 and Model 2 exhibit the two extremes of the controllability condition. Model 3 appears to be

somewhere in between as will be explained below. Approaching the controllability issue in this way sheds considerable light into a very complex topic.

The RUM actuated system consists of the six state variables previously defined in Chapter 5:

$$\begin{array}{ll}
 x_1 = q_1 & \text{(elev postion)} \\
 x_2 = q_2 & \text{(x-elev position)} \\
 x_3 = q_3 & \text{(RUM position)} \\
 x_4 = \dot{q}_1 & \text{(elev velocity)} \\
 x_5 = \dot{q}_2 & \text{(x-elev velocity)} \\
 x_6 = \dot{q}_3 & \text{(RUM velocity)}
 \end{array}$$

Putting the RUM actuated system into Equation (65) format results in Equation (70):

$$\dot{\vec{x}} = \begin{bmatrix} 0_{3 \times 3} & I_{3 \times 3} \\ 0_{3 \times 3} & -H^{-1}C \end{bmatrix} \vec{x} + \begin{bmatrix} 0_{3 \times 3} \\ H^{-1} \end{bmatrix} \tau \quad (70)$$

where: H and C were previously defined in the Chapter 4 calculations. The control input,  $\tau$ , is the single torque input to the RUM torque motors. This causes the system to be under-actuated as discussed previously. To accurately describe this under-actuated system for controllability analysis,  $g(x)$  must account for this single input.

Therefore, for  $\tau = [0 \ 0 \ \tau_3]^T$ ,  $f(\vec{x}) = \begin{bmatrix} 0_{3 \times 3} & I_{3 \times 3} \\ 0_{3 \times 3} & -H^{-1}C \end{bmatrix} \vec{x}$ ,  $g(\vec{x})$  is the last column of

$$\begin{bmatrix} 0_{3 \times 3} \\ H^{-1} \end{bmatrix}.$$

### 6.4.1 Model 1 Controllability Condition

For Model 1, the controllability condition matrix is Equation (71) where  $s(q_3)$  and  $c(q_3)$  stand for  $\sin(q_3)$  and  $\cos(q_3)$  respectively.

(71)

$$cc = \begin{bmatrix} 0 & 0 & -4d\dot{q}_3 \frac{s(q_3)}{rI_x} & -6d\dot{q}_3^2 \frac{c(q_3)}{rI_x} & 8d\dot{q}_3^3 \frac{s(q_3)}{rI_x} & 10d\dot{q}_3^4 \frac{c(q_3)}{rI_x} \\ 0 & 0 & 4d\dot{q}_3 \frac{c(q_3)}{rI_y} & -6d\dot{q}_3^2 \frac{s(q_3)}{rI_y} & -8d\dot{q}_3^3 \frac{c(q_3)}{rI_y} & 10d\dot{q}_3^4 \frac{s(q_3)}{rI_y} \\ 0 & -\frac{1}{mr^2} & 0 & 0 & 0 & 0 \\ 0 & 4d\dot{q}_3 \frac{s(q_3)}{rI_x} & 2d\dot{q}_3^2 \frac{c(q_3)}{rI_x} & -2d\dot{q}_3^3 \frac{s(q_3)}{rI_x} & -2d\dot{q}_3^4 \frac{c(q_3)}{rI_x} & 2d\dot{q}_3^5 \frac{s(q_3)}{rI_x} \\ 0 & -4d\dot{q}_3 \frac{c(q_3)}{rI_y} & 2d\dot{q}_3^2 \frac{s(q_3)}{rI_y} & 2d\dot{q}_3^3 \frac{c(q_3)}{rI_y} & -2d\dot{q}_3^4 \frac{s(q_3)}{rI_y} & -2d\dot{q}_3^5 \frac{c(q_3)}{rI_y} \\ \frac{1}{mr^2} & 0 & 0 & 0 & 0 & 0 \end{bmatrix}$$

There are several interesting observations:

1. The matrix (cc) is a function of RUM position and velocity only ( $q_3$  and  $\dot{q}_3$ ).
2. The matrix is full rank no matter what the RUM position is as long as the RUM is rotating (i.e. velocity  $\neq 0$ ).
3. Even though the matrix is full rank, the RUM position effects sparseness of the matrix. This in turn implies less control effectiveness to the RUM actuation. A comparable example would be control of the lateral dynamics of an airplane actuated using only rudder input [24]. Even though the controllability matrix has full rank and the system is controllable, the maneuverability of the airplane would

be greatly degraded with this type of control. "Controllability does not guarantee a high-quality control, it just guarantees that all the states can be manipulated to zero in some fashion in some finite time."

4. The above observation indicates the periodic nature of the controllability for the system as discussed in Chapter 2. Equations (72) and (73) show how the controllability matrix changes as the RUM position goes from  $q_3 = 0^\circ$  to  $q_3 = 90^\circ$  respectively. Note  $\dot{q}_3 = \pi$  rad/sec.

$$cc = \begin{bmatrix} 0 & 0 & 0 & -6d \frac{\pi^2}{rI_x} & 0 & 10d \frac{\pi^4}{rI_x} \\ 0 & 0 & 4d \frac{\pi}{rI_y} & 0 & -8d \frac{\pi^3}{rI_y} & 0 \\ 0 & -\frac{1}{mr^2} & 0 & 0 & 0 & 0 \\ 0 & 0 & 2d \frac{\pi^2}{rI_x} & 0 & -2d \frac{\pi^4}{rI_x} & 0 \\ 0 & -4d \frac{\pi}{rI_y} & 0 & 2d \frac{\pi^3}{rI_y} & 0 & -2d \frac{\pi^5}{rI_y} \\ \frac{1}{mr^2} & 0 & 0 & 0 & 0 & 0 \end{bmatrix} \quad (72)$$

$$cc = \begin{bmatrix} 0 & 0 & -4d \frac{\pi}{rI_x} & 0 & 8d \frac{\pi^3}{rI_x} & 0 \\ 0 & 0 & 0 & -6d \frac{\pi^2}{rI_y} & 0 & 10d \frac{\pi^4}{rI_y} \\ 0 & -\frac{1}{mr^2} & 0 & 0 & 0 & 0 \\ 0 & 4d \frac{\pi}{rI_x} & 0 & -2d \frac{\pi^3}{rI_x} & 0 & 2d \frac{\pi^5}{rI_x} \\ 0 & 0 & 2d \frac{\pi^2}{rI_y} & 0 & 2d \frac{\pi^4}{rI_y} & 0 \\ \frac{1}{mr^2} & 0 & 0 & 0 & 0 & 0 \end{bmatrix} \quad (73)$$

### 6.4.2 Model 2 Reachability Condition

For Model 2, the controllability condition matrix is given by Equation (74).

$$cc = \begin{bmatrix} 0 & -2d \frac{\cos(q_3)}{rI_x} & 0 & 0 & 0 & 0 \\ 0 & -2d \frac{\sin(q_3)}{rI_y} & 0 & 0 & 0 & 0 \\ 0 & -\frac{1}{mr^2} & 0 & 0 & 0 & 0 \\ 2d \frac{\cos(q_3)}{rI_x} & 2d\dot{q}_3 \frac{\sin(q_3)}{rI_x} & 0 & 0 & 0 & 0 \\ -2d \frac{\sin(q_3)}{rI_y} & -2d\dot{q}_3 \frac{\cos(q_3)}{rI_y} & 0 & 0 & 0 & 0 \\ \frac{1}{mr^2} & 0 & 0 & 0 & 0 & 0 \end{bmatrix} \quad (74)$$

There are several interesting observations made from this analysis:

1. The matrix is also a function of RUM position and velocity only.
2. The matrix never has full rank; it always has a rank of 2.
3. Since the matrix is less than full rank, Model 2 cannot be controlled at every instant in time. Scanning motion, however, is controllable for Model 2.

Conclusion: the system dynamics produce the necessary motion for scanning even though they are not always controllable.

4. In calculating the Lie Brackets for columns 3, 4, 5, and 6, the  $\nabla g \cdot f$  and  $\nabla f \cdot g$  terms completely negate each other, resulting in the zero vectors. This is due to the reaction terms in Model 2. Therefore, the reaction terms negate a significant part of the controllability of the system.

### 6.4.3 Model 3 Reachability Condition

For Model 3, the Lie Brackets associated with Equation (66) quickly become very complicated due to the complexity of the Model 3 representation. Maple<sup>TM</sup> was used to facilitate calculation of the Lie Brackets for Model 3. Because of the complexity and recursive nature of higher order Lie Brackets, Maple<sup>TM</sup> was only able to calculate the first three Lie Brackets. The calculations for the first three Lie Brackets show linearly independent vectors in the controllability condition matrix. The following conclusions result from the controllability analysis of Model 3:

1. The cc matrix is a function of all states.
2. Since the complexity of the Lie Brackets increases with each recursion, it appears that the controllability matrix will be full rank. The full rank matrix seems to be due primarily to the cross-coupling between axes which does not appear in Models 1 and 2. Because the cc matrix is a function of all states, there may be certain states (i.e. positions and velocities) that cause the cc matrix to lose rank and thus system controllability. This is unlikely because of the complexity of the matrix. However, a decrease in control effectiveness and system maneuverability may occur at certain states.
3. Because Model 3 encompasses both Models 1 and 2, it has a controllability condition somewhere between Models 1 and 2. Model 1 represents a system that is completely controllable and Model 2 represents a system that is not controllable at every instant in time.

4. The analysis done here and in Section 6.1 seems to indicate that Model 3 represents a situation where the system is controllable but the ‘maneuverability’ is poor and it must rely on large inputs and system dynamics to accomplish certain motions.

Since the RUM actuated system is under-actuated, the control input is based on the amount of coupling between the actuator and the telescope. Therefore, to further understand the controllability of Model 3, a coupling index measuring this coupling is necessary.

## 6.5 Coupling index – RUM Actuated System

Unlike Models 1 and 2, Model 3 lends significant insight into the amount of coupling available for control. In the next few sections the coupling index is calculated and compared for each model.

### 6.5.1 Model 1 Coupling index

Putting Model 1 into Equation (67) form results in Equation (75).

$$\begin{bmatrix} I_{RUM} & 0 & 0 \\ 0 & I_E & 0 \\ 0 & 0 & I_X \end{bmatrix} \begin{bmatrix} \ddot{q}_3 \\ \ddot{q}_1 \\ \ddot{q}_2 \end{bmatrix} + \begin{bmatrix} 0 \\ 2\dot{q}_3 mr \sin(q_3) \\ -2\dot{q}_3 mr \cos(q_3) \end{bmatrix} = \begin{bmatrix} \tau_3 \\ 0 \\ 0 \end{bmatrix} \quad (75)$$

Using (75) to calculate the  $M_c$  matrix results in Equation (76).

$$\begin{aligned}
 M_{pp} &= \begin{bmatrix} I_E & 0 \\ 0 & I_X \end{bmatrix} \\
 M_{pa} &= \begin{bmatrix} 0 \\ 0 \end{bmatrix} \\
 M_c &= M_{pp}^{-1} M_{pa} = \begin{bmatrix} 0 \\ 0 \end{bmatrix}
 \end{aligned} \tag{76}$$

The following observations are made from this result:

1. Indicates that it is not possible to control the elevation joint and cross-elevation joint at every instant via coupling to the RUM joint.
2. Appears to contradict earlier findings on controllability condition in Section 6.4.1. This index, however, measures inertia coupling only and does not account for coriolis or centripetal coupling which are important factors in RUM control.  $M_c = 0$  is consistent with the fact that Model 1 does not account for coupling of the elevation and cross-elevation axes to the RUM via inertia terms. This analysis shows that the inertia terms cannot be ignored in modeling the RUM actuated system.
3. The pointing motion observed in Model 1 tests are generated strictly from centripetal terms as previously observed.

### 6.5.2 Model 2 Coupling index

Putting Model 2 into Equation (67) form results in Equation (77).

$$\begin{bmatrix} I_{RUM} & 0 & 0 \\ -2mrd \cos(q_3) & I_E & 0 \\ -2mrd \sin(q_3) & 0 & I_X \end{bmatrix} \begin{bmatrix} \ddot{q}_3 \\ \ddot{q}_1 \\ \ddot{q}_2 \end{bmatrix} + \begin{bmatrix} 0 \\ 2\dot{q}_3 mr \sin(q_3) \\ -2\dot{q}_3 mr \cos(q_3) \end{bmatrix} = \begin{bmatrix} \tau_3 \\ 0 \\ 0 \end{bmatrix} \quad (77)$$

Using Equation (77) to calculate the  $M_c$  matrix results in Equation (78).

$$\begin{aligned} M_{pp} &= \begin{bmatrix} I_E & 0 \\ 0 & I_X \end{bmatrix} \\ M_{pa} &= \begin{bmatrix} -2mrd \cos(q_3) \\ -2mrd \sin(q_3) \end{bmatrix} \\ M_c &= M_{pp}^{-1} M_{pa} = \begin{bmatrix} -2mrd \cos(q_3) / I_E \\ -2mrd \sin(q_3) / I_X \end{bmatrix} \end{aligned} \quad (78)$$

The following observations are made from this result:

1. Indicates that the passive joints are both controlled via dynamic coupling with the active joints.
2. The terms in this coupling matrix were previously identified as the reaction terms in Chapter 2 analysis. These terms keep the telescope from pointing when a variable RUM velocity control is used. In essence, they “control” the telescope so that variable speed cannot affect pointing motion.
3. Since the number of active joints ( $r = 1$ ) is less than the number of passive ( $p = 2$ ), one of the passive joints cannot be independently controllable at every instant. In

fact, it appears there is a trade off between control of each axis as  $q_3$  rotates from 0 to  $2\pi$  again showing the periodic controllability of the system.

### 6.5.3 Model 3 Coupling index

Putting Model 3 into Equation (67) form results in Equation (79).

$$\begin{bmatrix} h_{33} & h_{31} & h_{32} \\ 2h_{13} & h_{11} & h_{12} \\ 2h_{23} & h_{21} & h_{22} \end{bmatrix} \begin{bmatrix} \ddot{q}_3 \\ \ddot{q}_1 \\ \ddot{q}_2 \end{bmatrix} + C(\vec{q}, \dot{\vec{q}})\dot{\vec{q}} = \begin{bmatrix} \tau_3 \\ 0 \\ 0 \end{bmatrix} \quad (79)$$

Where:  $H_{ij}$  is as previously defined in Chapter 4 and Appendix C and  $C(\vec{q}, \dot{\vec{q}})\dot{\vec{q}}$  are the coriolis and centripetal terms.

Using Equation (79) to calculate the  $M_c$  matrix results in:

$$\begin{aligned} M_{pp} &= \begin{bmatrix} h_{11} & h_{12} \\ h_{21} & h_{22} \end{bmatrix} \\ M_{pa} &= \begin{bmatrix} 2h_{13} \\ 2h_{23} \end{bmatrix} \\ M_c &= M_{pp}^{-1} M_{pa} = \begin{bmatrix} M_{c11} \\ M_{c21} \end{bmatrix} \end{aligned} \quad (80)$$

Where detailed values for  $M_c$  are shown in Appendix D. The following observations are made from this result:

1. The  $M_c$  matrix is a function of the RUM position angle and the cross-elevation position angle only. There is no elevation position term in the matrix. This indicates that the coupling of the RUM actuator to the elevation joint is through

the cross-elevation joint. This makes sense physically since the elevation joint is in the base frame.

2. The reaction terms are in the  $M_c$  matrix similar to Model 2 but there are other inertia terms that might be used for control.
3. Since the number of active joints ( $r = 1$ ) is less than the number of passive ( $p = 2$ ), one of the passive joints cannot be independently controllable at every instant of time.

#### 6.5.4 Summary

The coupling index is an important tool used in controllability and reachability analysis. In the RUM actuated case, however, it only shows part of the picture involved in control. It verifies the observations made in the variable RUM rate analysis and explains how the inertias couple to prevent pointing motion. It does not show the influence of coriolis and centripetal terms which are major factors generating scanning motion.

#### 6.6 Modifications to Control Input

The controllability condition analysis of Model 3 indicates that the RUM actuated system is controllable. The control index analysis indicates that the system is not controllable at every instant of time. It also indicates that the coupling, although present, may not be enough to affect an efficient pointing control scheme. This

section discusses possible control scheme changes that may achieve the desired pointing control.

Using Polites' original control scheme shown in Equation (62), one possible change in the control input would be to vary the RUM speed above the nominal speed instead of varying it above and below the nominal speed as suggested by Polites.

Figure 36 shows a comparison between the two speed profiles.

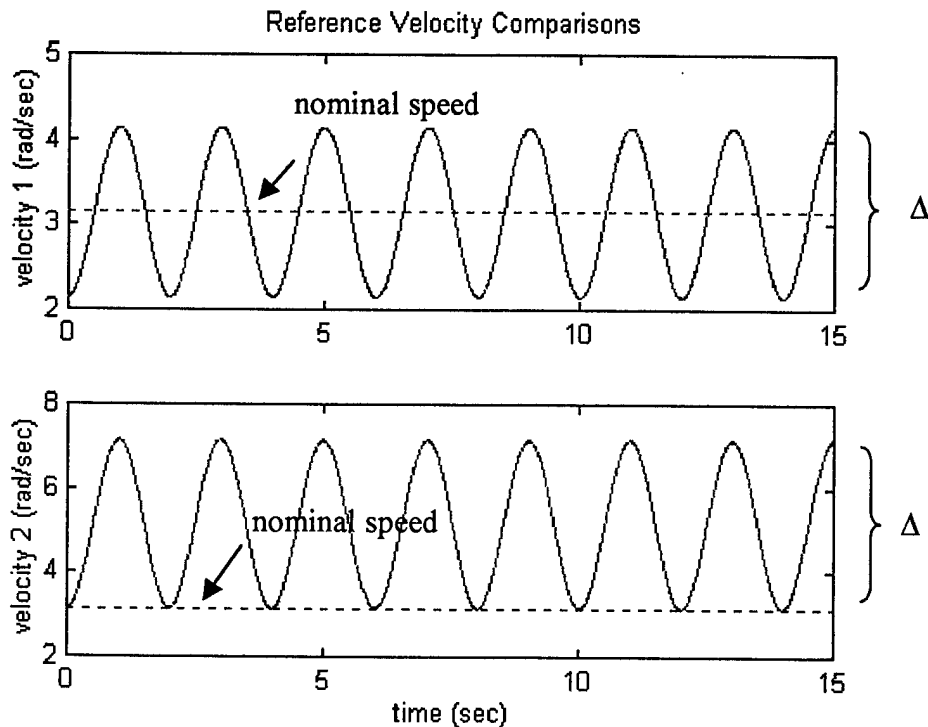


**Figure 36 Speed Profile Comparison**

This control is accomplished by using RUM velocity and position feedback and simply adding an off-set to the reference RUM speed as shown in Equation (81).

$$\dot{q}_{3(ref)} = (\text{nominal speed} + \frac{\Delta}{2}) + \frac{\Delta}{2} \cos(q_3 + \phi) \quad (81)$$

Where  $\Delta$  is the change in maximum to minimum RUM speed and  $\phi$  is a phase shift term used to adjust the location of RUM acceleration and deceleration in each revolution. By varying the RUM speed above the nominal speed, an average speed change occurs. Note that this is different than just changing the RUM velocity to a higher constant value. Changing to a higher constant RUM velocity results in a faster scan only, without pointing motion. Varying the RUM speed as shown in Figure 36 results in initiating multiple transient responses as the RUM speed goes from nominal speed to maximum speed. It is analogous to turning the system on and off and using the small transient behavior to affect pointing. Note that varying the RUM speed above the nominal also allows for a larger change in velocity ( $\Delta$ ) during each revolution of the RUM without worrying about the velocity going negative which is a problem with the original control input. Having a nominal speed above zero ensures a non-zero RUM velocity, essential for control. Theoretically there would be an infinitely large control input available for pointing actuation which may solve some of the control issues addressed earlier. Practically, however, power is limited and at a premium. Therefore it must be conserved and used efficiently. Figure 37 shows the results of the change in control input for cross-elevation axis motion using  $\Delta = 4$ .

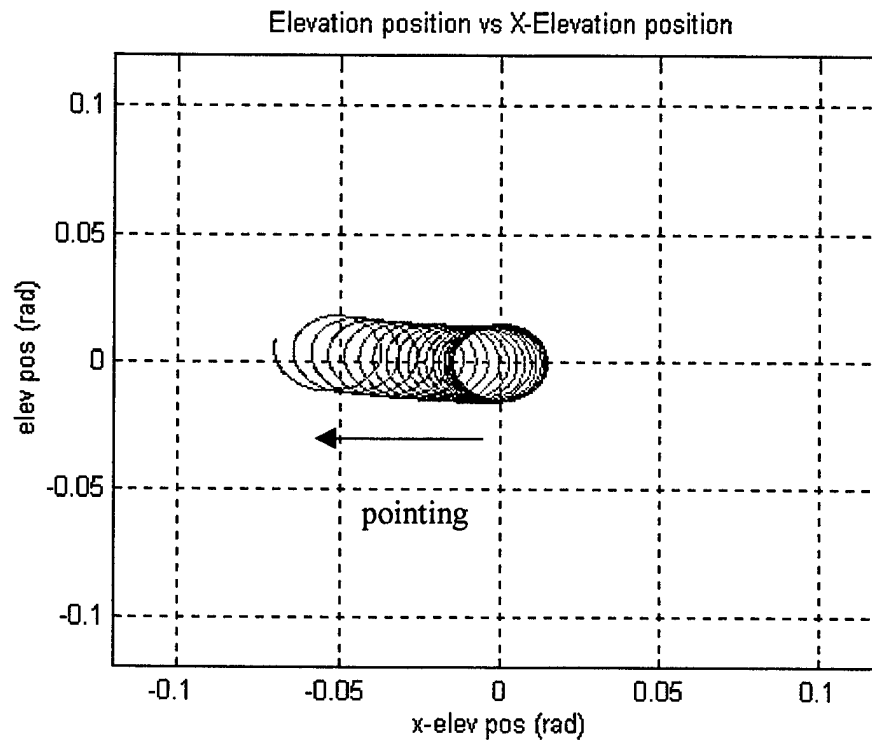


**Figure 37 Cross-Elevation Axis Motion with New Control (30 sec simulation)**

For elevation axis motion, a much larger  $\Delta$  is required in the reference speed to induce a similar amount of motion. Figure 38 shows the results of elevation axis motion for  $\Delta$  ten times that used for the cross-elevation motion.

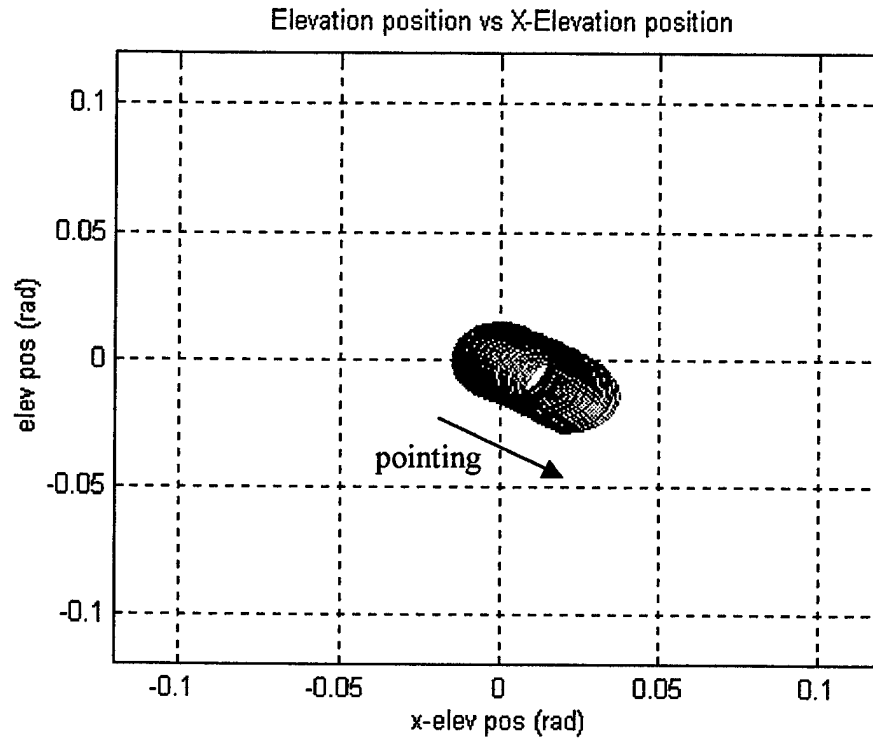


**Figure 38 Elevation Axis Motion with New Control ( $\Delta$  times 10)**

The following significant observations result from the new control input:

1. Hardware limitations and large input requirements will restrict the maximum RUM speed thus reducing the effectiveness of this control scheme. Another pointing strategy may be more appropriate. Note that this control scheme has not been tested on the actual system.
2. It would appear that the motion in cross-elevation axis and elevation axis should be symmetric. Linearized models of the system will be symmetric but non-linear models of the system may not be. Another example of the asymmetry in the system is the existence of a singularity in one axis but not in the other. Since the

elevation axis motion is defined in the base frame, the use of a universal (U) joint configuration at the gimbal mount in the RUM system introduces a singularity when the RUM rotation is in the same plane as the elevation axis motion. The singularity occurs because the RUM axis motion cannot be distinguished from elevation axis motion. This type of configuration contributes to the asymmetry in the motion of the elevation and cross-elevation axes. Even with this asymmetry, some pointing motion is possible with the new control input. Note that if the base frame motion is changed from elevation axis motion to cross-elevation axis motion, the singularity is switched as well.

3. The difference in cross-elevation axis and elevation axis motion and control requirements is also partly explained by the coupling index from Section 6.5.3. The absence of the elevation axis variable in the  $M_c$  matrix and the fact that there are more passive joints than active joints indicates that one passive joint cannot be controlled at every instant.
4. There is a significant amount of coupling between axes that in essence prevents large pointing motions in the elevation axis. This could account for the success of the disturbance test conducted in Chapter 2. A small disturbance in the elevation axis did not have much impact on the motion of the telescope when Polites' control scheme is implemented. Again, the coupling index from Section 6.5.3 helps explain this phenomenon.

## 6.7 System Configuration Changes

Using the single RUM control strategy only may not be the most efficient or practical means of controlling pointing. A possible solution to the under-actuated control issues raised previously is to add another actuator. One obvious solution is to allow the RUM arms to rotate without the  $180^\circ$  spatial displacement requirement. This would in essence add an additional actuator to the system by using the hardware already present. There would be four joints with 4 degrees of freedom and two actuators available to control them. This, however, would cause lateral motion about the center of mass of the telescope causing pendulum like oscillations in the balloon borne system. Polites originally designed the RUM actuated system with the  $180^\circ$  spatial displacement to prevent this lateral motion because it destabilizes the gondola platform and makes the balloon borne telescope unusable. This configuration, however, could be used for a space borne system since the lateral motion could be used for pointing. The space borne system will require extensive model changes due to the increased degrees of freedom compared to the current gimbal mounted model. This configuration will be addressed in the future work section of Chapter 7. Two other possible actuator additions are promising. They are a variable gimbal braking actuator and a variable RUM arm length actuator. These configurations are investigated in the next two sections.

### 6.7.1 Variable Gimbal Braking

One possible solution to reducing the auxiliary control system hardware may be to reduce the complexity of the system by using simple brakes at the gimbal mount instead of torque motors, reaction wheels or CMGs. Obviously this configuration would only be suitable for balloon borne systems because the braking system requires a platform to brake against. Simple brakes have been used on numerous occasions as a simple way to increase actuation for under-actuated systems [23,25]. A variable braking system would apply a friction force at the gimbal mount in the elevation and cross elevation axis. The RUM would rotate at a constant speed and the braking would be synchronized with the RUM position to affect pointing in different directions. Equation (82) shows an example of the friction force generated by the braking system necessary for pointing control.

$$\begin{aligned}\tau_1 &= -(0.5 + 0.5 \cos(q_3 + \phi))\dot{q}_1 \\ \tau_2 &= -(0.5 + 0.5 \cos(q_3 + \phi))\dot{q}_2\end{aligned}\tag{82}$$

This configuration would take advantage of the RUM motion and allow the telescope to continue scanning at the same time it was being pointed.  $\phi$  is used to change the direction of the pointing command. Figure shows the open loop response to such a command for  $\phi = 45^\circ$ .

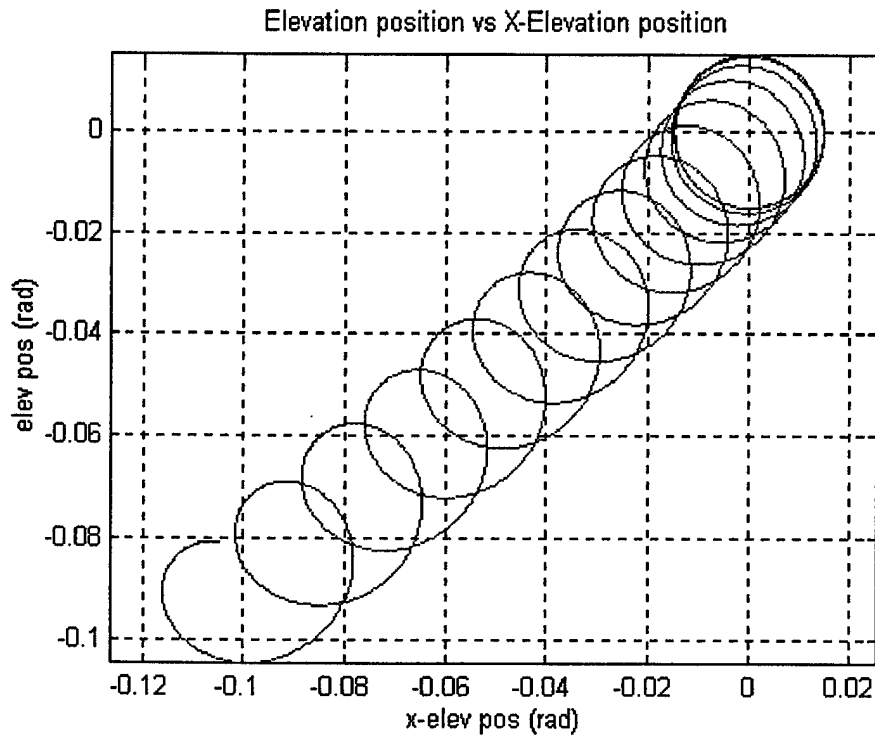


**Figure 39 Variable Gimbal Braking Pointing Actuation**

### 6.7.2 Pointing Control using Variable RUM Arm Length

Adding an actuator to vary the RUM arm length is another possible solution to the under-actuated control issues raised previously. In this configuration, the RUMs will continue to rotate as before (i.e.  $180^\circ$  spatial displacement) at a constant velocity but the RUM arm length would vary during each revolution. Since the variable arm length adds new dynamics to the system, a new model is required. Applying the Lagrange Formulation to this new configuration results in equations of motion given by Equation (83).

$$\begin{bmatrix} h_{11} & h_{12} & 2h_{13} & 2h_{14} \\ h_{21} & h_{22} & 2h_{23} & 2h_{24} \\ h_{13} & h_{23} & h_{33} & 0 \\ h_{14} & h_{24} & 0 & h_{44} \end{bmatrix} \begin{bmatrix} \ddot{q}_1 \\ \ddot{q}_2 \\ \ddot{q}_3 \\ \ddot{q}_4 \end{bmatrix} + \begin{bmatrix} c_{11} & c_{12} & 2c_{13} & 2c_{14} \\ c_{21} & c_{22} & 2c_{23} & 2c_{24} \\ c_{31} & c_{32} & c_{33} & c_{34} \\ c_{41} & c_{42} & c_{43} & c_{44} \end{bmatrix} \begin{bmatrix} \dot{q}_1 \\ \dot{q}_2 \\ \dot{q}_3 \\ \dot{q}_4 \end{bmatrix} = \begin{bmatrix} 0 \\ 0 \\ \tau_3 \\ \tau_4 \end{bmatrix} \quad (83)$$

where:  $\dot{q}_3$  and  $\ddot{q}_3$  are the RUM angular velocity and acceleration, respectively and  $\dot{q}_4$  and  $\ddot{q}_4$  are the RUM arm velocity and acceleration, respectively. Varying the RUM arm length by as little as 1.2 inches (from 6 inches to 7.2 inches) generates considerable pointing motion as shown in Figure 40.

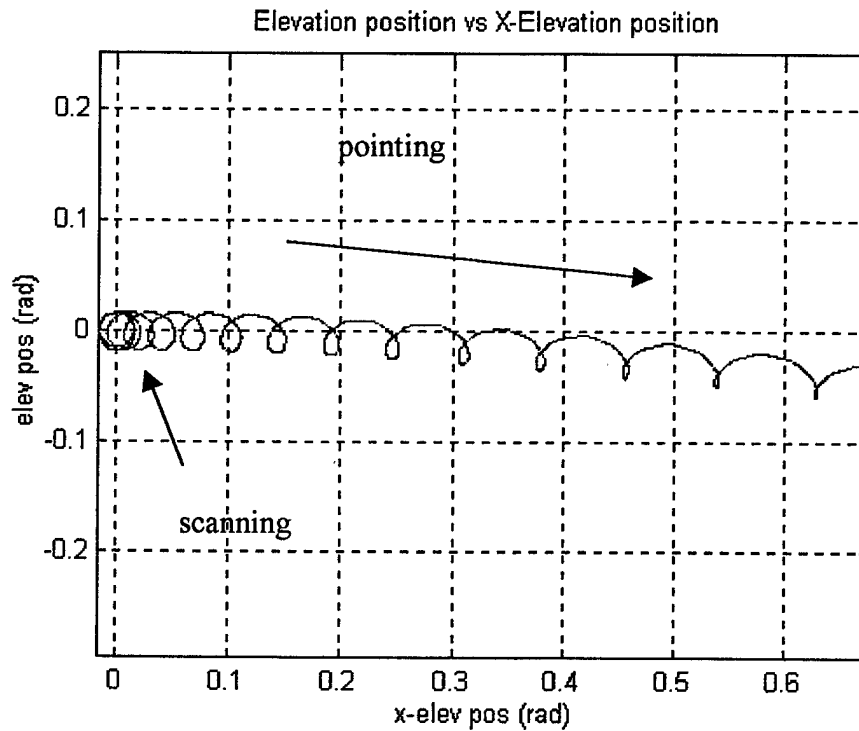


Figure 40 Variable RUM Arm Length Pointing Actuation

Therefore, variable RUM arm length appears to be an effective method for accomplishing scanning and pointing. Since the  $180^\circ$  spatial displacement in RUM positions is maintained, lateral motion should be eliminated making this configuration suitable for both balloon and space borne systems. Varying the RUM arm length, however, will require another actuator, meaning major hardware changes to the physical system. This will require an investigation into the mechanical implementation of another actuator. Some suggested ideas are a geared camshaft that can provide a variable arm length at different locations in the RUM's rotation or a spring loaded telescoping arm. This configuration does eliminate the requirement for an auxiliary control system but it may be difficult and complicated to implement physically.

## **6.8 Conclusions**

This chapter investigates the feasibility of pointing control using RUM actuators. System controllability condition and coupling index are two valuable tools used in reachability analysis. Each has its limitations and must be used carefully. The controllability matrix can be quite complex and the coupling index shows only the inertia coupling. This chapter also provides a sampling of different pointing control strategies and configurations. Model 3 provides a detailed representation available for control, but discovering that control scheme will require considerable research. Simple control schemes, such as a variable RUM rate control do not appear to be highly

effective for pointing control at this point in the research. Two simpler solutions are variable gimble braking or variable RUM arm length configurations and control schemes. Implementation of these will require substantial hardware changes but will reduce or eliminate the auxiliary control system requirements. Much more research is required to determine a control strategy and configuration that will be effective and efficient for pointing actuation.

The RUM actuated system contains very complex dynamics. Under-actuated system analysis has shown that a 3 degree of freedom system cannot be controlled at every instant of time by a single actuator. That does not mean, however, that the RUM actuated system is not usable. For example, a single RUM actuator successfully produces accurate scanning motion. This begs the question, “Is the motion generated by the actuator a motion we can use (but may not be able to control at every time instant but possibly on average)?” In other words, if the RUM device actuates motion that can be used for scanning, perhaps other physical properties of the RUM device can be controlled to give the pointing motion desired. Further research is required in this area.

## CHAPTER 7

### FUTURE WORK AND CONCLUSIONS

The RUM device was developed at NASA to partially meet the unique control challenges of space and balloon-borne gamma ray and x-ray imaging telescopes. This dissertation takes the analysis of this unique actuator to a new level. It provides a systematic method of modeling the RUM actuated system. The modeling approach draws from robotics but extends the application of the Denavit-Hartenberg (DH) coordinate convention and the Lagrange Formulation to this unusual “robot” configuration. The RUM actuated system is unique in a robotic sense since it is not an efficient use of joints or links and is under-actuated, having only the RUM torque motors for actuation. Through the application of this modified modeling approach, this dissertation provides the first known complete model of the RUM actuated system. Prior models do not accurately account for coupling between the telescope axes and the RUM device or provide an accurate prediction of telescope motion under all operating conditions.

Obtaining this complete model facilitates detailed control analysis, which helps determine the feasibility of pointing actuation using the RUM device. This analysis draws from non-linear reachability conditions and the dynamic coupling index. The results of the feasibility study indicate that simple variable RUM rate control schemes

do not appear to be highly effective for pointing control. Experimental simulations give insight into the physical behavior of the system. The results show that pointing motion generated by RUM rotation is due primarily to start-up transient behavior. System configuration changes, such as variable gimbals braking or variable RUM arm length, appear to be effective means of obtaining pointing but substantial hardware changes are necessary. These approaches, however, will help simplify or eliminate the auxiliary control system. The feasibility study also points out the limitations of existing analysis tools. For complex systems, the Lie Bracket calculations quickly become unmanageable and the coupling index provides valuable information about the inertia coupling but does not account for coriolis or centripetal coupling, a major factor in RUM actuated motion. Analysis of the RUM actuated system is a rich and in-depth area of research. It yields numerous other areas of study that will lead to years of future research topics as discussed in the next section.

## **7.1 Future Research**

### **1. RUM Phasing**

Allowing the RUM arms to rotate independently from each other seems to be the next logical approach for increasing the number of actuators since the hardware is already in place, i.e. the two RUM actuators can be phased different by control alone. Increased computing power will be required and there are certain drawbacks to using the RUMs in this manner as discussed in Chapter 6. Also, since lateral motion may be a by-product of the RUM phase approach, some experiment modification will be

necessary. The telescope ('I' beam) must be suspended to simulate a gondola configuration. Suspending the telescope will allow lateral motion and a more accurate experimental setup. Model 3 must be modified to allow for lateral motion in the cross-elevation and elevation axis plus rotational motion in the line of sight axis.

## 2. Variable RUM Arm Length

Simulations involving variable RUM arm length appear to show a promising method for accomplishing scanning and pointing. Varying the RUM arm length, however, requires another actuator which means major hardware changes. Investigation into the mechanical implementation of another actuator is necessary. Some suggested ideas are a geared camshaft that can provide a variable arm length at different locations in the RUM's rotation. The development of a closed loop control scheme incorporating elevation and cross-elevation motion is necessary as well.

## 3. Variable Gimbal Braking

Variable gimbal braking appears to be the most effective and accurate pointing control scheme studied in this dissertation. It takes advantage of the RUM motion and is considerably less complex than other Auxiliary Control System (ACS) hardware. Again, hardware changes are necessary along with the development of a closed loop control scheme

## 4. Linear Scan Configuration

The circular scan was originally studied because two axis pointing is necessary for telescope applications and both elevation axis and cross-elevation axis motion are

affected with the circular scan configuration. Since it was shown (in Chapter 6) that 3-degrees of freedom cannot be controlled at every instant by a single RUM actuator, perhaps a step back is necessary. The linear scan configuration meets the minimum coupling index criteria (i.e. there must be at least as many active joints as passive joints). Studying the linear scan motion may provide some clues and possible solutions to using a single actuator to accomplish pointing along a single axis (i.e. one axis pointing may be possible with a single actuator). This is an easier problem that may shed light on single actuator control but it may not directly apply to the circular scan configuration.

#### 5. Unique Actuators

Unique types of actuators, such as the RUM device, provide a wealth of potential research topics in the area of controlling mechanical systems. The RUM device is a unique actuator because it uses centripetal force to affect motion. Further investigation is warranted to determine what other types of actuators are available and whether they have similar modeling and analysis issues as those encountered with the RUM actuated system. The question to ask when looking at these types of actuators is not whether they are completely controllable but whether the motion generated by the actuators can be used in some form to control mechanical system behavior? Perhaps another actuator can provide the pointing motion as part of its physical properties.

## 6. Under-actuated Systems

Under-actuated system analysis has shown that a 3-degree of freedom system cannot be controlled at every instant by a single actuator. But, the RUM system is controlled in the scanning mode with a single actuator. This is because the motion of one axis depends on the motion of the other axis. This dependence is very predictable and can be controlled by changing system parameters such as RUM arm length and RUM mass. The RUM actuated system appears to fit into the category of 'nonholonomic' systems. Nonholonomic systems are best described by comparing them to 'holonomic' systems. Given two points in space, A and B, a holonomic systems can take arbitrary paths to get from one point to the other. For nonholonomic systems, motion between points A and B are constrained to specific paths [26]. Examples of nonholonomic systems are automobiles, space-based robot manipulators, and orbiting satellites. A classic example of controlling a nonholonomic system is parallel parking a car. The car must be moved along a certain path to move the car into the parking space. Backing the car into the space is the optimum solution. The RUM system may be a similar situation. The RUM must rotate in order to affect elevation and cross-elevation axes motion. This motion constrains the path that the elevation and cross-elevation axes can take. If unlimited power is available, RUM rate variations will generate pointing along this constrained path. If not, another approach is necessary similar to backing the car into the parking space. The discovery of these types of control are usually ad hoc in nature and will require considerable research.

## 7. Additional Non-linear Analysis Tools

Limitations in the reachability analysis tools appear to indicate a need for additional non-linear analysis tools. A tool that is not unduly complicated is needed to analyze the coupling of centripetal, coriolis, and gravitational terms. These three terms may be significant factors in the control actuation of certain systems (e.g. gravity gradient control of space satellites). Having an analysis tool that can describe their coupling with other system dynamics would greatly facilitate reachability analysis.

### 7.2 Summary of Contributions

The research presented in this dissertation provides a number of contributions in the area of RUM actuated system modeling, analysis, and control as follows:

- Developed the first model that accounts for nonlinear coupling between payload axes and the RUM devices (Chapter 4).
- Showed that the model agrees with pointing control experimental results (Chapter 5). In contrast, earlier models give incorrect predictions.
- Identified dynamic effects (terms in the model) that prevent pointing (Chapter 6).
- Placed the pointing problem in the framework of under-actuated robotic systems (Chapter 6). Showed that necessary conditions for pointing control are not satisfied by present system.
- Identified several potential solutions to the pointing problem (Chapter 6).
- Identified numerous other areas of study that will provide years of future research.

### **7.3 Closing Thoughts**

This dissertation has taken a significant step toward the development of a comprehensive attitude control strategy for RUM actuated systems by providing the first complete system model and initial control analysis. The detailed model developed in this dissertation provides a valuable tool for continued research in the area of pointing control. Even though the system does not appear to be completely controllable, that doesn't mean it is not useable. Perhaps it is a matter of determining a better control approach that accounts for these system limitations.

## BIBLIOGRAPHY

- [1] M.E. Polites, "New Method for Scanning Spacecraft and Balloon-Borne/Space-Based Experiments," *Journal of Guidance, Control and Dynamics*, vol. 14, No. 3, May-June 1991, pp. 548-553.
- [2] M.E. Polites, "Rotating-Unbalanced-Mass Devices and Methods of Scanning Balloon-Borne Experiments, Free-Flying Spacecraft, and Space Shuttle/Space Station Attached Experiments," U.S. Patent #5, 129,600, NASA, Washington, D.C. July 14, 1992.
- [3] D.C. Alhorn and M.E. Polites, "Rotating Unbalanced-Mass Devices for Scanning : Results from the Proof-of-Concept Test," *Guidance and Control 1994*, Vol. 86, *Advances in the Astronautical Sciences*, Edited by R.D. Culp and R.D. Rausch, American Astronautical Society, 1994.
- [4] J. Cornell and J. Carr, Editors, *Infinite Vistas: New Tools for Astronomy*, New York, Charles Scribner's Sons, 1985.
- [5] M. Bass, Editor in Chief, *Handbook of Optics*, McGraw-Hill, Inc. 1995
- [6] R.A. Sunyaev, et al, "Highlights from the KVANT Mission," *Advances in Space Research*, Vol 10, No. 2, 1990, pp. 41-46.
- [7] J.J. Sellers, *Understanding Space: An Introduction to Astronautics*, McGraw-Hill, Inc. 1994.
- [8] J.P. Ducarteron and J.P. Treilhou, "Resonance Frequencies of a Gondola Submitted to a Forced Rotation under a Stratospheric Balloon," *Advances in Space Research: Scientific Ballooning*, Vol 13, No. 2, Feb
- [9] J.Y. Hung, D.A. McGee, M.E. Polites, D. Alhorn, "Spacecraft Pointing and Scanning using Rotating Unbalance Masses," Project Summary Report, NASA/ASEE Summer Faculty Fellowship Program, Marshall Space Flight Center, Huntsville, AL, Aug 1996.
- [10] A.J. Koivo, *Fundamentals for Control of Robotic Manipulators*, John Wiley & Sons, 1989
- [11] B. Friedland, *Advanced Control Techniques*, McGraw-Hill, 1995.

- [12] Z. Qu and D.M. Dawson, *Robust Tracking Control of Robot Manipulators*, IEEE Press, 1996.
- [13] J.-J.E. Slotine and W. Li., *Applied Nonlinear Control*, Prentice Hall, 1991.
- [14] C.A. Bishop, J.Y. Hung, M.E. Polites, D.C. Alhorn, "Pointing and Scanning Control of Optical Instruments using Rotating Unbalanced Masses," *Guidance and Control 1997*, Vol. 94, *Advances in the Astronautical Sciences*, Edited by R.D. Culp and S.B. Wiens, American Astronautical Society, 1997.
- [15] Goldstein, H., *Classical Mechanics*, Addison-Wesley, 1959.
- [16] H. Asada and J.J.E. Slotine, *Robot Analysis and Control*, John Wiley and Sons, 1986.
- [17] M.W. Spong and M. Vidyasagar, *Robot Dynamics and Control*, John Wiley and Sons, 1989.
- [18] J.H. Ginsberg, *Advanced Engineering Dynamics*, Cambridge University Press, 1995.
- [19] J.Y. Hung, J.M. Gallaspy, C. A. Bishop, M.E. Polites, D.C. Alhorn, "Dynamic Models of Instruments Using Rotating Unbalanced Masses," Project Summary Report, ASEE/NASA Summer Faculty Fellowship Program, Marshall Space Flight Center, Huntsville, AL, Aug 1997.
- [20] D.C. Alhorn and M.E. Polites, "Results of a Laboratory Experiment That Tests Rotating Unbalanced-Mass Devices for Scanning Gimbaled Payloads and Free-Flying Spacecraft," NASA TP-3458, NASA Marshal Space Flight Center, AL, January 1994.
- [21] C. Moler, "Golden ODEs, "New Ordinary Differential Equation Solvers for Matlab and Simulink," Matlab News and Notes, Summer 1996.
- [22] K. Ogata, *Modern Control Engineering*, Prentice Hall, Inc., Englewood Cliffs, N.J., 1970.
- [23] M. Bergerman, C.Lee, Y. Xu, "A Dynamic Coupling Index for Underactuated Manipulators," *Journal of Robotic Systems*, 12 (10), 1995, pg 693-707.

- [24] W.L. Brogan, *Modern Control Theory*, Prentice Hall Inc., Englewood Cliffs, N.J., 1991.
- [25] M. Bergerman and Y. Xu, "Robust Joint and Cartesian Control of Underactuated Manipulators," *Journal of Dynamic Systems, Measurement, and Control*, Vol 118, Sept. 1996, 557-565.
- [26] A.W. Divilbiss, "Nonholonomic Motion Planning in the Presence of Obstacles," Ph.D. dissertation, Dept. of Electrical Engineering, Rensselaer Polytechnic Institute, Troy, New York, Dec. 1993.

## APPENDIX A

### KINEMATIC MODELING DETAILS

#### 1. Homogeneous Transformations:

$$A_{01} := \begin{bmatrix} \cos(\theta_1) & 0 & \sin(\theta_1) & 0 \\ \sin(\theta_1) & 0 & -\cos(\theta_1) & 0 \\ 0 & 1 & 0 & 0 \\ 0 & 0 & 0 & 1 \end{bmatrix}$$

$$A_{12} := \begin{bmatrix} -\sin(\theta_2) & 0 & \cos(\theta_2) & 0 \\ \cos(\theta_2) & 0 & \sin(\theta_2) & 0 \\ 0 & 1 & 0 & 0 \\ 0 & 0 & 0 & 1 \end{bmatrix}$$

$$A_{23} := \begin{bmatrix} 1 & 0 & 0 & 0 \\ 0 & 1 & 0 & 0 \\ 0 & 0 & 1 & d \\ 0 & 0 & 0 & 1 \end{bmatrix}$$

$$A_{34} := \begin{bmatrix} \cos(\theta_4) & -\sin(\theta_4) & 0 & r \cos(\theta_4) \\ \sin(\theta_4) & \cos(\theta_4) & 0 & r \sin(\theta_4) \\ 0 & 0 & 1 & 0 \\ 0 & 0 & 0 & 1 \end{bmatrix}$$

$$A_{25} := \begin{bmatrix} 1 & 0 & 0 & 0 \\ 0 & 1 & 0 & 0 \\ 0 & 0 & 1 & -d \\ 0 & 0 & 0 & 1 \end{bmatrix}$$

$$A56 := \begin{bmatrix} \cos(\theta_6) & -\sin(\theta_6) & 0 & -r \cos(\theta_6) \\ \sin(\theta_6) & \cos(\theta_6) & 0 & -r \sin(\theta_6) \\ 0 & 0 & 1 & 0 \\ 0 & 0 & 0 & 1 \end{bmatrix}$$

## 2. Kinematic Equations:

$A04 :=$

$$\begin{aligned} & [-\cos(\theta_1) \sin(\theta_2) \cos(\theta_4) + \sin(\theta_1) \sin(\theta_4), \\ & \cos(\theta_1) \sin(\theta_2) \sin(\theta_4) + \sin(\theta_1) \cos(\theta_4), \\ & \cos(\theta_1) \cos(\theta_2), -\cos(\theta_1) \sin(\theta_2) r \cos(\theta_4) \\ & + \sin(\theta_1) r \sin(\theta_4) + \cos(\theta_1) \cos(\theta_2) d] \\ & [-\sin(\theta_1) \sin(\theta_2) \cos(\theta_4) - \cos(\theta_1) \sin(\theta_4), \\ & \sin(\theta_1) \sin(\theta_2) \sin(\theta_4) - \cos(\theta_1) \cos(\theta_4), \\ & \sin(\theta_1) \cos(\theta_2), -\sin(\theta_1) \sin(\theta_2) r \cos(\theta_4) \\ & - \cos(\theta_1) r \sin(\theta_4) + \sin(\theta_1) \cos(\theta_2) d] \\ & [\cos(\theta_2) \cos(\theta_4), -\cos(\theta_2) \sin(\theta_4), \sin(\theta_2), \\ & \cos(\theta_2) r \cos(\theta_4) + \sin(\theta_2) d] \\ & [0, 0, 0, 1] \end{aligned}$$

$A06 :=$

$$\begin{aligned} & [-\cos(\theta_1) \sin(\theta_2) \cos(\theta_6) + \sin(\theta_1) \sin(\theta_6), \\ & \cos(\theta_1) \sin(\theta_2) \sin(\theta_6) + \sin(\theta_1) \cos(\theta_6), \\ & \cos(\theta_1) \cos(\theta_2), \cos(\theta_1) \sin(\theta_2) r \cos(\theta_6) \\ & - \sin(\theta_1) r \sin(\theta_6) - \cos(\theta_1) \cos(\theta_2) d] \\ & [-\sin(\theta_1) \sin(\theta_2) \cos(\theta_6) - \cos(\theta_1) \sin(\theta_6), \\ & \sin(\theta_1) \sin(\theta_2) \sin(\theta_6) - \cos(\theta_1) \cos(\theta_6), \\ & \sin(\theta_1) \cos(\theta_2), \sin(\theta_1) \sin(\theta_2) r \cos(\theta_6) \\ & + \cos(\theta_1) r \sin(\theta_6) - \sin(\theta_1) \cos(\theta_2) d] \\ & [\cos(\theta_2) \cos(\theta_6), -\cos(\theta_2) \sin(\theta_6), \sin(\theta_2), \\ & -\cos(\theta_2) r \cos(\theta_6) - \sin(\theta_2) d] \\ & [0, 0, 0, 1] \end{aligned}$$

## APPENDIX B

### VELOCITY JACOBIANS

#### 1. Linear Velocity Jacobians:

$$JL1 := \begin{bmatrix} 0 & 0 & 0 & 0 \\ 0 & 0 & 0 & 0 \\ 0 & 0 & 0 & 0 \end{bmatrix}$$

$$JL2 := \begin{bmatrix} 0 & 0 & 0 & 0 \\ 0 & 0 & 0 & 0 \\ 0 & 0 & 0 & 0 \end{bmatrix}$$

$$JL3 := \begin{bmatrix} 0 & 0 & 0 & 0 \\ 0 & 0 & 0 & 0 \\ 0 & 0 & 0 & 0 \end{bmatrix}$$

$JL4 :=$

$$\begin{aligned} & [\sin(\theta_1) \sin(\theta_2) r \cos(\theta_4) + \cos(\theta_1) r \sin(\theta_4) \\ & - \sin(\theta_1) \cos(\theta_2) d, \\ & -\cos(\theta_1) \cos(\theta_2) r \cos(\theta_4) - \cos(\theta_1) \sin(\theta_2) d, \\ & \sin(\theta_1) r \cos(\theta_4) + \sin(\theta_2) \cos(\theta_1) r \sin(\theta_4), 0] \\ & [-\cos(\theta_1) \sin(\theta_2) r \cos(\theta_4) + \sin(\theta_1) r \sin(\theta_4) \\ & + \cos(\theta_1) \cos(\theta_2) d, \\ & -\sin(\theta_1) \cos(\theta_2) r \cos(\theta_4) - \sin(\theta_1) \sin(\theta_2) d, \\ & -\cos(\theta_1) r \cos(\theta_4) + \sin(\theta_2) \sin(\theta_1) r \sin(\theta_4), 0] \\ & [0, -\sin(\theta_2) r \cos(\theta_4) + \cos(\theta_2) d, -\cos(\theta_2) r \sin(\theta_4), 0] \end{aligned}$$

$$JL5 := \begin{bmatrix} 0 & 0 & 0 & 0 \\ 0 & 0 & 0 & 0 \\ 0 & 0 & 0 & 0 \end{bmatrix}$$

$JL6 =$

$$\begin{aligned}
 & [-\sin(\theta_1) \sin(\theta_2) r \cos(\theta_6) - \cos(\theta_1) r \sin(\theta_6) \\
 & + \sin(\theta_1) \cos(\theta_2) d, \\
 & \cos(\theta_1) \cos(\theta_2) r \cos(\theta_6) + \cos(\theta_1) \sin(\theta_2) d, 0, \\
 & -\sin(\theta_1) r \cos(\theta_6) - \sin(\theta_2) \cos(\theta_1) r \sin(\theta_6)] \\
 & [\cos(\theta_1) \sin(\theta_2) r \cos(\theta_6) - \sin(\theta_1) r \sin(\theta_6) \\
 & - \cos(\theta_1) \cos(\theta_2) d, \\
 & \sin(\theta_1) \cos(\theta_2) r \cos(\theta_6) + \sin(\theta_1) \sin(\theta_2) d, 0, \\
 & \cos(\theta_1) r \cos(\theta_6) - \sin(\theta_2) \sin(\theta_1) r \sin(\theta_6)] \\
 & [0, \sin(\theta_2) r \cos(\theta_6) - \cos(\theta_2) d, 0, \cos(\theta_2) r \sin(\theta_6)]
 \end{aligned}$$

2. Angular Velocity Jacobian:

$$JA1 = \begin{bmatrix} 0 & 0 & 0 & 0 \\ 0 & 0 & 0 & 0 \\ 1 & 0 & 0 & 0 \end{bmatrix}$$

$$JA2 = \begin{bmatrix} 0 & \sin(\theta_1) & 0 & 0 \\ 0 & -\cos(\theta_1) & 0 & 0 \\ 1 & 0 & 0 & 0 \end{bmatrix}$$

$$JA3 = \begin{bmatrix} 0 & \sin(\theta_1) & 0 & 0 \\ 0 & -\cos(\theta_1) & 0 & 0 \\ 1 & 0 & 0 & 0 \end{bmatrix}$$

$$JA4 = \begin{bmatrix} 0 & \sin(\theta_1) & \cos(\theta_1) \cos(\theta_2) & 0 \\ 0 & -\cos(\theta_1) & \sin(\theta_1) \cos(\theta_2) & 0 \\ 1 & 0 & \sin(\theta_2) & 0 \end{bmatrix}$$

$$JA5 = \begin{bmatrix} 0 & \sin(\theta_1) & 0 & 0 \\ 0 & -\cos(\theta_1) & 0 & 0 \\ 1 & 0 & 0 & 0 \end{bmatrix}$$

## APPENDIX C

### H AND C MATRIX VALUES

Notational note for  $H(q)$  and  $C(q, \dot{q})$  calculations:

$$\theta_1 = q_1$$

$$\dot{\theta}_1 = \dot{q}_1$$

$$\theta_2 = q_2$$

$$\dot{\theta}_2 = \dot{q}_2$$

$$\theta_4 = \theta_6 = q_3$$

$$\dot{\theta}_4 = \dot{\theta}_6 = \dot{q}_3$$

1.  $H(q)$  Matrix:

$$H_{[1,1]} = \left( -2 mRUM r^2 \cos(\theta_4)^2 + 2 mRUM d^2 + I_{elX} \right) \cos(\theta_2)^2 - 4 mRUM \sin(\theta_2) r \cos(\theta_4) \cos(\theta_2) d + 2 mRUM r^2$$

$$H_{[1,2]} = \left( -2 mRUM r^2 \cos(\theta_2) \cos(\theta_4) - 2 mRUM r \sin(\theta_2) d \right) \sin(\theta_4)$$

$$H_{[1,3]} = -mRUM r \cos(\theta_2) d \cos(\theta_4) + mRUM r^2 \sin(\theta_2)$$

$$H_{[1,4]} = -mRUM r \cos(\theta_2) d \cos(\theta_4) + mRUM r^2 \sin(\theta_2)$$

$$H_{[2,1]} = (-2 mRUM r^2 \cos(\theta_2) \cos(\theta_4) - 2 mRUM r \sin(\theta_2) d) \sin(\theta_4)$$

$$H_{[2,2]} = ItelY + 2 mRUM d^2 + 2 mRUM r^2 \cos(\theta_4)^2$$

$$H_{[2,3]} = -mRUM r \sin(\theta_4) d$$

$$H_{[2,4]} = -mRUM r \sin(\theta_4) d$$

$$H_{[3,1]} = -mRUM r \cos(\theta_2) d \cos(\theta_4) + mRUM r^2 \sin(\theta_2)$$

$$H_{[3,2]} = -mRUM r \sin(\theta_4) d$$

$$H_{[3,3]} = mRUM r^2$$

$$H_{[3,4]} := 0$$

$$H_{[4,1]} := -mRUM r \cos(\theta_2) d \cos(\theta_4) + mRUM r^2 \sin(\theta_2)$$

$$H_{[4,2]} := -mRUM r \sin(\theta_4) d$$

$$H_{[4,3]} := 0$$

$$H_{[4,4]} := mRUM r^2$$

## 2. $C(q, \dot{q})$ Matrix Values

$$\begin{aligned} c_{[1,1]} := & \left( -4 mRUM \cos(\theta_2)^2 r \cos(\theta_4) d \right. \\ & + \left( -\text{iteIX} - 2 mRUM d^2 + 2 mRUM r^2 \cos(\theta_4)^2 \right) \sin(\theta_2) \cos(\theta_2) \\ & + 2 mRUM r \cos(\theta_4) d \left. \right) \theta_2 \dot{\theta}_2 + \left( \right. \\ & 2 mRUM \cos(\theta_2)^2 r^2 \cos(\theta_4) \sin(\theta_4) \\ & + 2 mRUM \sin(\theta_2) r \sin(\theta_4) \cos(\theta_2) d \left. \right) \theta_4 \dot{\theta}_4 \end{aligned}$$

$$\begin{aligned}
c_{[1,2]} = & \left( -4 mRUM \cos(\theta_2)^2 r \cos(\theta_4) d \right. \\
& + \left( -ItelX - 2 mRUM d^2 + 2 mRUM r^2 \cos(\theta_4)^2 \right) \sin(\theta_2) \cos(\theta_2) \\
& + 2 mRUM r \cos(\theta_4) d \left. \right) \theta_1 \dot{\theta}_1 + \left( \right. \\
& 2 mRUM r^2 \sin(\theta_4) \sin(\theta_2) \cos(\theta_4) \\
& - 2 mRUM r \sin(\theta_4) \cos(\theta_2) d \left. \right) \theta_2 \dot{\theta}_2 + \\
& + \left( 2 mRUM r^2 - 2 mRUM r^2 \cos(\theta_4)^2 \right) \cos(\theta_2) \theta_4 \dot{\theta}_4
\end{aligned}$$

$$\begin{aligned}
c_{[1,3]} = & \left( mRUM \sin(\theta_2) r \sin(\theta_4) \cos(\theta_2) d \right. \\
& + mRUM \cos(\theta_2)^2 r^2 \cos(\theta_4) \sin(\theta_4) \left. \right) \theta_1 \dot{\theta}_1 \\
& + \left( -mRUM r^2 \cos(\theta_4)^2 + mRUM r^2 \right) \cos(\theta_2) \theta_2 \dot{\theta}_2 \\
& + mRUM r \sin(\theta_4) \cos(\theta_2) d \theta_4 \dot{\theta}_4
\end{aligned}$$

$$\begin{aligned}
c_{[1,4]} = & \left( mRUM \sin(\theta_2) r \sin(\theta_4) \cos(\theta_2) d \right. \\
& + mRUM \cos(\theta_2)^2 r^2 \cos(\theta_4) \sin(\theta_4) \left. \right) \theta_1 \dot{\theta}_1 \\
& + \left( -mRUM r^2 \cos(\theta_4)^2 + mRUM r^2 \right) \cos(\theta_2) \theta_2 \dot{\theta}_2 \\
& + mRUM r \sin(\theta_4) \cos(\theta_2) d \theta_4 \dot{\theta}_4
\end{aligned}$$

$$\begin{aligned}
c_{[2,1]} = & \left( 4 mRUM \cos(\theta_2)^2 r \cos(\theta_4) d \right. \\
& + \left( -2 mRUM r^2 \cos(\theta_4)^2 + 2 mRUM d^2 + ItelX \right) \sin(\theta_2) \cos(\theta_2) \\
& - 2 mRUM r \cos(\theta_4) d \left. \right) \theta_1 \dot{\theta}_1 + \\
& \left( -2 mRUM r^2 \cos(\theta_4)^2 \cos(\theta_2) - 2 mRUM r \cos(\theta_4) \sin(\theta_2) d \right) \\
& \theta_4 \dot{\theta}_4
\end{aligned}$$

$$c_{[2,2]} = -2 mRUM r^2 \cos(\theta_4) \sin(\theta_4) \dot{\theta}_4$$

$$c_{[2,3]} = \left( -mRUM r^2 \cos(\theta_4)^2 \cos(\theta_2) - mRUM r \cos(\theta_4) \sin(\theta_2) d \right) \dot{\theta}_1 - mRUM r^2 \cos(\theta_4) \sin(\theta_4) \dot{\theta}_2 - mRUM r \cos(\theta_4) d \dot{\theta}_4$$

$$c_{[2,4]} = \left( -mRUM r^2 \cos(\theta_4)^2 \cos(\theta_2) - mRUM r \cos(\theta_4) \sin(\theta_2) d \right) \dot{\theta}_1 - mRUM r^2 \cos(\theta_4) \sin(\theta_4) \dot{\theta}_2 - mRUM r \cos(\theta_4) d \dot{\theta}_4$$

$$c_{[3,1]} = \left( -mRUM \cos(\theta_2)^2 r^2 \cos(\theta_4) \sin(\theta_4) - mRUM \sin(\theta_2) r \sin(\theta_4) \cos(\theta_2) d \right) \dot{\theta}_1 + \left( mRUM r \cos(\theta_4) \sin(\theta_2) d + mRUM r^2 \cos(\theta_4)^2 \cos(\theta_2) \right) \dot{\theta}_2$$

$$c_{[3,2]} = \left( mRUM r \cos(\theta_4) \sin(\theta_2) d + mRUM r^2 \cos(\theta_4)^2 \cos(\theta_2) \right) \dot{\theta}_1 + mRUM r^2 \cos(\theta_4) \sin(\theta_4) \dot{\theta}_2$$

$$c_{[3,3]} = 0$$

$$c_{[3,4]} = 0$$

$$c_{[4,1]} = \left( -mRUM \cos(\theta_2)^2 r^2 \cos(\theta_4) \sin(\theta_4) \right. \\ \left. - mRUM \sin(\theta_2) r \sin(\theta_4) \cos(\theta_2) d \right) \dot{\theta}_1 + \\ \left( mRUM r \cos(\theta_4) \sin(\theta_2) d + mRUM r^2 \cos(\theta_4)^2 \cos(\theta_2) \right) \dot{\theta}_2$$

$$c_{[4,2]} = \left( mRUM r \cos(\theta_4) \sin(\theta_2) d + mRUM r^2 \cos(\theta_4)^2 \cos(\theta_2) \right) \dot{\theta}_1 + \\ mRUM r^2 \cos(\theta_4) \sin(\theta_4) \dot{\theta}_2$$

$$c_{[4,3]} = 0$$

$$c_{[4,4]} = 0$$

## APPENDIX D

### COUPLING INDEX – MODEL 3

Notational note for coupling index calculations:

$$\theta_1 = q_1$$

$$\theta_2 = q_2$$

$$\theta_4 = \theta_6 = q_3$$

$$\begin{aligned}
 Mc11 = & 2 r mRUM \left( ItelY \cos(\theta_2) d \cos(\theta_4) - ItelY r \sin(\theta_2) \right. \\
 & + 2 mRUM d^3 \cos(\theta_2) \cos(\theta_4) - 2 mRUM r^3 \cos(\theta_4)^2 \sin(\theta_2) \\
 & + 2 mRUM r^2 \cos(\theta_2) \cos(\theta_4) d - 2 r mRUM d^2 \sin(\theta_2) \cos(\theta_4)^2 \left. \right) \\
 & \left( -\cos(\theta_2)^2 ItelX ItelY - 2 \cos(\theta_2)^2 ItelX mRUM d^2 \right. \\
 & - 2 \cos(\theta_2)^2 ItelX mRUM r^2 \cos(\theta_4)^2 - 2 \cos(\theta_2)^2 mRUM d^2 ItelY \\
 & - 4 \cos(\theta_2)^2 mRUM^2 d^4 + 2 \cos(\theta_2)^2 mRUM r^2 \cos(\theta_4)^2 ItelY \\
 & + 4 mRUM \sin(\theta_2) r \cos(\theta_4) \cos(\theta_2) d ItelY \\
 & + 8 mRUM^2 \sin(\theta_2) r \cos(\theta_4) \cos(\theta_2) d^3 - 2 mRUM r^2 ItelY \\
 & - 4 mRUM^2 r^4 \cos(\theta_4)^2 + 4 mRUM^2 r^4 \cos(\theta_2)^2 \cos(\theta_4)^2 \\
 & + 8 mRUM^2 r^3 \cos(\theta_2) \cos(\theta_4) \sin(\theta_2) d \\
 & - 4 mRUM^2 r^2 d^2 \cos(\theta_2)^2 - 4 mRUM^2 r^2 d^2 \cos(\theta_4)^2 \\
 & \left. + 4 mRUM^2 r^2 d^2 \cos(\theta_2)^2 \cos(\theta_4)^2 \right)
 \end{aligned}$$

$$\begin{aligned}
Mc21 = & 2 mRUM r \sin(\theta_4) \cos(\theta_2) \left( -2 mRUM r^3 \cos(\theta_4) \sin(\theta_2) \right. \\
& - 2 mRUM r \sin(\theta_2) d^2 \cos(\theta_4) + 2 mRUM r^2 d \cos(\theta_2) \\
& \left. + d \cos(\theta_2) ItelX + 2 mRUM \cos(\theta_2) d^3 \right) / \left( -\cos(\theta_2)^2 ItelX ItelY \right. \\
& - 2 \cos(\theta_2)^2 ItelX mRUM d^2 - 2 \cos(\theta_2)^2 ItelX mRUM r^2 \cos(\theta_4)^2 \\
& - 2 \cos(\theta_2)^2 mRUM d^2 ItelY - 4 \cos(\theta_2)^2 mRUM^2 d^4 \\
& + 2 \cos(\theta_2)^2 mRUM r^2 \cos(\theta_4)^2 ItelY \\
& + 4 mRUM \sin(\theta_2) r \cos(\theta_4) \cos(\theta_2) d ItelY \\
& + 8 mRUM^2 \sin(\theta_2) r \cos(\theta_4) \cos(\theta_2) d^3 - 2 mRUM r^2 ItelY \\
& - 4 mRUM^2 r^4 \cos(\theta_4)^2 + 4 mRUM^2 r^4 \cos(\theta_2)^2 \cos(\theta_4)^2 \\
& + 8 mRUM^2 r^3 \cos(\theta_2) \cos(\theta_4) \sin(\theta_2) d \\
& - 4 mRUM^2 r^2 d^2 \cos(\theta_2)^2 - 4 mRUM^2 r^2 d^2 \cos(\theta_4)^2 \\
& \left. + 4 mRUM^2 r^2 d^2 \cos(\theta_2)^2 \cos(\theta_4)^2 \right)
\end{aligned}$$